
# BRNO UNIVERSITY OF TECHNOLOGY

VYSOKÉ UČENÍ TECHNICKÉ V BRNĚ

## CENTRAL EUROPEAN INSTITUTE OF TECHNOLOGY BUT

STŘEDOEVROPSKÝ TECHNOLOGICKÝ INSTITUT VUT


# UTILIZATION OF THEORETICAL AND EXPERIMENTAL APPROACHES TO SINTERING FOR TAILORING THE MICROSTRUCTURE AND PROPERTIES OF ADVANCED CERAMIC MATERIALS

VYUŽITÍ TEORETICKÝCH A EXP. PŘÍSTUPŮ KE SLINOVÁNÍ PRO ZÍSKÁNÍ OPTIMÁLNÍ MIKROSTRUKTURY A VLASTNOSTÍ POKROČILÝCH KERAMICKÝCH MATERIÁLŮ

SHORT VERSION OF DOCTORAL THESIS

TEZE DIZERTAČNÍ PRÁCE


**AUTHOR**
AUTOR PRÁCE

Ing. Tomáš Spusta

**SUPERVISOR**
ŠKOLITEL

prof. RNDr. Karel Maca, Dr.



BRNO 2019

# Abstract

This thesis is focused on possibility of microstructure tailoring of selected oxide advanced ceramic materials (alumina, cubic and tetragonal zirconia) by post-Hot isostatic pressing (post-HIPing) method in order to produce samples with full density and minimal grain size. Considering that the post-HIPing is in majority of cases the finishing technique, the pre-sintering (preparation of specimens in close porosity stage) was also heavily studied. Extensive theoretic and experimental research of pre-sintering advanced oxide materials resulted in several observations. It was found out, that pore closure is material characteristic governed by interfacial energies (pore closure ranging from 92 to 96% t.d. in dependence on used material), it is independent on green body processing and it is also independent on sintering history.

In order to examine the microstructure via scanning electron microscope and to increase the efficiency of the microstructure analysis, the novel low temperature thermal etching method was developed. The low temperature 900 °C for 1 hour allows to thermally reveal microstructure for both partially sintered and fully dense specimens without thermal contamination (increase in the density and grain size) of the examined samples.

The pre-sintered samples were post-HIPed at designed combinations of temperature (1200-1400 °C), applied pressure (50 and 200 MPa) and dwell time (0.5-9 hours) in order to examine influence of these post-HIPing parameters on the microstructure of the samples. The most important observation was minimal influence of the applied pressure on the grain growth during post-HIPing, while it has significant densification capability. The sintering temperature and dwell time also exhibit densification potential, however with negative effect on the grain size inhibition after post-HIPing respecting kinetic grain growth reaction – exponential effect for temperature and parabolic for dwell time.

Such observations were accompanied to prepare optimized post-HIPing cycles for observed materials, resulting into the specimens with density above 99.7 % t.d. and with only minimal (below 10 %) increase in the grain size compared to pre-sintered grain size.

Obtained knowledge was applied for production of transparent alumina ceramics doped by erbium with photo luminescent properties. Obtained HV 10 hardness (26.9 GPa) and real inline transmittance (RIT 56 %) are the highest values among the rare-earth doped alumina published so far.

# Key Words

Oxide ceramics, pre-sintering, post-HIPing, microstructure tailoring

# Abstrakt

Táto práca sa zaoberá prispôsobením (tailoring) mikroštruktúry vybraných pokročilých keramických materiálov (oxid hlinitý, kubický a tetragonálny oxid zirkoničitý) metódou izostatického lisovania za tepla (post-HIPing) s cieľom pripraviť vzorky s teoretickou hustotou and minimálnou veľkosťou zŕn. Vzhľadom na to, že izostatické lisovanie je vo väčšine prípadov používané ako dokončovacia metóda, pred-slinovanie (príprava vzoriek v štádiu uzavretej pórovitosti) bolo tiež dopodrobna študované. Extenzívny teoretický a experimentálny výskum pred-sintrovania pokročilých keramických materiálov ukázal niekoľko výsledkov. Bolo zistené, že uzatváranie pórov je materiálová charakteristika riadená medzi-povrchovými energiami (uzatváranie pórov nastáva pri 92-96 % t.d. pre skúmané materiály), je nezávislé na technológii prípravy keramického polotovaru a je nezávislé na histórii sintrovacieho procesu.

Pre analýzu mikroštruktúry skenovacím elektrónovým mikroskopom a výrazné zvýšenie efektivity mikroštruktúrnej analýzy, bola vyvinutá nízkoteplotná metóda termálneho leptania. Táto metóda umožňuje zviditeľnenie leštenej mikroštruktúry pri leptacej teplote 900 °C a výdrži 1 hodina čiastočne sintrovaných a plne hutných vzoriek bez teplotnej kontaminácie (zvýšenie hustoty a veľkosti zŕn).

Pred-sintrované vzorky boli post-HIPované nadizajnovaným kombináciami teploty (1200-1400 °C), aplikovaného tlaku (50 a 200 MPa) a času výdrže (0,5 až 9 hodín) s cieľom štúdia vplyvu týchto post-HIPovacích parametrov na mikroštruktúru vzoriek. Najdôležitejší výsledok experimentov je, že aplikovaný tlak vykazuje iba minimálny vplyv na rast zŕn v priebehu post-HIPovania, pričom výrazne posilňuje zhutňovanie. Sintrovacia teplota a čas výdrže tiež vykazovali zhutňovací potenciál, avšak s negatívnym efektom na veľkosť zŕn počas post-HIPovania rešpektujúc kinetickú rovnicu rastu zŕn – exponenciálny rast pre teplotu a parabolický rast pre čas.

Tieto výsledky boli použité pre optimalizáciu post-HIPovacích cyklov pre študované materiály. Výsledné vzorky boli zhutnené nad 99,7 % t.d. a s minimálnym (pod 10 %) nárastom veľkosti zŕn v porovnaní s pred-sintrovanou veľkosťou zŕn.

Aplikáciou získaných znalostí bola pripravená transparentná korundová keramika dopovaná erbiom s fotoluminiscenčnými vlastnosťami. Pripravená vzorka s tvrdosťou HV 10 26,9 GPa a so skutočnou inline priepustnosťou RIT 56 % vykazuje najlepšie hodnoty tvrdosti a priepustnosti v doposiaľ publikovaných korundových keramických materiáloch dopovaných prvkami vzácnych zemín.

# Kľúčové slová

Oxidová keramika, pred-sintrovanie, post-HIPovanie, optimalizácia mikroštruktúry

# Bibliographic Citation

SPUSTA, Tomáš. *Využití teoretických a exp. přístupů ke slinování pro získání optimální mikrostruktury a vlastností pokročilých keramických materiálů*. Brno, 2020. Dostupné také z: https://www.vutbr.cz/studenti/zav-prace/detail/125609. Dizertační práce. Vysoké učení technické v Brně, Středoevropský technologický institut VUT, Středoevropský technologický institut VUT. Vedoucí práce Karel Maca.

# Declaration

I declare that this master's thesis was worked out on my own using mentioned literature and under supervision of above named supervisor.

In Brno on the 15th of January 2020

.....

Ing. Tomáš Spusta

# Acknowledgements

I would like to thank to my supervisor prof. RNDr. Karel Maca, Dr. for valuable and experienced scientific supervision, patience and professional approach. Furthermore, I would like to thank to all my colleagues from the CEITEC research group Advanced Materials for their assistance in execution of experiments. I would also like to thank my family for their consistent support through the years of my study.

# Table of Content


1. Introduction ..... 2
2. Theoretical Part ..... 4
   2.1. Sintering Basics ..... 4
   2.2. Issues with Pressureless Sintering ..... 4
   2.3. Benefits of Sintering with Applied Pressure ..... 5
   2.4. Hot Isostatic Pressing Basics ..... 7
      2.4.1. Post-HIPing of Pre-sintered Green Bodies ..... 8
   2.5. Hot Isostatic Pressing Maps – Theoretical Models ..... 9
   2.6. Hot Isostatic Pressing – Experimental Observations ..... 9
   2.7. Influence of the Grain Size on the Properties of Ceramic Materials ..... 16
      2.7.1. Strength and Hardness ..... 16
      2.7.2. Transparency in Visible Spectrum ..... 17
      2.7.3. Piezoelectric Coefficient $d_{33}$ ..... 18
   2.8. Personal Thoughts on the Experimental Review ..... 19
3. Objectives of the Ph.D. Thesis ..... 21
4. Pre-sintering Regime Optimization - Study of Pore Closure Phenomena ..... 22
5. Low Temperature Technique for Thermal Etching ..... 24
6. Doped Transparent Alumina Ceramics with Photo-luminescent Properties ..... 26
7. Microstructure Development During Post-HIPing - Experimental Part ..... 28
   7.1. Preparation of Green Bodies ..... 28
   7.2. Preparation of Pre-sintered Bodies ..... 28
   7.3. Preparation of Post-HIPed Samples ..... 28
   7.4. Density Measurements ..... 29
   7.5. Microstructure Analysis ..... 30
8. Microstructure Development During Post-HIPing - Results ..... 32
   8.1. Green Bodies ..... 32
   8.2. Pre-sintered Samples ..... 33
   8.3. Post-HIPed Samples ..... 34
      8.3.1. Post-HIPed Alumina TM-DAR ..... 34
      8.3.2. Post-HIPed Zirconia TZ3Y ..... 36
      8.3.3. HIPed Zirconia TZ8Y ..... 38
      8.3.4. Post-HIPed Zirconia TZ8YSB ..... 40
9. Microstructure Development During Post-HIPing - Discussion ..... 42
   9.1. Green Body Preparation ..... 42
   9.2. Repeatability of Pre-sintering Process ..... 43

9.3. Errors of Density and Grain Size Measurements ..... 43
9.4. Influence of HIPing Variables on the Microstructure ..... 44
9.4.1. Influence of the Time on the Microstructure ..... 44
9.4.2. Influence of the Temperature on the Microstructure ..... 46
9.4.3. Influence of the Pressure on the Microstructure ..... 49
9.4.4. Optimization of the HIPing Process ..... 52
9.4.5. Trading of the HIPing Parameters ..... 54
10. Conclusions ..... 56
11. Bibliography ..... 57
12. Appendix ..... 65
13. Author's publications and other outputs ..... 66

# 1. Introduction

In a general way, a term tailoring comes from the fashion industry and it means the production of clothes, which exactly fit the customers' size and demands. In the case of the advanced ceramic processing, the tailoring is understood as a way of controlling the microstructure of the material to achieve the properties fitting demands on a certain ceramic product. The example of ceramic microstructure tailoring can be demonstrated on alumina ceramics designed for two different purposes: ceramic filters and protective transparent shields.

For the ceramic foam filters used in a metal casting industry high porosity (80-90 vol. %) is required to separate a molten metal from possible solid inclusions created during melting – the slag. The size of pores has to be designed in a certain way to respect viscosity of the metal, the size of inclusions, etc. If the pores are too tiny, the molten metal could not penetrate the filter due to the capillary forces, and on the contrary, if the pores are excessively large, the filter will not be effective in removing the inclusions. On the other hand, for the transparent protective shielding, the transparency in the visible spectra is required alongside with mechanical resistance against the impact of flying objects. Such properties could be achieved by producing the alumina ceramics with theoretical density (zero porosity) and grain size below 350 nm [1–3]. In this particular combination of material (crystallographic structure) and grain size, the visible light will not be scattered on the grain boundaries or pores – which will create transparency in visible light. In addition, according to the empirical Hall-Petch equation [4], fine-grained microstructure also provides increased mechanical strength and hardness.

The traditional sintering process (pressureless heating of ceramic green body) is unable to provide such dense and fine grained microstructure due to accelerated grain growth in the final stage of sintering [5, 6]. Therefore more advanced sintering methods have to be accompanied. One of the specialized sintering technologies is pressureless pre-sintering followed by hot isostatic pressing (so-called post-HIPing). The HIPing is technology, which profits from the combination of the thermal energy and the isostatic pressure of a gas, which provides an additional energy input to the system. This combination of energies allows decreasing the HIPing temperature below the pressureless sintering one, which will eventually lead to the smaller grain size with the comparable (or even higher) density after HIPing [7].

Unfortunately, because of present gas creates the isostatic pressure, there are strict requirements on the sample. Although the sample could be any shape, the sample surface has to be air-tight, which means that either all open pores (net of tubular pores in a ceramic body) have to be annihilated by pre-sintering, or the ceramic specimen has to be encapsulated into the container made of appropriate glass or metal to seal up the surface of the sample. Both approaches have difficult steps to master: pre-sintering requires an additional amount of time, experiments and material to determine the critical relative density of the pore closure [8]. On the other hand, the glass or metal coatings are difficult to find, because they have to respect the shrinkage of coated ceramics and after HIPing they have to be chemically or mechanically removable without affecting the sintered sample [9, 10].

In addition, due to high equipment and operating costs, incomparable with the pressure-less sintering, HIPing is only justified for ceramic products with high additional value (transparent polycrystalline ceramics, biological implants, etc.), or in ceramics used in extreme conditions (turbines, bearings, cutting tools, etc.). In those cases either the product cannot be manufactured by any other technology or the investment of HIPing will provide longer life or additional functional and/or mechanical properties.

There are several articles in the relevant literature dealing with the influence of the HIPing variables on the densification either in the experimental or the theoretical way. However, according to the author's best knowledge, there is not the complex study of the impact of the HIPing temperature, the applied pressure and the dwell time on the grain growth in the post-HIPing process. Therefore, this empty space opens the window of opportunity for studying these phenomena. Such research could be beneficial for the optimization of already developed HIPing cycles and it also could reveal new facts about the post-HIPing process.

Therefore, the main focus of this thesis, in order to study the microstructure development during post-HIPing, is to prepare pre-sintered specimens, introduce etching technique suitable for partially dense and fully dense samples, analyse the influence of HIPing parameters (applied pressure, temperature and dwell time) on the microstructure and eventually utilize the post-HIPing observations in the proper application, where the post-HIPing provides enhanced results.

# 2. Theoretical Part

## 2.1. Sintering Basics

In the vast majority of ceramic processing techniques, it is required to densify the green body (shaped ceramic powder) by applying thermal energy to change weak connection realized by van der Waals forces to more durable connection by covalent, ion or ion-covalent bonding. Generally, when the green body particles are in point contact and thermal energy is applied (temperature in the furnace rises) there are several processes, which will simultaneously change the powder green body to the almost fully dense ceramic material. In general, the green body has 45-65 % of material theoretical density (t.d.) depending on the powder characteristics and the shaping technique (uniaxial pressing, cold isostatic pressing, slip casting, gel casting, injection moulding, etc.), therefore 55-35 % of green body is air, which has to be removed.

The sintering is usually divided into 3 stages, which correspond to the geometry changes according to Coble's model [5]. When the particles in point contact are heated, point contacts are enlarged and necks are formed. As temperature increases, the curvature gradients created by necks are smoothened by diffusion mechanisms, which can be densifying or non-densifying in their nature. The densifying mechanisms (the distance between particle centres is shortened) are welcomed and there is an aspiration to keep them online as long as possible. On the other hand, non-densifying (e.g. surface diffusion) mechanisms are contra-productive and there is a demand to restrict their influence to the minimum. With increasing temperature, necks will increase the contact area, which creates a tubular pore structure among particles connected with the outside atmosphere.

During the densification, conditions for stability of the tubular voids start to diminish. As the density increases (particles advance to each other) diameter of the tubular voids decreases. It is important to notice, that the tubular pore structure is not smooth as a drinking straw, but rather wavy as electromagnetic waves with wavelength and amplitudes [11, 12]. Therefore, at certain conditions (pore length, diameter, amplitude, wavelength, etc.) tubular pore structure will break up into spherical (lenticular) pores accommodated on grain boundaries.

## 2.2. Issues with Pressureless Sintering

The simplest approach to sintering is to increase the sintering temperature and dwell time until the density is at the desired value. However, after the pore structure transforms into discrete individual pores, grain boundary motion is no longer retarded by pore structure, which leads to excessive grain growth in the ceramic volume. The direct impact of excessive grain growth (increased mobility of grain boundaries) is other disturbing phenomena – pores leave the grain boundaries and enter into grain volume. This basically prevents to fully densification of the material, unless extreme temperature and holding times are accompanied.

Knowing these facts, several advanced techniques were developed to diminish those negative effects and produce ceramic products with fine grains and full density. The simplest way how to reduce the grain size during sintering is to lower the temperature after the closure of super-critical pores and increase the dwell time (basically, temperature vs. time trade-off). Such sintering regime is known as two-step sintering [13, 14]. The advantage and simplicity of this technique are in the fact that there is no need to use any special furnace. The disadvantage, mainly for the industry, is too long time for sintering (tens of hours).

Another approach is to combine thermal energy with mechanical energy. The mechanical energy will introduce beneficial forces, which will help to densify the samples, decrease

sintering temperature and even decrease dwell time. The mechanical energy could be delivered to the system by punches in Spark Plasma Sintering and Hot Pressing, or by gas (usually inert, but it depends on the construction of the machine) in Hot Isostatic Pressing.

## 2.3. Benefits of Sintering with Applied Pressure

In the case of conventional (pressureless) sintering without chemical reaction, the driving force for densification (lowering the free surface energy) is provided by curvature gradients of the particles. At the start, particles are in unnatural, high energy state and the aim of the sintering is to lower this energetic state. The intensity of this energetic misbalance represents how effectively the particles will densify – the more free surface energy, the less temperature is needed to densification (simplified). An example could be 1 mole of powder consisting of spherical particles with radius $r$. Number of particles $N$ in the molar volume of the powder is

$$N = \frac{3V_m}{4\pi r^3} \tag{1}$$

where $V_m$ is molar volume defined as

$$V_m = \frac{M}{\rho} \tag{2}$$

where $M$ is molecular weight and $\rho$ is the density of the particle material. Therefore surface area $S$ of the particle system can be presented as

$$S = 4\pi r^2 N = \frac{3V_m}{r}. \tag{3}$$

The surface free energy associated with the mentioned system is

$$E_S = \frac{3\gamma_s V_m}{r} \tag{4}$$

where $\gamma_s$ is specific surface energy per unit area.

$E_S$ represents the decrease in surface free energy of the system if a fully dense material were to be formed from the particle compact [15]. In the case of used powders in the following experimental research Taimicron TM DAR ($Al_2O_3$, $r = 75\,nm$, $\gamma_s = 1\,J/m^2$, $V_m = 2.56 \cdot 10^{-5} m^3/mol$), the free energy would be around $1000\,J/mol$, in the case of Tosoh TZ3Y ($ZrO_2$, $r = 40\,nm$, $\gamma_s = 1.5\,J/m^2$, $V_m = 2.02 \cdot 10^{-5} m^3/mol$) the free energy would be around $2200\,J/mol$.

Additional energy which could be added to sintering particle system is mechanical pressure – that is why the name "pressure-assisted" sintering. The effectivity of such complementary process is presented in the following calculation. The external pressure applied on 1 mole of particles will do work on the system, which can be approximated as

$$W = p_a V_m \tag{5}$$

where $p_a$ is applied pressure, $W$ represents the driving force for densification due to application of external pressure. As an example $p_a = 200\,MPa$ normally used in HIPing process and molar volume of alumina $V_m = 2.56 \cdot 10^{-5}\,m^3/mol$ gives work $5110\,J/mol$. In the case of zirconia ($V_m = 2.02 \cdot 10^{-5}\,m^3/mol$) the work is $4050\,J/mol$. From these basic, simple and approximate calculations it can be seen enormous potential in the densification capabilities when pressure is applied during sintering.

Previous calculations were focused on the moment when powder compact is sintered with or without pressure from the start. However, when sintering approaches the final stage (pores are

closed) situation with pressure in the pores is different. When powder compact enters into the final stage of sintering, gas is entrapped into the isolated pores with the pressure of sintering atmosphere (for conventional sintering it will be air with a pressure of 1 $bar$). During further densification spherical pores will shrink until they reach equilibrium between sintering pressure and pressure emitted from pressurized gas inside the pore (Equation (6)) [16]:

$$P_i\left[\left(\frac{r_i}{r_f}\right)^3 - 1\right] = \frac{2\gamma_s}{r_f} \tag{6}$$

where $P_i$ is the initial pressure of the gas, $r_i$ is the radius of pore just after closure (initial) and $r_f$ is the final radius of isolated pore. When this equilibrium is attained, basically no shrinkage/densification will longer occur unless coalescence of pores occurs. Kang and Yoon [17] studied such phenomena and in Figure 1A it can be seen that large pores have significant stopping power for densification. However, as the pore radius decreases influence of the pore on final density also decreases – entrapped gas in a pore with radius under 0.5 μm has almost no effect. On the other hand, when pressure is applied to the material with isolated pores even several tens bars could drastically improve the ability to densify – as can be seen in Figure 1B [18].

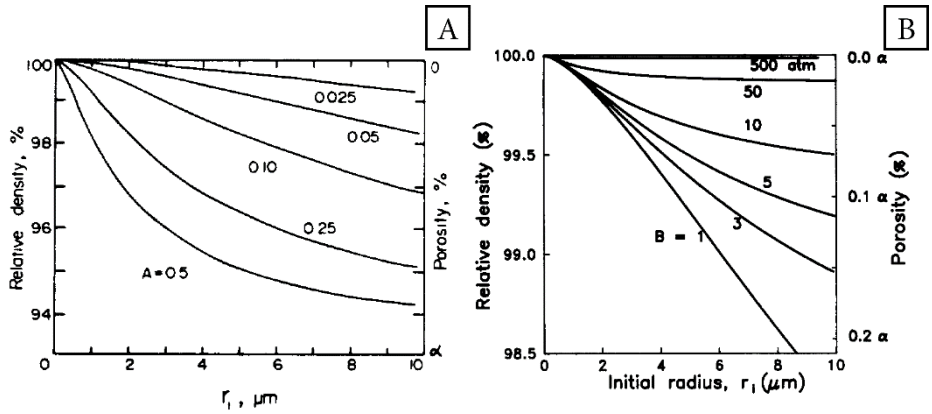


*Figure 1: Presence of pores during the final stage of sintering. A – Influence of pore size on densification during pressureless sintering, the larger the pore, the less maximum achievable density* [17].*Parameter* $A = P_i/2\gamma_s\ \mu m$. *B – Influence of pressure during the densification. The higher the pressure, the denser the final product is, even with large pores* [18]. *Parameter B is pressure in atm.*

Considering the previously mentioned theory, there are several reasons why to use pressure during sintering. Pressure assisted sintering primarily introduces additional force acting as a driving force for densification. An impact of this additional force is tremendous:

- Densification (sintering) can be performed at lower temperature to achieve similar or even better final density.
- Dwell times of sintering cycles could be shortened.
- The decrease in the sintering temperature could prevent activation of grain growth mechanisms and therefore produce finer microstructure.
- Densification of complex or materials difficult to densify is now possible because of additional energy.

## 2.4. Hot Isostatic Pressing Basics

A hot isostatic press (HIP) machine (Figure 2) can be described as a furnace with the ability to hold high gas pressure during the sintering. It has to be pointed out, that there are no dies present, which are otherwise needed to transmit pressure to the sample's body (like graphite tools in Hot Press or SPS).

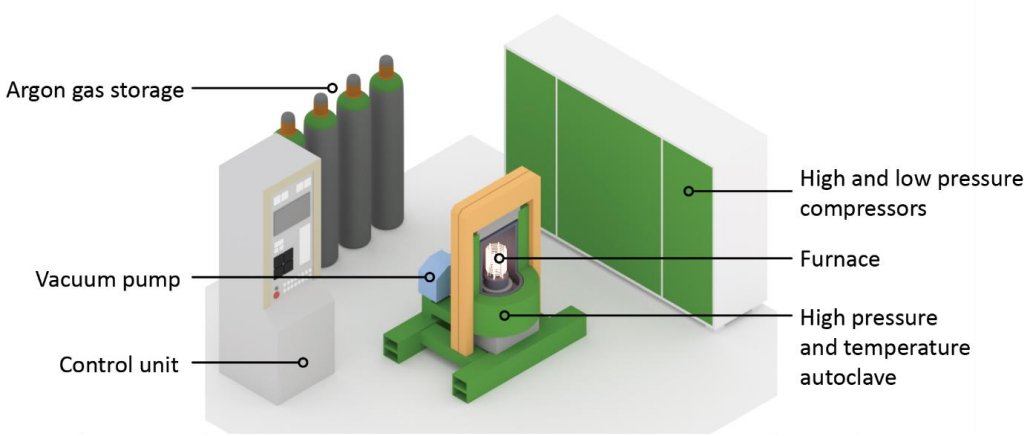


*Figure 2: Hot isostatic press. At the beginning of the HIPing cycle, the furnace is evacuated and purged with argon several times. At first, only by the pressure gradient between the furnace and the gas storage, followed by pressurizing by compressors to the desired value. After completing the HIPing cycle, the majority of used argon is pumped from the furnace back to the gas storage.*

Although the configuration of the hot isostatic press is similar for every machine, the procedures of the hot isostatic pressing are different and they can be divided accordingly to how they prevent the gas from entering to the pores of the powder body. This thesis will follow the terminology from the work of Larker & Larker [7], which grouped HIPing methods into two categories:

- Direct HIPing (also known as an encapsulated HIP, glass encapsulated HIP, glass HIP, capsule HIP or container HIP) – the core technique in this approach is to establish continuous gas impermeable barrier around the evacuated porous body before the HIPing starts. Only suitable glasses and metals have to be used for the encapsulation purpose.
- Post-HIPing (also known as cladless HIP, sinter-HIP or sinter plus HIP) – in this method a green body is sintered to a state with no surface connected porosity before pressurization.

### 2.4.1. Post-HIPing of Pre-sintered Green Bodies

Post-HIPing [19] of partially sintered ceramics (Figure 3) is an alternative to direct HIPing, which does not use the encapsulation procedure. A ceramic specimen is sintered to the state of closed porosity, which creates airtight surface and post-HIPing can be successfully applied. This technique is used in the experimental part of this thesis.

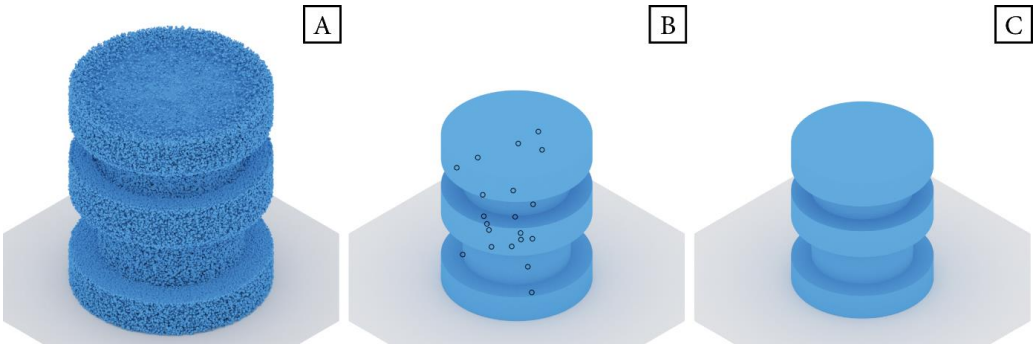


*Figure 3: Post-HIPing of the partially sintered body.*
*A - The green body is shaped by the chosen technology. B - The green body is subsequently sintered to closed porosity stage. After HIPing the closed pores are removed resulting with the fully dense specimen, without the necessity of removing any envelope - C.*

In this case gas (mostly inert argon) is allowed to act directly on the surface of the sample ending with fully dense material (after application of proper temperature /pressure/ time regime). The necessity of pre-sintering to high density (92+ % t.d.) limits the materials suitable for this method. Such materials have to be able to sinter to require densities without unacceptable deterioration of microstructure, phase composition, shape etc. For many ceramic materials with high strength at high temperatures, other limitations can occur. For example in the pre-sintering of silicon nitride elongated beta silicon nitride grains are formed and often create a very rigid and interlocking structure [7].

As it was mentioned in the Introduction, the limitation of utilisation of the full potential of this hot isostatic pressing method is the precise determination the conditions when the specimen reaches the close porosity stage. The importance of pre-sintering process optimization can be demonstrated on results of Maca et al. [20]. The work is dealing with the optimization of pre-sintering regime of alumina magnesia spinel ($MgAl_2O_4$) prior to the post-HIPing (1500 °C, 200 MPa, 1 h), in order to prepare transparent ceramics suitable for ballistic protection. Due to cubic lattice, conditions for spinel transparency are only impurities-free and pore-free structure with no limitation in grain size. As can be seen in Figure 4, there is a visible relationship between pre-sintering density and transparency after post-HIPing. The sample on the left was pre-sintered at ideal density (94.9 % t.d.) and the result is a fully dense specimen with high real in-line transparency (RIT 60 %). On the other hand, the sample on the right was pre-sintered to unnecessary high density (99.5 % t.d.), which caused decrease of the final transparency (RIT 7.3 %). This drop in the transparencies authors relates to trapped pores in the grains' interior due to extensive grain growth during excessive pre-sintering [20].

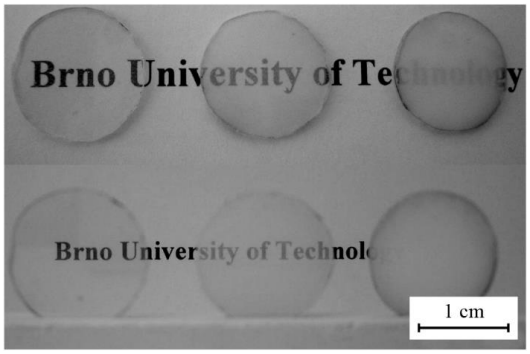


*Figure 4: The optical transparency of spinel ceramics (thickness 1.1mm) prepared with different pre-sintered densities (from left: 94.9, 97.9 and 99.5 % t.d.). In the upper image, the samples are lying immediately on the sheet of paper bearing the text; in the lower one, they are 5 cm above it* [20].

## 2.5. Hot Isostatic Pressing Maps – Theoretical Models

Hot isostatic pressing maps, firstly created by Swinkels, Ashby and Arzt [21–23], represent a theoretical approach with the ambition to determine the dominant densifying mechanism during hot isostatic pressing.

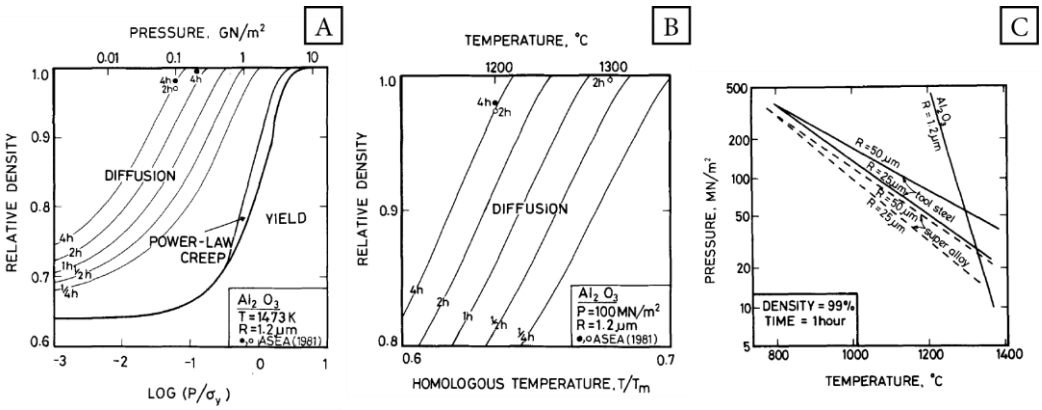


*Figure 5: Various HIPing maps of the influence of HIPing variables on densification of the alumina* [22]. *A – Influence of the used pressure on the HIPing time, B – Influence of the temperature on the HIPing time, C – Relation between pressure and temperature used in HIPing cycle for metals and alumina ceramic.*

Presented results (Figure 5) focused on the HIPing of alumina reveal a unique set of information valuable for optimization the HIPing cycle. Figure 5A demonstrates that the increase in the sintering pressure will lead to the reduction of sintering time required to achieve the full density. Increasing the sintering temperature (Figure 5B) will also reduce the sintering time needed to fully densified sample. Figure 5C illustrates trading mechanical energy for thermal energy required for densification.

Such theoretical models are highly appreciated because according to this relation (or trading) it should be possible to sinter the powder material into the fully dense specimen without entering the stage where exaggerated (uncontrolled) grain growth is present.

## 2.6. Hot Isostatic Pressing – Experimental Observations

As it was mentioned before, accommodating HIPing as a technique for ceramic processing in the academic and industrial applications is relatively limited. Sample preparation, coating/pre-sintering, equipment costs, experiment running costs, maintenance costs, etc. predetermine

HIPing usage only for applications with the high added value acquired after HIPing (transparent ceramics, joint/bone replacements, etc.). Therefore, after HIPing boom in the 1980s, where the number of articles had exponentially rising tendency, after mid-1990s number of articles dealing with issues concerning HIPing ceramics saturated (Figure 6). The reasons for such development could be that scientists discovered benefits and limitations of HIPing fairly quickly and implemented such observations into ceramic industry, although they were limited by technology of that time. On the other hand, there are still undiscovered/unexplained issues concerning HIPing requiring modern equipment or methods (unavailable in 1980s) and that is the reason of continuous research and article publication in the field of Hot Isostatic Pressing of ceramic materials.

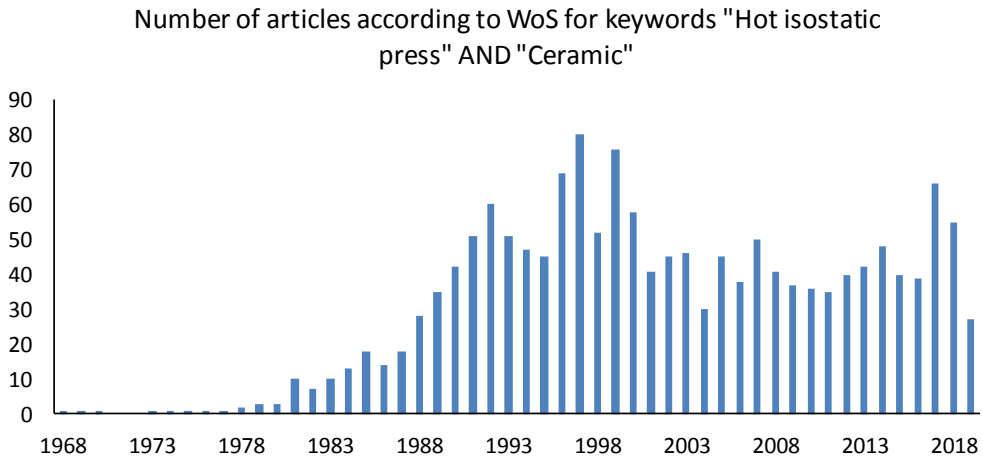


*Figure 6: Number of articles through the time concerning the HIPing process with ceramics according to Web of Science* [24].

As it was pointed out at the end of the previous chapter, HIPing variables have a significant impact on the results of the HIPing procedure in terms of achieving density and cutting off the sintering time. Härdtl (1975) [19] described the influence of HIPing parameters (temperature, pressure and time) on the densification of various pre-sintered ceramic materials – mainly $BaTiO_3$ and $SrTiO_3$. Unfortunately, the density of pre-sintered ceramic bodies is quite high (97.5 % for $BaTiO_3$ and 98.5 % for $SrTiO_3$) therefore only very little of HIPing potential could be accompanied.

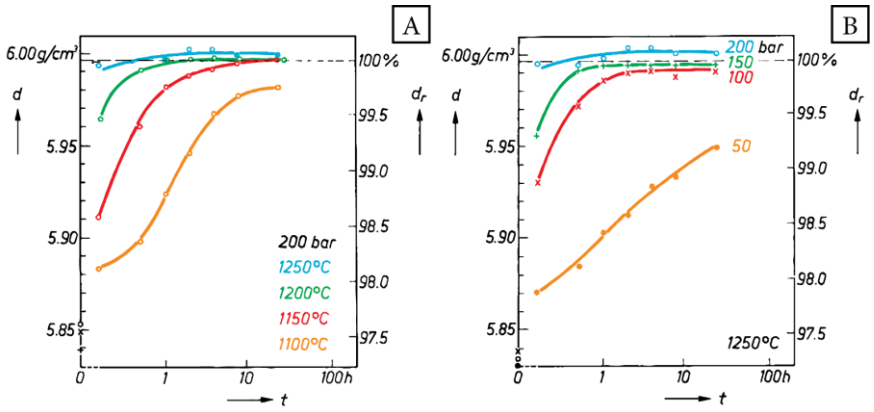


*Figure 7: The influence of the temperature, pressure and time on the densification of $BaTiO_3$ during the post-HIPing process* [19]. *A – Increasing the temperature at constant pressure. The higher the temperature, the less time is needed to full densification. B – Increasing the pressure at a constant temperature. The higher pressure at a given temperature, the less time is needed to reach full density.*

Figure 7 (post-HIPing of $BaTiO_3$, pre-sintered at 4 hours, at 1315 °C in oxygen atmosphere) shows that according to fundamental expectations, increasing temperature (Figure 7A), time and pressure (Figure 7B) increase density of post-HIPed specimens. The author also presented interesting simplified idea, that "in general, doubling the pressure has the approximately same effect as increasing the temperature by 50 °C". Another important observation is that according to author there is no change in grain size during HIPing in the studied temperature range.

Interesting observations concerning the porosity remaining in the ceramic volume after pre-sintering cycle in connection with sintering temperature and trapped isolated pores in grain volume published Kwon in1987 [25]. According to his observations, alumina specimens which were introduced to the HIPing process containing open pores increased in weight by 0.4-0.6 %. This is enormously disturbing, because it means that HIPing gas at high pressure (in this case Argon at 150 MPa) could be enclosed into pores even during HIPing. Entrapped gas after HIPing, which estimated pressure is 25 MPa after cooling to room temperature, will cause massive problems in the use of such components at high working temperatures.

Kim et al. (1990) [26] studied densification of several kinds of Y-TZP (yttria-stabilized tetragonal zirconia made by various producers) pre-sintered at 1200 – 1500 °C and post-HIPed at various conditions: HIPing temperature: 1100 – 1400 °C, pressure: 5 – 200 MPa and dwell time: 0.5 – 4 h.

In this work, it is easy to demonstrate the theoretical assumptions from HIPing maps (Chapter 2.5) about trading one HIPing parameter for another one. Specimen A (orange colour) has 0 % open porosity at 1300 °C (Figure 8A) at 94.5 % t.d. – therefore it is a suitable candidate for post-HIPing process. Almost full density after HIPing can be achieved by:

- Increasing HIPing temperature to 1300 °C/ 50 MPa/ 1 h (Figure 8B). This is not the perspective way, because increasing the HIPing temperature close to the pre-sintering one could have a negative effect on grain size in fully dense product.
- Increasing time to 1200 °C/50 MPa/4 h (Figure 8C). This could be the possible way for densification as it resembles the two-step sintering mechanism – lowering sintering temperature and increasing sintering time [13].
- Increasing pressure to 1200 °C/200 MPa/1 h (Figure 8D). This way accompanies most of the gas pressure capabilities of HIP and decreases the final time of the sintering process. Such optimization could lead to ideal post-HIPing treatment with maximum density and minimum grain growth after pre-sintering.

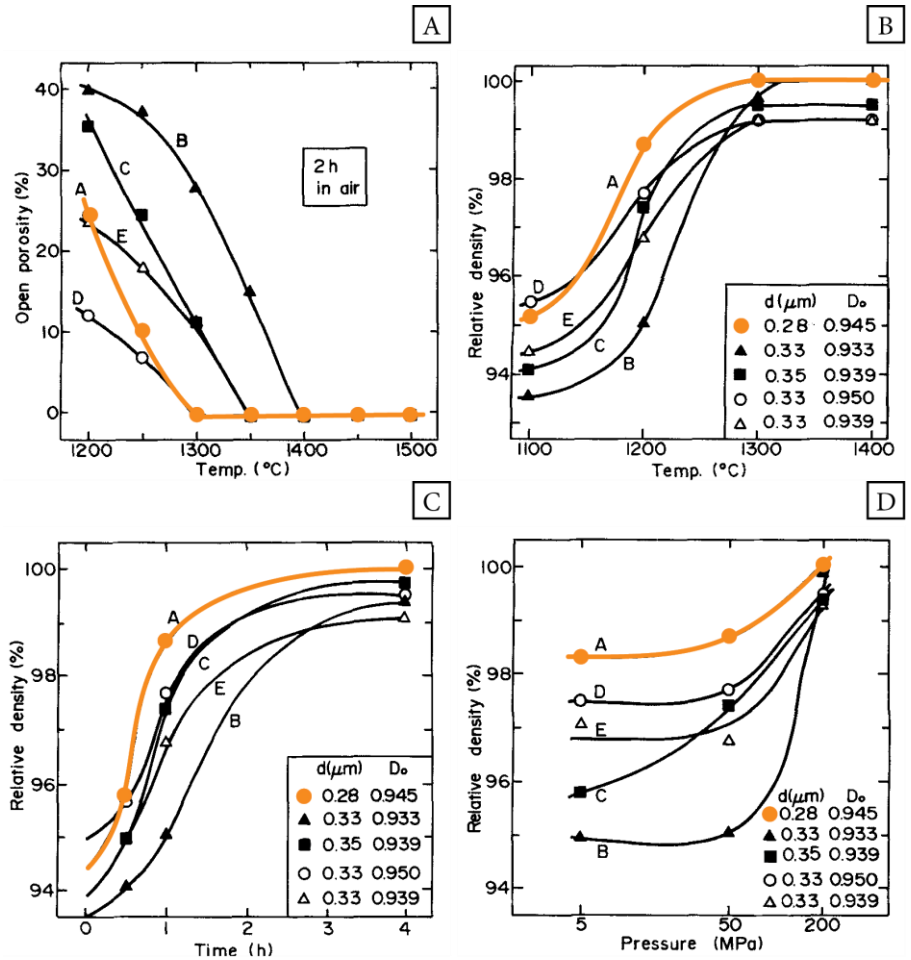


*Figure 8: The influence of HIPing variables on post-HIPing of tetragonal zirconia (colourized)* [26]*. Samples were pre-sintered at various temperatures to achieve closed porosity stage – A, characterized by d (grain size) and $D_o$ (relative density). It was demonstrated the influence of post-HIPing temperature at 50 MPa for 1 h - B, time at 1200 °C and 50 MPa - C and pressure at 1200 °C for 1 h - D on densification.*

Kim et al. [26] also observed grain growth during HIPing, which indicates the logarithmical dependence of porosity reduction versus grain growth (Figure 9A). Unfortunately, the results are quite strict concerning the amount of data. There is missing information about which of HIPing approach was used to achieve certain grain size because in the results they are mixed together, therefore there is no possible way, how to evaluate which of HIPing setting produce "the best" (the lowest grains, full density) results. Another work of Kim et al. [27] describes similar observation also for the capsulated HIP of zirconia powder compacts. Interesting observation is, that grain growth is present even in capsule HIP (Figure 9B), although it did not exhibit such strong, exponential, uncontrolled grain growth in the final stage of densification as during pressureless sintering.

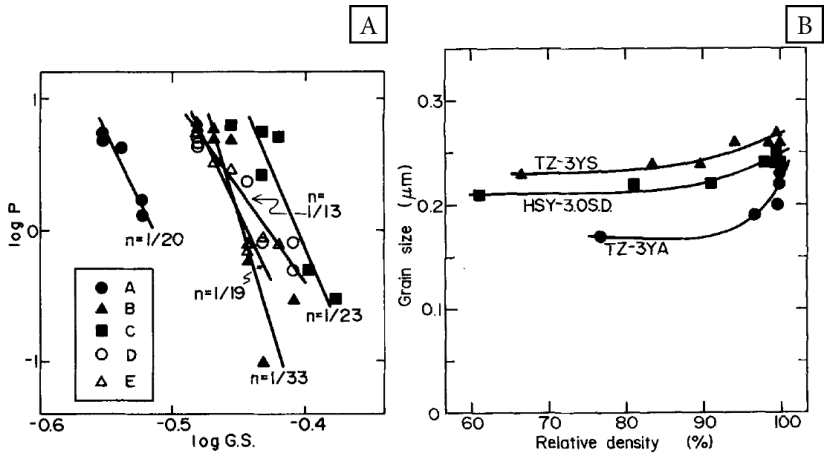


*Figure 9: A - Relation between the logarithm of porosity and logarithm of grain size* [26]. *B - Change of grain size with densification during HIPing* [27].

Works of Uematsu et al. (1989-1990) [28, 29] are focused on HIPing of alumina under various conditions: temperature: 1100 – 1400 °C, pressure: 5 – 200 MPa and dwell time: 0.5 – 4 h. This work provides similar results as were shown by previous authors and confirms their observations about trading the HIPing variables to achieve full density. Moreover, detailed grain evolution data are provided (Figure 10D). As it can be seen in Figure 10D exponential grain growth in the final densification stage is present.

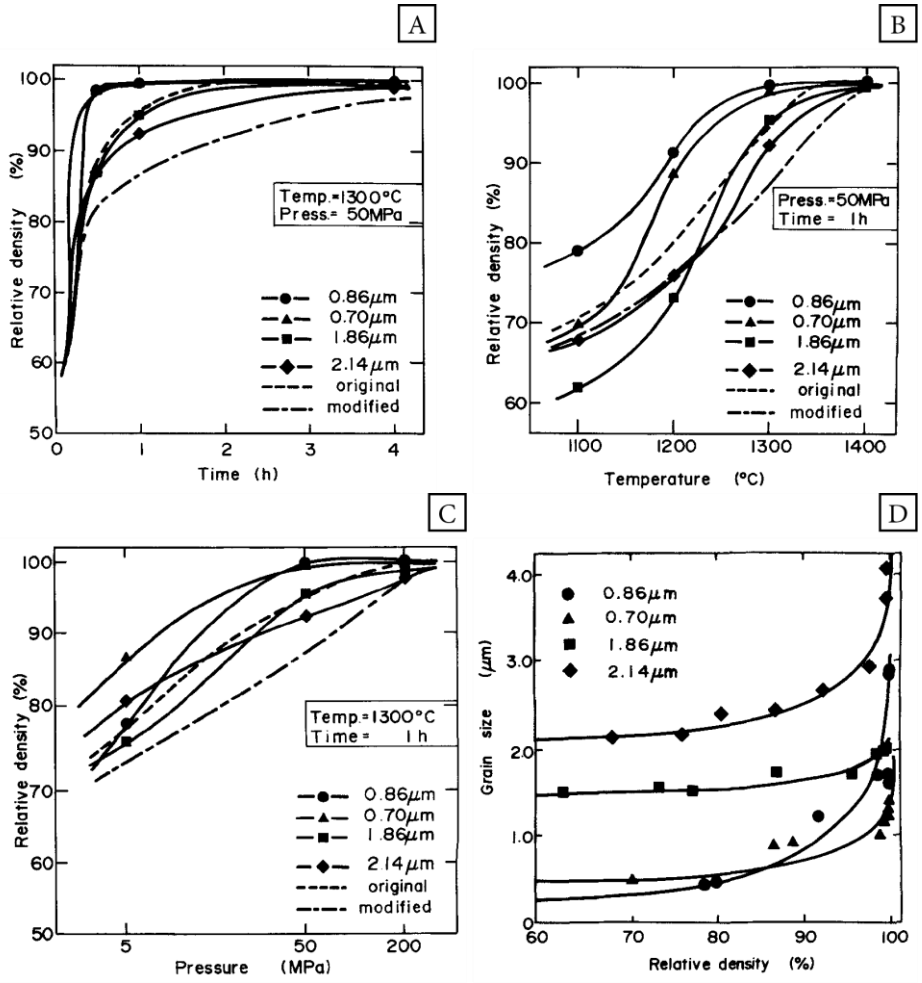


*Figure 10: Influence of HIPing variables on final density and gain size after direct HIPing of alumina* [28]. *Time - A, temperature - B and pressure - C HIPing maps for four alumina*

*powders with various initial particle sizes. D - Grain size after HIPing at various temperatures, 50 MPa and 1 h. Symbols represent initial particle size (according to* [28] *analysis).*

Besson and Abouaf (1989-1991) [30, 31] used direct HIPing (1300 °C, various dwell time, various pressures) of alumina to observe its densification and grain growth. According to authors increasing the HIPing pressure has an enhancing effect on the grain growth (and the densification) – Figure 11A and C. Several statements were made:

- The grain size after the direct HIPing increases as a linear function of the HIPing pressure (Figure 11A).
- The HIPing pressure of 200 MPa is less effective for the densification than lower pressures (Figure 11C).
- The pressure has no effect on already dense samples (Table 1). This observation is in good agreement with [32], where authors propose, that the pressure inhibiting the grain growth in polycrystalline cadmium has to be relatively high (i.e. 2000 – 3000 MPa).

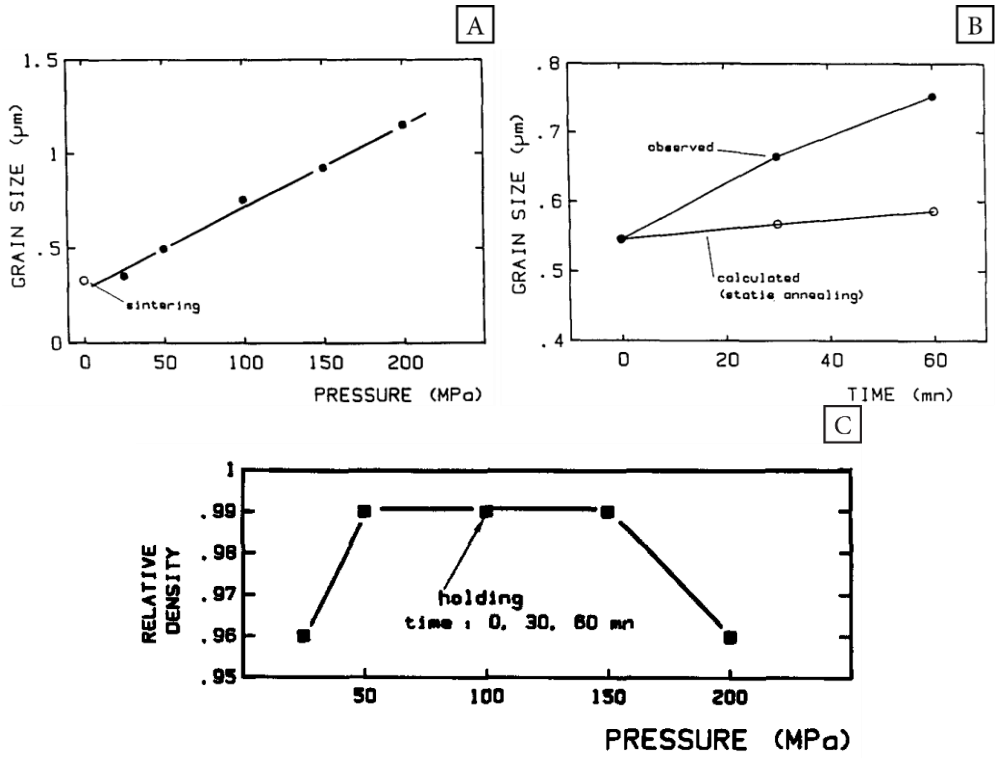


*Figure 11: A - The influence of the pressure on grain growth of directly HIPed alumina after 1 h dwell time at 1300 °C.B - The influence of the HIPing dwell time at 1300 °C and 100 MPa on the grain growth. C - The influence of the HIPing pressure on densification at 1300 °C and 1 h dwell time* [30].

*Table 1: Observed grain growth in dense and porous materials during HIP (holding time 60 min, temperature 1300 °C)* [30].

| Pressure [MPa] | Initial density [% t.d.] | Initial grain size [µm] | Observed final grain size [µm] |
|---|---|---|---|
| 25 | 51 | 0.25 | 0.35 |
| | 98 | 0.59 | 0.62 |
| 100 | 51 | 0.25 | 0.75 |
| | 98 | 0.59 | 0.62 |

Presented observations, mainly concerning the influence of the applied pressure on the grain evolution, were not published by other authors, and therefore provide new valuable information in the field of tailoring the material. The drop in the density at 200 MPa (Figure 11C) authors describes as a presence of abnormal grain growth (which is documented by SEM images), which was not present at lower pressures. Such observations put even more stress on the optimization procedures.

Park and Park (2001) [34] present the study of the grain growth during post-HIPing and pressureless sintering of alumina ceramics. The experiment starts with the preparation of samples – pre-sintering: 1600 °C, 1h and post-HIPing 1600 °C, 150 MPa, 0.5 h. One batch of such samples was further post-HIPed at 1600 °C, 150 MPa for 1-8 hours. The second batch was further sintered without pressure at 1600 °C for 1-8 hour as is illustrated in Figure 12. The application of pressure 150MPa caused inhibition of grain growth in comparison with pressureless sintering. Authors considered the high-temperature deformation as a critical factor for grain growth inhibition. During this process, alumina grains will interlock each other which is, according to authors, more plausible under pressure.

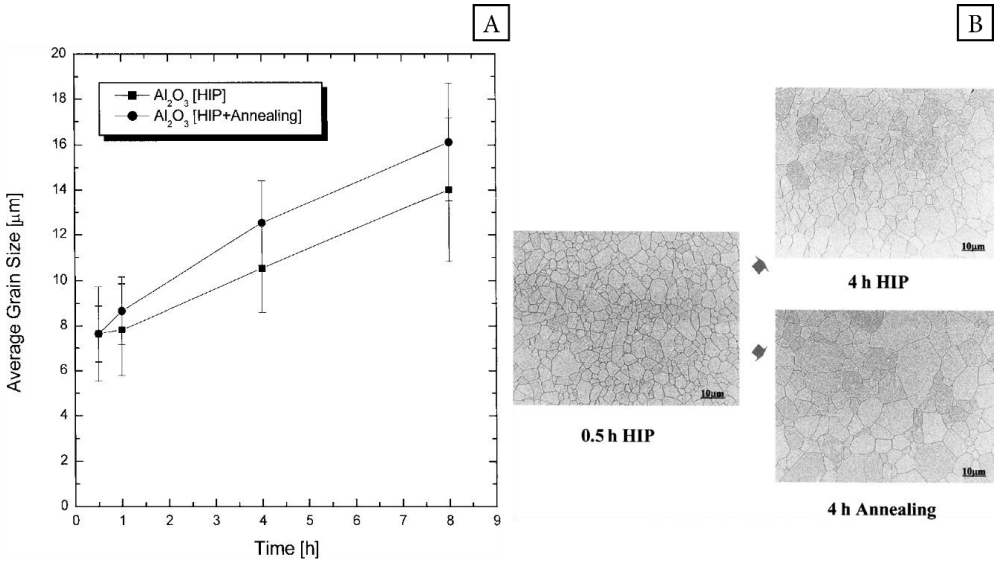


*Figure 12: A - Comparison of the grain growth after post-HIPing (150 MPa, 1600 °C) and pressureless annealing (1600 °C) during long periods of time in alumina. B – SEM micrographs of alumina after heat treatment at 1600 °C for 4 h.* [34]

Kishimoto et al. (2007) [35] observe the grain growth and densification of magnesia under various HIPing pressures. Authors used post-HIPing treatment (pre-sintering: 1600 °C, 2 h, post-HIPing: 1600 °C, 0.5 h, 50 - 195 MPa) on fine magnesia powder doped with coarse magnesia powder with various ratios (0, 0.5, 5, 20 wt. %).

*Table 2: Relative density of magnesia ceramics derived from different coarse powder ratios before and after post-HIP treatment* [35]

| Coarse powder ratio [%] | Relative density [% t. d.] | | | | |
|---|---|---|---|---|---|
| | Before post-HIP treatment | Post-HIP pressure | | | |
| | | 0.1 [MPa] | 50 [MPa] | 100 [MPa] | 195 [MPa] |
| 0 | 96.60 | 97.65 | 98.34 | 99.59 | 100.00 |
| 0.5 | 96.62 | 97.50 | 98.44 | 99.40 | 100.00 |
| 5 | 97.90 | 98.17 | 99.17 | 99.52 | 99.70 |
| 20 | 97.00 | 97.30 | 98.91 | 99.26 | 99.65 |

This doping results in the decrease in the grain size during HIPing at high pressures (Figure 13A). However, for pure fine powder an increasing of HIPing pressure results in grain growth as a linear function of the applied isostatic pressure (as already observed in [30]). Additionally, as it was mentioned above, the applied pressure helps the densification (Table 2).

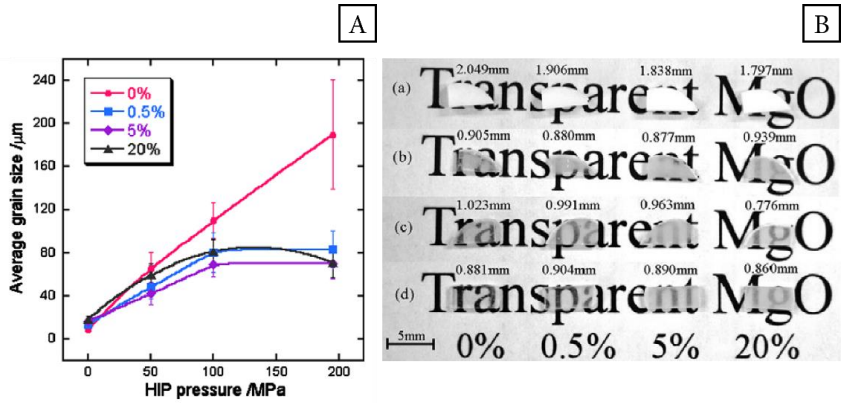


*Figure 13: A - The grain growth under various pressures (1600 °C, 0.5 h) during the post-HIPing of MgO. B – Photographs of magnesia ceramics derived from different coarse powder ratios (a) Before post-HIPing, (b) post-HIPing 50 MPa, (c) post-HIPing 100 MPa and (d) post-HIPing 195 MPa.* [35]

In addition to presented selected papers, there are some other articles dealing with other aspects of HIPing. There are several reviews on the HIPing process [10, 36–38], articles dealing with modelling of the parts or whole HIPing process [39–46], other articles are more focused on production of transparent ceramics [46–53] or they are focused on the influence of HIPing on mechanical properties of ceramics [54–59].

## 2.7. Influence of the Grain Size on the Properties of Ceramic Materials

The advanced ceramic materials are in the majority of the cases polycrystalline materials composed of numerous connected crystals – grains. The average size and the distribution of grains play significant role in the quality of many different properties of ceramic materials. From the variety of the properties (hardness, fracture toughness, creep, bending strength, chemical resistance, wear resistance, transparency, magnetic properties, dielectric properties, piezoelectric properties, thermal conductivity, electrical resistivity, etc.) following three (strength/hardness, transparency and $d_{33}$ constant) were chosen to represent the influence of grain size on these properties. These three cases demonstrate that there is not a simple relation between grain size and properties, although it is presented, that grain size optimization has significant impact on the performance and final product.

### 2.7.1. Strength and Hardness

The ceramic materials due to the covalent, ion and ion-covalent bonding are hard, with high compression strength, high Young's modulus, etc. However, they are brittle (low fracture toughness) due to lack of the slip systems for the dislocation movement.

In order to estimate the influence of the grain size on the mechanical properties, empirical Hall-Petch relation [64, 65] was proposed:

$$\sigma_y = \sigma_0 + \frac{k_y}{\sqrt{d}}, \tag{7}$$

where $\sigma_y$ is the yield stress, $\sigma_0$ is a material constant for the starting stress for dislocation movement, $k_y$ is the strengthening coefficient (specific for the material) and $d$ is the average grain diameter.

The relation propose the idea, that the mechanical properties can be increased as the grain size is decreased. When the stress is applied on the ceramic material, dislocations slip through the grain until they reach the grain boundary, which impede the dislocation movement. The dislocations then pile-up at grain boundaries and at certain critical moment, a dislocation traverses the grain boundary and travels from grain to grain, which will eventually lead to failure of the system (deformation, crack, fracture, etc.). However, as grains become smaller, a higher stress has to be applied to propagate dislocations from grain to grain and permanently deform the material, increasing the mechanical properties. There are numerous scientific observations [4, 66–68], which confirms traditional Hall-Petch relation for sub-micron ceramics (Figure 14A). However, there are several cases where the nano-sized grains exhibits an inverse phenomenon: in [67] authors present, that in the MgO ceramics with grain size lower than 20 nm with decreasing the grain size, hardness also decrease (Figure 14A). However this inverse/abnormal Hall-Petch behaviour is relatively new observation and it is heavily studied – mainly because the results are not uniform for every material.

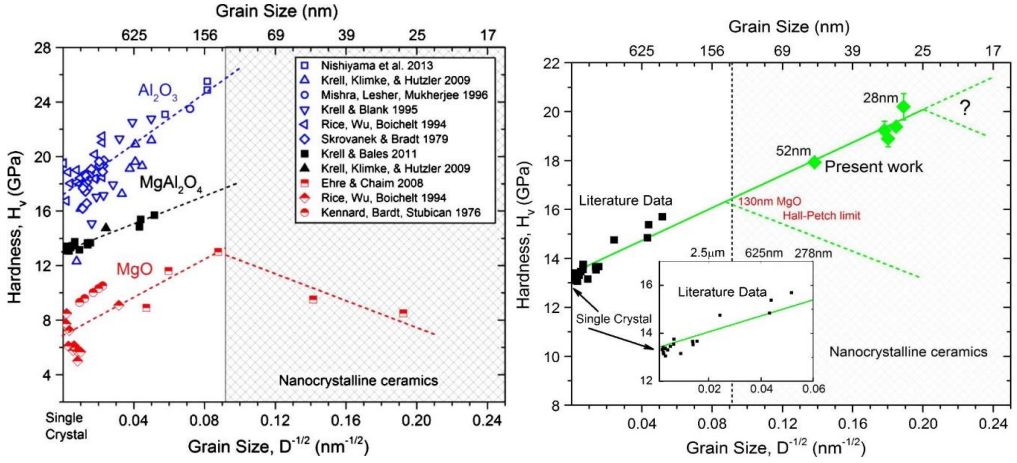


*Figure 14: Vickers hardness influenced by grain size for various ceramic materials. In the case of the MgO it can be seen that inverse Hall-Petch behaviour appeared* [67]. *However, for the $MgAl_2O_4$ such behaviour is not present.* [4]

## 2.7.2. Transparency in Visible Spectrum

Some of the ceramics, for example alumina, zirconia, magnesia alumina spinel, yttria or YAG are capable to exhibit transparency in the visible spectrum and be transparent for human eye. However due to polycrystalline nature of the ceramics in general, there are several-light scattering sources (Figure 15), from which the primary ones are pores. Due to different refractive indexes between ceramics and air (in pores), scattering of the light beam is extremely significant.

The next scattering centres are grain boundaries. One way how to increase the transparency is to produce ceramics with huge grains and thus reduce number of grain boundaries to eliminate scattering on them. However, as the grain size increases significant decrease in the mechanical properties of the ceramic materials is present. Quite the opposite idea is to produce ceramic materials with as fine grain as possible, ideally smaller than the wavelength of the interacting light. When the grains are smaller than the wavelength of the passing light, the light will not interact on the grain boundaries and thus it will not scatter (lose intensity). Moreover, the

symbiotic effect of small grains on the mechanical properties will provide materials suitable for the transparent ballistic armours [1, 70].

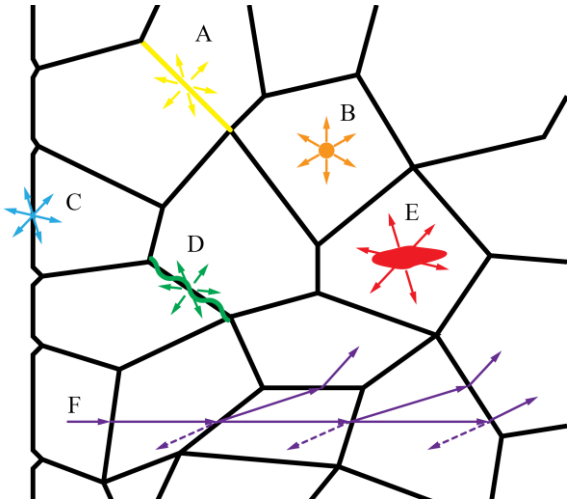


*Figure 15: Schematic illustration of various light-scattering sources.* [69]
*A – grain boundary, B – porosity, C – surface roughness, D – secondary phases, E – inclusions, F – Double refractions.*

The ideal candidates for the transparent polycrystalline ceramics are ceramics with cubic crystallographic structure, e.g. cubic zirconia, alumina-magnesia spinel or yttrium aluminum garnet. For such materials, due to isotropy of the refraction indexes of the crystallographic structure the requirement for the transparency is to remove the porosity in the volume and maintain the purity of the material. In [71] there is visible comparison between the volumes of porosity – it is clear, that the pores are enemy of the transparency number 1, when even 0.3 % of pores in volume creates opaque ceramics, while 0.03 % porosity provides transparency.

On another hand, there are ceramics with anisotropic crystallographic structures, e.g. alumina or tetragonal zirconia. The alfa alumina with hexagonal lattice has different refraction indexes between a and c lattice direction and therefore the light passes differently through the volume of the sample according to the orientation of the grains. Such effect is called birefringence. Therefore, the grains have to be smaller than the wavelength of the visible light so the light wave can pass through the grains without interaction [72].

### 2.7.3. Piezoelectric Coefficient $d_{33}$

In the latest years, after the European Union ban of ceramics containing lead, e.g. lead-based piezo electric materials for sensors, fuel injectors, actuators, transducers, etc., intensive research arises to replace them with perovskite type lead-free ceramic materials with piezoelectric properties. One of the most promising piezo-ceramics is barium calcium zirconium titanate - BCZT $(Ba_{0.85}Ca_{0.15})(Zr_{0.1}Ti_{0.9})O_3$. There are several observations for pure and doped BCZT ceramics, which present that grain size is one of the significant aspects which effect the functional properties [73]. The influence of the grain size on the piezoelectric coefficient $d_{33}$ in the BCZT ceramics are presented in Figure 16. The authors tested, among other things, the influence of the different composition and different initial particle size (in Figure 16 it is 5/5, which stands for 0.5BZT–0.5BCT composition and initial particle sizes 1, 3, 5 μm) on various piezoelectric properties. It is visible, that the $d_{33}$ changes with the grain size. However, the change is not linear, but more complex, exhibiting maximum peak proposing that there is an ideal grain size for $d_{33}$ and for other piezoelectric properties for BCZT ceramics (and for ceramics with similar structure).

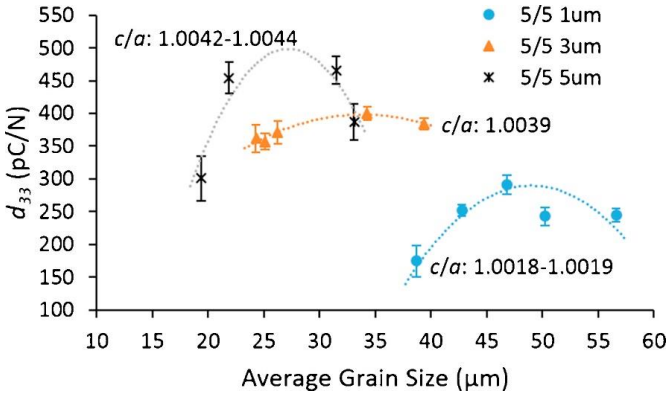


*Figure 16: Influence of the grain size on the piezoelectric coefficient $d_{33}$ in BCZT piezoelectric ceramics* [73]

On the other hand, for Potassium sodium niobate ($K_{0.5}Na_{0.5}NbO_3$), which is another promising piezoelectric ceramic material, the influence of the grain size is different. In [74] Malic et. al. observed that when the largest grain size decreased from 20 µm to 1.3 µm the $d_{33}$ changes from 80 pC/N to 100 pC/N, which suggest that the smaller grains could be beneficial for the piezoelectric properties in KNN. In addition the KNN ceramics contain volatile elements (Na, K), which evaporates during sintering at excessive high temperatures, therefore the HIPing pressure assisted densification provides ideal technique to produce dense KNN ceramics.

## 2.8. Personal Thoughts on the Experimental Review

The findings from the literature mentioned in the previous chapter are not easily interpretable, due to complex interplay of many independent variables – applied pressure, dwell time, HIPing temperature, sample microstructure and physical properties, etc. Another important aspect of HIPing temperature is connected with pre-sintering temperature, whether the HIPing temperature is lower, higher or the same as the pre-sintering one. Generally, the full density of the ceramic specimen could be achieved by various ways, which is the most visible in Kim's et al. paper [27], where optimization of HIPing parameters always led to the full density of tetragonal zirconia specimen "A" (Figure 8B-D).

On the other hand, the influence of HIPing variables on the grain growth is rarely analysed in the relevant literature and presented results are rather confusing. There are two instances of the grain evolution analysis and according to Besson et al. [30, 31] and Kishimoto et al. [35] increasing the pressure during HIPing at constant temperature will lead to coarser grains (Figure 11A and Figure 13A) for both capsule HIPing and capsule-free HIPing. Even it could be misleading to make a definitive conclusions from only two sources, the observations induce thoughts that the HIPing pressure should be kept on the lowest possible level to minimize the grain growth, which is rather confusing while using the pressure assisted sintering.

Additionally, there are few articles focused on the influence of the pressure on the grain growth in the spark plasma sintering [75–78], which are similarly confusing. However, Kim et. al. [77] presented the theory of such inconsistent behaviour of ceramic materials under pressure. In their study (Figure 17) both situation appeared – pressure has minimal effect on grain size at 1100 °C and linear effect at 1200 °C. They propose, that the pressure applied during spark plasma sintering increase the grain boundary sliding and deformation rate introducing dynamic grain growth. Therefore, the grain growth during spark plasma sintering will be affected by combination of the applied pressure and sintering temperature – the dynamic grain growth will only appear when the grain mobility is sufficiently high. However, in the SPS the pressure is propagated to the system from direction of the pistons, in one axis – uniaxially, while during

HIPing the pressure is propagated from all directions – isostatically, which could make a difference in the pressure influence on the grain growth.

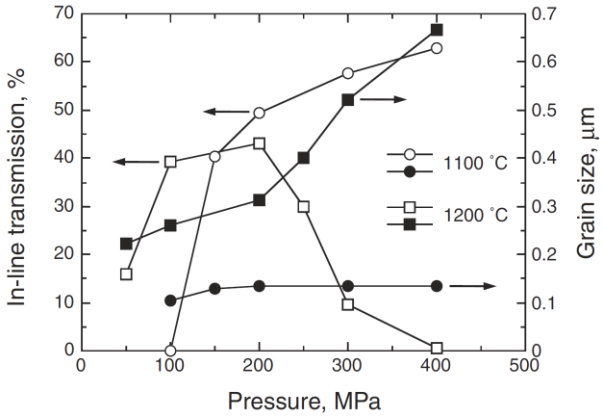


*Figure 17: Influence of the SPS pressure at various temperatures on the grain size of alumina ceramics* [77].

Therefore, according to my opinion, observations presented in HIPing articles have to be presented by a similar way as for SPS. When the temperature is above certain threshold, the grain boundary motion is then activated and applied pressure provides the forces for the easier grain sliding, which will lead to the movement of the grain boundaries. Grains will eventually find proper orientation and fuse together, leading to increased average grain size.

It is well known, that grain growth kinetics in pressureless sintering follows parabolic equation expressed as [6, 79–81]:

$$G^n - G_0^n = k_G \cdot t \tag{8}$$

where $G$ is actual grain size, $G_0$ is initial grain size, $k_G$ is kinetic constant, $n$ is an exponent of growth, $t$ is time. The kinetic exponent $k_G$ is dependent on temperature by Arrhenius-type equation as:

$$k_G = k_0 exp\left(\frac{-Q_G}{RT}\right) \tag{9}$$

where $k_0$ is constant, $Q_G$ is activation energy for boundary mobility, $R$ is gas constant and $T$ is absolute temperature. According to Equations (8) and (9) grain size can be directly affected by the increase in the temperature and/or time.

In the case of pressure-assisted sintering the similar equation considering influence of the applied pressure was not, according to author's best knowledge, reported yet, which leaves open space for further research.

However, even with limited theoretical background of the pressure influence on the grain growth, the experimental study can be performed. In order to produce specimens with maximum density and minimal grain size the optimization of the HIPing parameters has to be focused on the specific densification procedure minimizing the effects on the mobility of grain boundaries. Accompanying the Equations (8) and (9) for the pressureless sintering, the HIPing cycle has to be performed with the lowest possible temperature (minimize its exponential effect on grain growth), it has to be the shortest (minimize the effect of the time on grain growth) and with maximized pressure effect (maximizing the densification potential).

# 3. Objectives of the Ph.D. Thesis

Based on the literature review, there is a visible window for further and deeper research in the field of HIPing, mainly focusing on the influence of the post-HIPing parameters on the grain size (microstructure) development during post-HIPing. Therefore the objectives of this Ph.D. thesis are as follows:

(1) Optimization of the single step pre-sintering regime for selected oxide ceramic materials (alumina, tetragonal and cubic zirconia) including the study of the reproducibility of the pre-sintering to the value of open porosity below 0.1 vol%.

(2) Development of the optimal thermal etching procedure for evaluation of the microstructure of partially dense specimens, without affecting the density or the grain size.

(3) The systematic study of the densification and grain growth of selected ceramic materials (alumina, tetragonal and cubic zirconia) as a function of post-HIPing temperature, applied pressure and dwell time. Construction of sintering trajectories (the dependence of the average grain size on the final density) and their dependences on the HIPing variables.

(4) Optimization of the post-HIPing regimes for studied materials in order to achieve full density with minimal grain growth (relatively to pre-sintering average grain size).

During my Ph.D. study several goals of this thesis were already published in scientific journals. Therefore, results of those observations are summarized in this thesis in the form of extended abstracts and relevant articles are attached in the Appendix section. The optimisation of the pre-sintering regimes (objective No. 1) was published in [8] and it is summarized in Chapter 4. The novel etching technique (objective No. 2), which significantly simplifies the microstructure analysis of studied ceramic materials is published in [82] and summarized in Chapter 5.

The application of the pre-sintering optimization (objective No. 1) and preliminary post-HIPing results (objective No. 3) were incorporated during production transparent alumina ceramics with photo-luminescent properties, which was published in [83] and it is summarized in Chapter 6.

Yet unpublished work concerning the influence of HIPing parameters on the microstructure development (objectives No. 3 and No. 4) is the main focus of this thesis with adequate description of the experimental methods, results and discussion mentioned in Chapter 7, Chapter 8 and Chapter 9, respectively.

# 4. Pre-sintering Regime Optimization - Study of Pore Closure Phenomena

Optimization of the pre-sintering regime was done in several steps. The initial step, dealing with pore closure phenomena, was the topic of my diploma thesis and of the first year of my Ph.D. study year results subsequently published in [8]. The main aim of this work was to theoretically and experimentally define conditions of the transition from open to closed porosity stage.

Several theoretical models [12, 84–87] dealing with pore closure phenomena in ceramic materials show, that the pore closure is controlled by the dihedral angle, which is determined by surface energies of grain boundaries and free surface of the pore. Therefore, the transition from open to closed pores is a material characteristic and for given material it should occur at same critical density (Figure 18) independently on the sintering process.

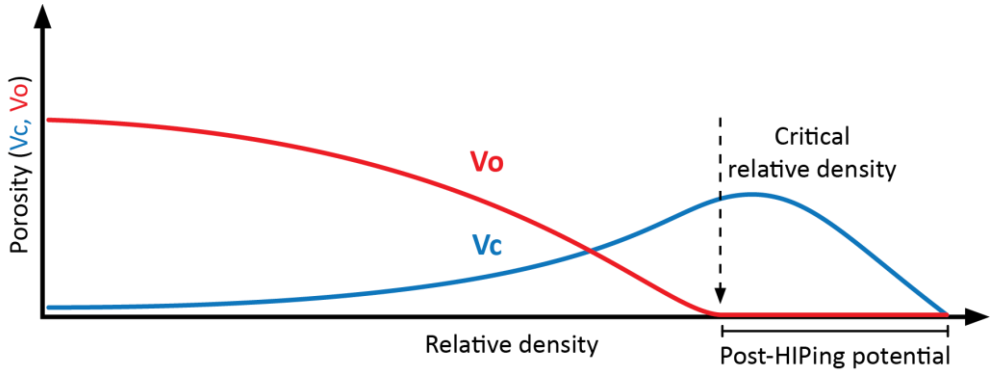


*Figure 18: Illustration of critical density and post-HIPing potential for densification. Vo and Vc represent the volume of open and closed pores, respectively.*

An experimental study to confirm or disprove the theoretical models by experimental determination of critical density was performed. Hence, several commercially available oxide ceramic materials (alumina, alumina-magnesia spinel, tetragonal and cubic zirconia) with various initial particle size and different green body microstructure were chosen as representative candidates for this research. Details about used powders, used shaping methods, microstructure after powder shaping, sintering cycles etc. are summarized in [8].

The powders were cold isostatically pressed at 100 and 300 MPa (ensuring different microstructure of green bodies – density of the samples and pore size distribution) and sintered in an air atmosphere to temperatures where pore closure is expected according to dilatometry measurements. After sintering, density and volume of open and closed pores were measured by Archimedes method. The sintering temperature was optimized in order to obtain ceramic bodies with 0.1 % of open pores (Figure 18). Such pre-sintered samples are ideal candidates for HIPing process because at this point closed pores are accommodated on grain boundaries and they are easily removable by HIPing.

Summarized results of pore closure determined by theoretical models and experimental approach are presented in Figure 19. It can be seen, that theoretical models of Beere [85] and Carter and Glaeser [86] predict pore closure with reasonable accuracy for materials with cubic lattice (cubic zirconia and magnesia alumina spinel), but have problems with the prediction of pore closure for alumina with a hexagonal lattice. Such differences can be caused by more symmetric cubic lattice, which is more similar to tetrakaidecahedron used in models, than hexagonal lattice in alumina, which could cause a shift of pore closure to higher densities.

Model of Svoboda et al. [87] is unfortunately unable to predict the complete pore closure (when all open pores are transformed to closed), instead of it predicts rather where the pore closure starts (when the first open pores are transformed).

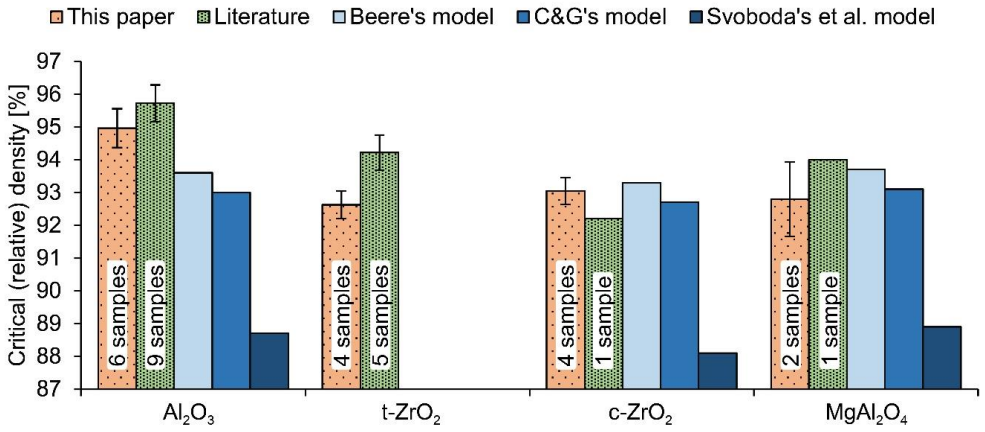


*Figure 19: Summarized results of pore closure determined by theoretical models and experimental approach* [8].

The obtained results were summarized into several conclusions to optimize pre-sintering regimes:

- Critical density of studied materials is material characteristic controlled by dihedral angle, independently on shaping pressure and initial particle size.
- Theoretical models of Beere and Carter & Glaeser successfully predict pore closure for materials with cubic lattice, which was confirmed experimentally. However, predictions of these models and experimental results do not match in case of hexagonal materials.
- Critical density of alumina is cca 95-96 % t.d.
- Critical density of alumina magnesia spinel is cca 92-93% t.d.
- Critical density of cubic and tetragonal zirconia is cca 92-93% t.d.

In addition, since in the previous research [8] the influence of heating rate on pre-sintering was not taken into account, we performed the study to evaluate its influence on the grain size after pre-sintering by increasing (100 °C/min) or decreasing (2 °C/min) heating rate relatively to standardly used 10 °C/min.

Figure 20 [88] shows that even when the temperature profile of the sintering cycle is very different, pore closure occurs at the same density.

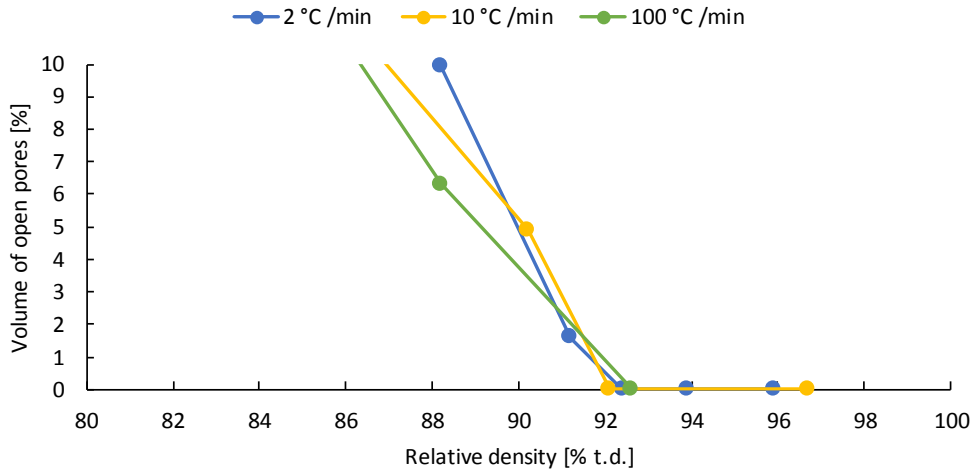


*Figure 20: Pore closure of TZ3Y during sintering by various heating rates* [88].

# 5. Low Temperature Technique for Thermal Etching

As it was previously mentioned, the microstructure of the polished ceramic materials can be revealed by various methods. During this work several attempts to reveal the microstructure differently than by thermal etching were performed. The alternative approach is needed because the standard thermal etching is performed at 100-200 °C below sintering temperature, therefore while preserving consistency in the whole set of experiments, for every pre-sintering and for every post-HIPing cycle it has to be determined the temperature of the thermal etching. The chemical etching and ion milling were probed as possible candidates for microstructure revelation and because they are not connected with elevated temperature, they could be used as convenient methods for every sample despite the sintering temperature. Unfortunately, none of tried methods provided sufficient revelation of the microstructure for all selected materials (chemical etching) or provided results in a reasonable time frame (ion milling).

Considering the failures during etching experiments, the thermal etching becomes the only usable choice. However, with the accompanying additional thermal energy to already sintered samples, there is a risk of alteration of the microstructure – increase in grain size or increase in the density after etching. Therefore, alternative approach to thermal etching was studied and used in this work. The idea of "low-temperature etching" is based on assumption, that there has to be temperature (or combination of time and temperature) at which the microstructure of polished surface starts to change to the etched surface via surface diffusion, which is a non-densifying mechanism (therefore, the density should not change during etching).

In the work, ceramic oxide materials were sintered to pre-sintering state (92-96 % t.d. correspondingly to [8]) and to fully dense state (99+ % t.d.). In the next step samples were polished to 1 µm surface roughness and etched by two approaches:

- The first approach represents a variation of standard thermal etching, where samples were etched at various temperatures below (50, 150, 250, 350 °C) sintering (Ts) temperature.
- The second approach deals with the question "What etching temperature is sufficient to reveal the grain microstructure?" Samples were therefore etched at low temperatures (900, 1000, 1100 °C) for 1 hour.

Our published results [82] show that it is possible to reveal microstructure by thermal etching at low temperature and a long time for all studied materials (alumina, cubic and tetragonal zirconia) independently on the sample density and also independently on sintering temperature

without altering the microstructure or increase density. As can be seen in Figure 21, at 900 °C/1 h the average grain size is the lowest, grain boundaries are safely visible and the specimen is without density increase after etching.

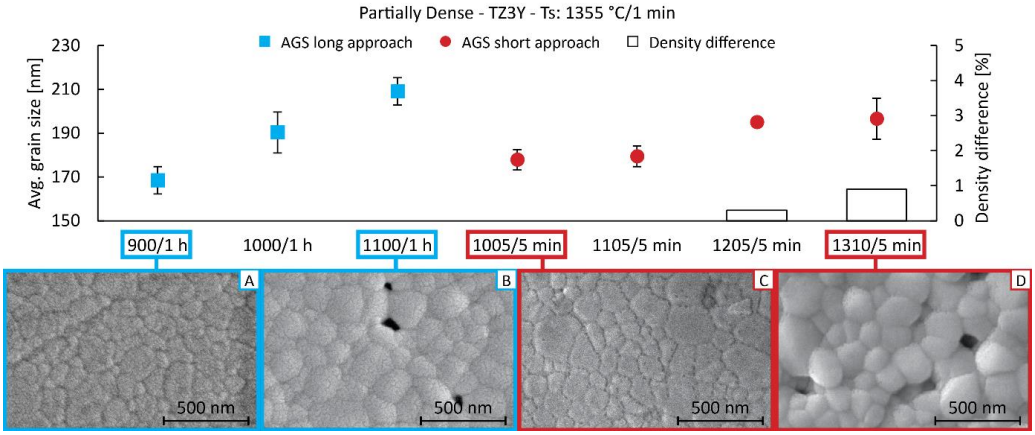


*Figure 21: Dependence of relative density change (after and before etching) and grain size of the partially dense tetragonal zirconia (TZ3Y) on etching temperature* [82] .

Similarly, as for pre-sintered samples, etching at 900 °C/1 h of fully dense samples (Figure 22) presents the lowest average grain size and clear visibility of grain boundaries.

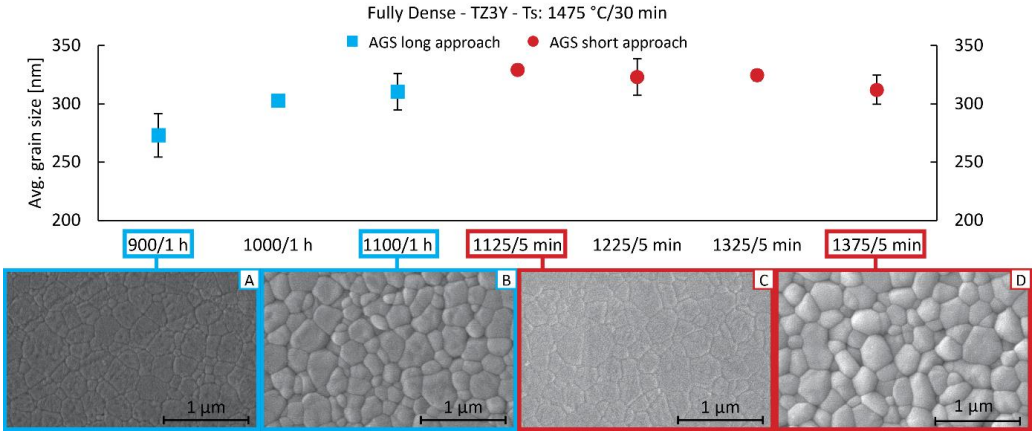


*Figure 22: Dependence of grain size of fully dense tetragonal zirconia (TZ3Y) on etching temperature* [82].

It can be noted, that TZ3Y has relatively fine grain microstructure and it could appear, that this technique only works with fine grain samples. However, Figure 23 shows an example of the coarse grain structure of fully sintered TZ8YSB and it can be seen that average grain size is again at minimum, grain boundaries are clearly visible, although the image has to be zoomed in digitally, due thin grain boundaries. Therefore, despite the alternative "long dwell" approach was not tested on other materials or compositions, it could be the way how to find universal thermal etching settings.

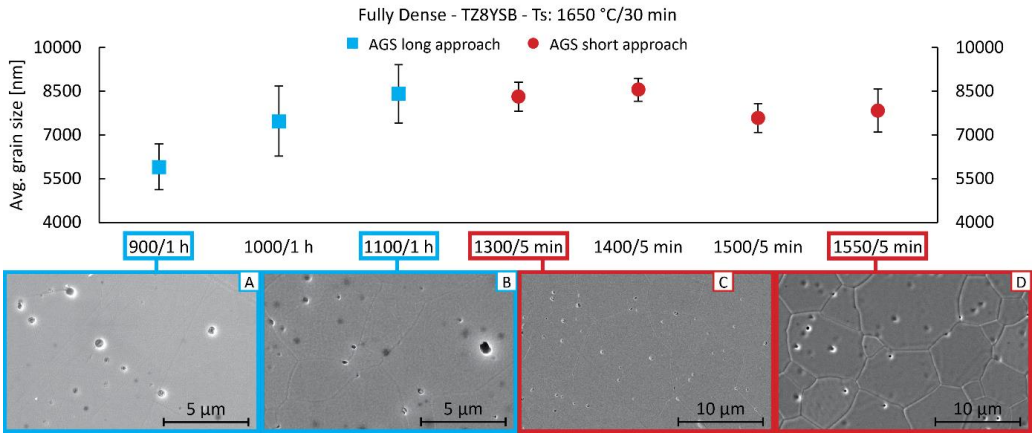


*Figure 23: Dependence of grain size of fully dense cubic zirconia (TZ8YSB) on etching temperature* [82].

# 6. Doped Transparent Alumina Ceramics with Photo-luminescent Properties

With proper microstructure, alumina ceramics provide transparency for visible light and with proper doping the already transparent samples could exhibit photo-luminescent properties (emitting the light of one wavelength after excited by another light with smaller wavelength).

The example of such synergic effects is preparation of erbium doped transparent alumina ceramics with photo-luminescent properties [83]. In this case, the crucial elements of the specimen preparation were optimization of the pre-sintering and post-HIPing regimes. Essentials for the pre-sintering optimisation were the published article [8] dealing with pore closure phenomena and its most important conclusion was that the pore closure is independent on the sintering history.

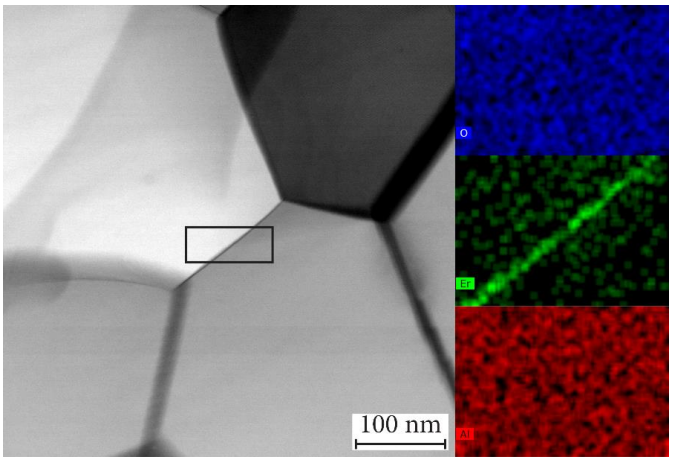


*Figure 24: EDX image of distribution of the Er dopant along alumina grain boundaries* [83].

Basic single-step pre-sintering regime provides the proper conditions for post-HIPing, which resulted in full dense specimen with fine grain size. However, the dopants were accommodated in relatively large clusters [83] , which created additional scattering centres and therefore decrease the final transparency. Alternative two-step pre-sintering provides similar microstructure (grain size at critical density), however significantly increase final transparency (Table 3) with higher amount of dopant. The explanation is that two-step pre-sintering provides sufficient temperature and time to redistribute the dopant ions alongside the grain boundaries (Figure 24) and reduce the size of the dopant clusters.

*Table 3: Mean grain size and real inline transmittance of Er-doped alumina after HIP (1280 °C/ 200 MPa/ 3 h)*

| Er doping | SSP + HIP | | | TSP + HIP | | |
|---|---|---|---|---|---|---|
| [at. %] | MGS [nm] | SD/n [nm/-] | RIT [%] | MGS [nm] | SD/n [nm/-] | RIT [%] |
| 0.1 | 450 | 60/20 | 49 | 390 | 50/20 | 52 |
| 0.17 | 370 | 50/20 | 28 | 350 | 40/20 | 34 |

MSG → Mean grain size, SD/n → Standard deviation of MSG from n measurements, RIT → Real in-line transmittance

The preliminary post-HIPing results of the thesis were also accompanied in this research and helped to optimize the finishing process. After refining the processing parameters of powder consolidation, the final specimen (Figure 25) doped with 0.1 % Er ions, pre-sintered with two-step regime (1430 °C → 1280 °C for 10 hours) and post-HIPed at 1280 °C/ 200 MPa/ 3 h, achieved real inline transmittance up to 56 % which is the highest RIT of rare-earth-doped alumina published so far. Furthermore, the refinement in the grain size also provides increase in the measured Vicker's hardness HV 10 which reached 26.9 GPa, which is highest observed hardness among doped, luminescent, transparent alumina ceramics [89].

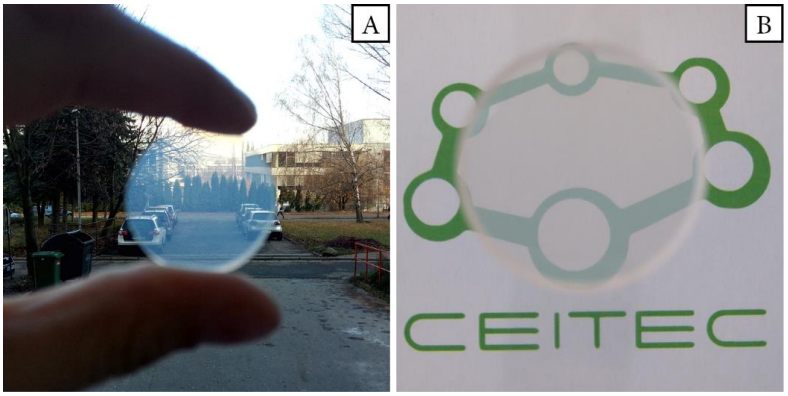


*Figure 25: Transparent alumina doped by Er with real inline transmittance of 56 %. A shows view to the distance and B shows sample 1 cm above the backing.*

# 7. Microstructure Development During Post-HIPing - Experimental Part

## 7.1. Preparation of Green Bodies

Commercially available ceramic powders (Table 4) were uniaxially pressed into cylinders (diameter 32 mm, height 10 mm) at approx. 20 MPa and subsequently cold isostatically pressed (Autoclave Engineering, Inc., USA) at 300 MPa. Formed discs were fired (800°C, 1 hour dwell and heating rate of 2 °C/min) to burn out organic additives and residues from uniaxial pressing and to increase mechanical (handling) strength of samples. The relative density of one random green body sample from every powder type was measured by Archimedes method [90] at scales equipped with density kit (Mettler Toledo XSE105) and another one was measured by mercury porosimetry (Pascal 440, Thermo Fisher Scientific) for pore size distribution analysis. Another random green body sample was infiltrated with resin and analysed by SEM (Verios 460L, FEI)

*Table 4: Summary of used ceramic powder types*

| Material | Powder type | Producer | Particle size [nm] | Theoretical density [g/cm$^3$] | Lattice |
|---|---|---|---|---|---|
| $Al_2O_3$ | TM-DAR | Taimei Chemicals | 150 | 3.99 [91] | Hexagonal |
| t-$ZrO_2$ | TZ3Y | Tosoh | 80 | 6.08 [92] | Tetragonal |
| c-$ZrO_2$ | TZ8Y | Tosoh | 80 | 5.99 [93] | Cubic |
| c-$ZrO_2$ | TZ8YSB | Tosoh | 140 | 5.99 [93] | Cubic |

Particle size is provided by the manufacturer and confirmed with SEM grain size analysis

## 7.2. Preparation of Pre-sintered Bodies

Numerous (approx. 20 for each powder type) pre-sintered bodies were prepared by pressureless sintering in super-kanthal furnace (Heraeus KT 1700/1, Germany). The pre-sintering temperatures were set in order to reach critical density (Vo < 0.1 %), which according to our already published studies [8] corresponds to densities in the range of 92-96 % t.d. depending on the material. After pre-sintering, relative density and volume of open and closed pores were measured for every sample. Linear-intersection method [62] was used for grain size analysis with a correction factor of 1.56 [94] using SEM. Analysed samples were thermally etched at 900 °C with 1 hour dwell time to minimize grain growth and further densification, which is the etching procedure developed during the Ph.D. study [82] (see Chapter 5).

## 7.3. Preparation of Post-HIPed Samples

Pre-sintered samples were post-HIPed (ABRA Shirp, Switzerland) in Argon atmosphere by regime illustrated in Figure 26. In order to observe the influence of all HIPing parameters on the density and the grain size, matrix of HIPing parameters was created (Table 5).

*Table 5: List of the post-HIPing experiments*

| Temperature [°C] | Pressure [MPa] | Time [h] |
|---|---|---|
| 1200 | 50 | 1, 4 |
| | 200 | 0.5, 1, 3, 4, 6, 9 |
| 1250 | 50 | 1, 4 |
| | 200 | 1, 4 |
| 1300 | 50 | 1, 4 |
| | 200 | 1, 4 |

The basic set of experiments consists of three various temperatures (1200, 1250, 1300 °C), two pressures (50 and 200 MPa) and two dwell times (1 and 4 hours). In addition, short regime (1200 °C, 0.5 hours and 200 MPa) and high-temperature regime (1400 °C, 4 hours and 200 MPa) were performed. To obtain additional experimental data to further examine the time influence in the HIPing process three pre-sintered samples for each powder type were HIPed at 1200 °C, 200 MPa for 3, 6 and 9 hours. The density and average grain size were determined in the same way as for the pre-sintering samples.

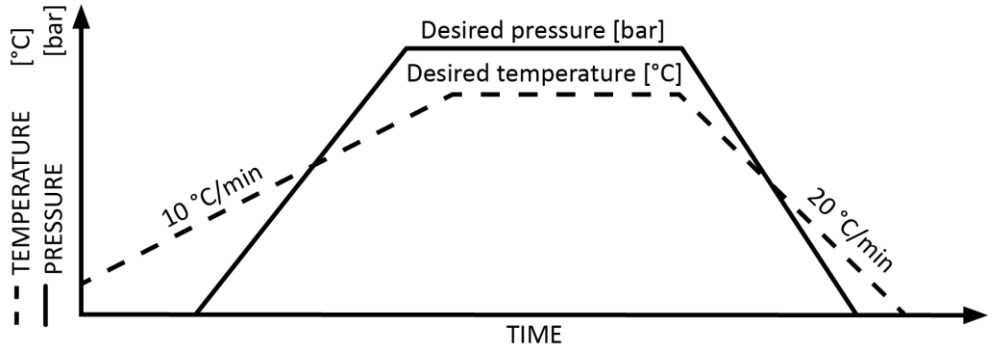


*Figure 26: Illustration of post-HIPing regime.*

## 7.4. Density Measurements

Density, the ratio of open and closed porosity of pre-sintered and HIPed samples were measured by immersion Archimedes method [90] using analytic balances Mettler Toledo XSE105 equipped with density kit with precision 0.1 mg by the following procedure:

1. Samples were placed under the infra-red lamp and heated up to 110 °C for 1 hour to remove adsorbed of water. After drying mass $m_1$ was measured. This value represents the dry mass of the sample (Figure 27A).
2. Samples were inserted into the vacuum chamber and kept under vacuum (50 mbar) for 30 minutes ensuring the air is removed from pores connected to the outer atmosphere (Figure 27B).
3. Samples were, under vacuum, immersed by distilled water (ChromAR HPLC, Macron), which density is known with a precision of 0.0001 g/cm$^3$ and with addition of wetting agent (Pervitro 75%) and kept under vacuum for another 30 minutes ensuring that samples were properly saturated by water (Figure 27C).
4. The air was admitted to the vacuum chamber to reach atmospheric pressure. Samples were then kept immersed in the water for another 30 minutes to eliminate temperature and pressure differences.
5. Each sample was then inserted into water (same as saturation water) on the density kit and the mass $m_2$ was measured. The mass $m_2$ represents the mass of the sample weighted in water.
6. The surface of the sample was carefully dried by wet laboratory paper to remove water from the surface, but to keep the water inside the open pores (Figure 27D). The mass $m_3$ was measured in air. The mass $m_3$ represents the mass of the sample with water inside the open porosity system. If open porosity is not present within the sample, $m_3$ is equal to $m_1$. Otherwise, there will be a difference between $m_1$ and $m_3$. Sample during $m_3$ measurement will be heavier. Sample, after drying the surface, should be measured as fast as possible because the water in the open pores starts to evaporate, which would lead to inaccurate measurement.

With all required inputs: theoretical density of the material $\rho_{teor}$, $m_1$, $m_2$, $m_3$ and temperature of the water during the experiment it is possible to evaluate the apparent relative density $\rho_{rel}$:

$$\rho_{rel} = \frac{m_1}{(m_3 - m_2)} \cdot \frac{\rho_{H2O}}{\rho_{teor}} \ [\%], \tag{10}$$

where $\rho_{H2O}$ is the density of used water based on its temperature $T_{H2O}$ in °C :

$$\rho_{H2O} = \frac{(0.997 - 0.9984)}{5 \cdot (T_{H2O} - 20)} + 0.9984 \ [kg \cdot m^{-3}]. \tag{11}$$

Additionally, the percentual volume of open ($V_O$) and closed ($V_C$) pores can be expressed with Equation (12) and Equation (13).

$$V_O = \frac{m_3 - m_1}{m_3 - m_2} \cdot 100 \ [\%], \tag{12}$$

$$V_C = \left(\frac{m_1 - m_2}{m_3 - m_2} \cdot 100\right) - \ \rho_{rel} \ [\%]. \tag{13}$$

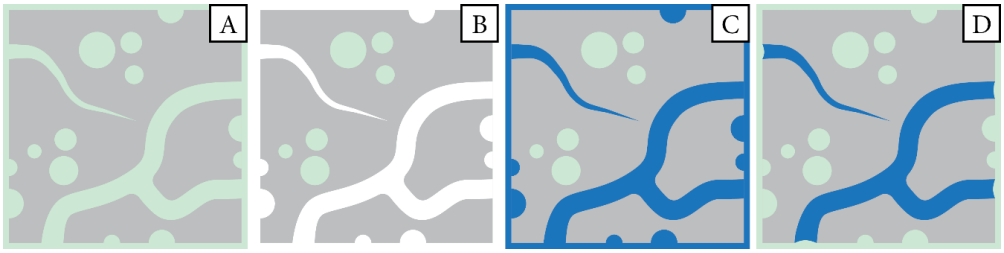


*Figure 27: Illustration of the basics of the Archimedes method. A – Every pore is filled with air (sintering in the air). B – Pores connected to the surface are evacuated by the vacuum pump. C – Pores are intruded by water. D – Water on the surface is removed, which leaves the water only inside the open pores.*

## 7.5. Microstructure Analysis

The microstructure analysis of grain size development for pre-sintered and HIPed samples was performed according to EN standard [62] from digital SEM images. Images were uploaded to Inkscape [95] software, which is free software for illustrations with the ability to measure the dimensions in virtual space. The average grain size of the samples was calculated according to the following procedure:

1. Five representative SEM view fields (images) with proper magnification corresponding to the number of grain boundaries which will be intersected – in this thesis minimum number of total intersections per sample was set to 400.
2. In Inkscape software, 6 randomly oriented lines were drawn and the total length of lines was measured ($L_t$).
3. Number of intersections ($N_i$) between the lines and grain boundaries according to rules displayed in Figure 28 were counted on every image.
4. The total length of lines divided by the number of intersections ($N_i$) from all images represents average grain size in digital space (in software) - $AGS_d$.
5. To convert $AGS_d$ to real average grain size $AGS_r$, the magnification coefficient has to be applied. From real view field ($V_r$) provided on SEM image and measured distance of the width of image – digital view field ($V_d$) in the software magnification coefficient is $V_r/V_d$.

6. Therefore real average grain size $AGS_r$ is:

$$AGS_r[\mu m] = \frac{L_t[mm]}{N_i\,[-]} \cdot \frac{V_r\,[\mu m]}{V_d\,[mm]}. \tag{14}$$

7. In order to respect the probability of cutting the grains differently than in the centre, it is required to multiply $AGS_r$ by 1.56 correction factor suggested in [94].

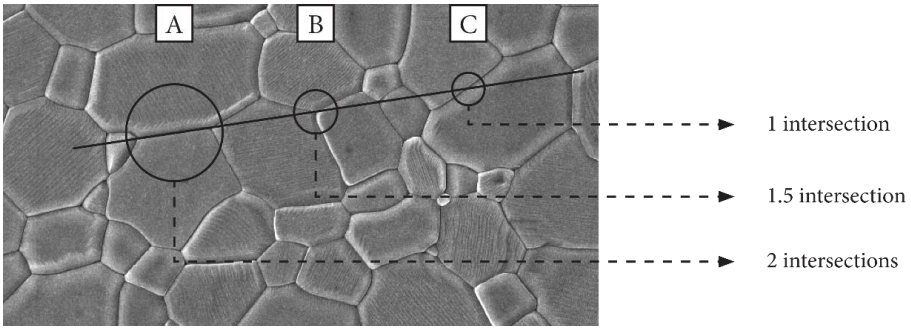


*Figure 28: Illustration of the intersection counting rules. A – Represents the case when intersection line goes along the grain boundary – it is counted as 2 intersections. B – Represents the case when the line intersects triple junction point – it is counted as 1.5 intersections. C – Represents standard case, when the line intersects just one grain boundary – it is counted as 1 intersection.*

# 8. Microstructure Development During Post-HIPing - Results

The Results chapter is divided into several sub-chapters in accordance with the experimental work schedule, starting with analysis of green bodies, following with analysis of pre-sintered samples and analysis of HIPed samples.

## 8.1. Green Bodies

The density of the green bodies measured by Archimedes method, the largest and the most present pore are summarized in Table 6.

*Table 6: Summarized data of green body analysis*

| Powder type | GB density [%] | s GB density | Radius of the most present pore [nm] | Radius of the largest pore [nm] |
|---|---|---|---|---|
| TM-DAR | 57.8 | 0.2 | 29 | 34 |
| TZ3Y | 49.9 | 0.3 | 25 | 28 |
| TZ8Y | 50.0 | 0.3 | 27 | 30 |
| TZ8YSB | 52.9 | 0.2 | 52 | 72 |

GB density, s GB density → average density and std. dev. calculated from 3 measurements

The whole measured range of porosity analysis (limited by used machine from 2.35 nm to cca 7000 nm) is presented in Figure 29 and detailed pore radius (zoomed) range (2.35 nm to 100 nm) is presented in Figure 30.

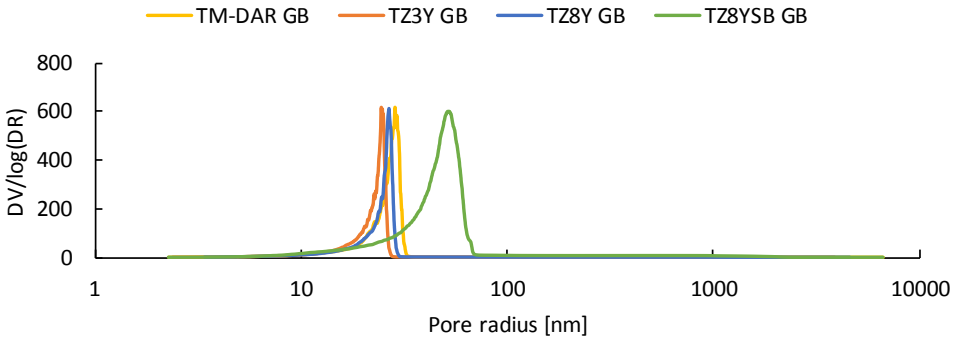


*Figure 29: Pore size distribution in the green bodies.*

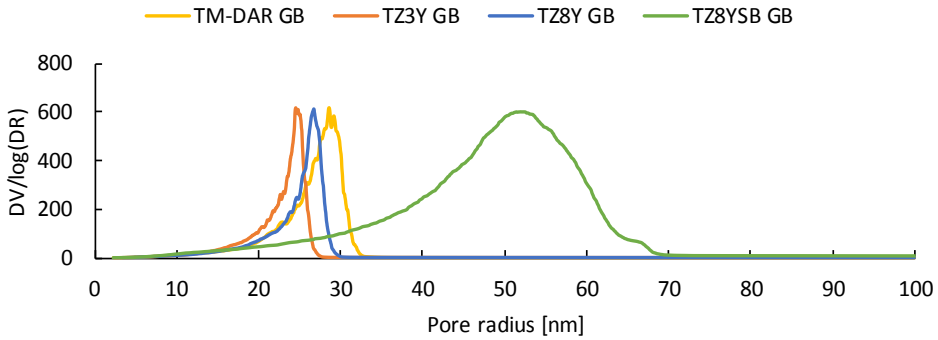


*Figure 30: Pore size distribution in the green bodies - detail.*

## 8.2. Pre-sintered Samples

Summary of characteristics of the pre-sintered (PS) samples (pre-sintering temperature and time, pre-sintered density and pre-sintered grain size) are presented in Table 7. Pre-sintered density was obtained from measuring cca 15-20 samples (each one 3 times) with open porosity below 0.2 % (Figure 31) and from these samples, 4 were chosen as representatives for microstructure observation and grain size evaluation.

*Table 7: Summary of pre-sintered samples which are input to the research*

| Powder type | PS temperature [°C] | PS density [%] | s PS density [-] | PS AGS [nm] | s PS AGS [-] |
|---|---|---|---|---|---|
| T | 1360/1min | 96.2 | 0.3 | 498 | 23 |
| 3Y | 1345/1min | 92.3 | 0.2 | 204 | 9 |
| 8Y | 1380/1min | 93.5 | 0.4 | 472 | 33 |
| 8YS | 1445/1min | 92.5 | 0.3 | 757 | 44 |

PS density, s PS density → average density and its std. dev. after pre-sintering calculated from 15-20 x 3 measurements

AGS, s AGS → average grain size and its std. dev. of pre-sintered samples calculated from 30 x 4 measurements

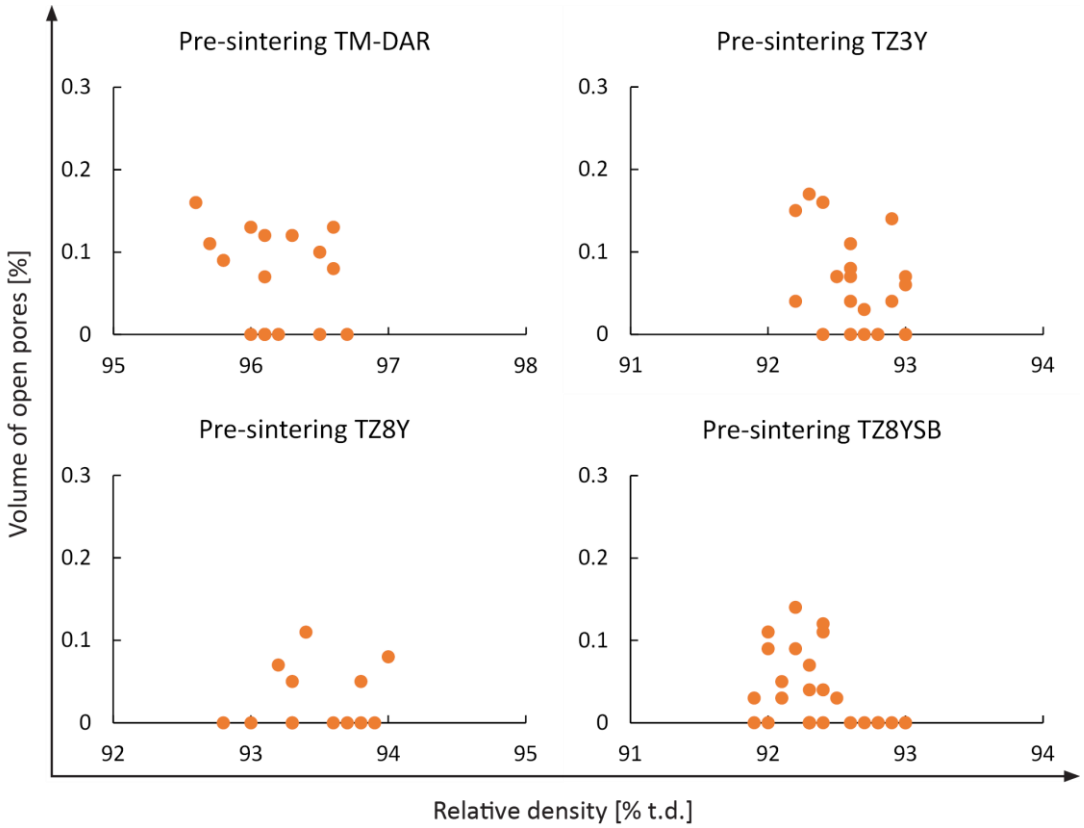


*Figure 31: Volume of open pores at specific relative density of pre-sintered samples subsequently used for HIPing.*

## 8.3. Post-HIPed Samples

### 8.3.1. Post-HIPed Alumina TM-DAR

The data obtained after the analysis of HIPed alumina TM-DAR specimens are summarized in Table 8 and important selected data (average grain size at specific relative density) are presented in Figure 32. It can be seen, that samples were densified to the range of 99.5 – 99.9 % t.d. According to grain size and density characteristics, the best post-HIPing regime is 1200 °C/ 200 MPa/ 1 hours providing a sample with density 99.7 % t.d. and grain size 535 nm. Representative microstructures of green body, pre-sintered sample and post-HIPed sample are presented in Figure 33.

*Table 8: Detailed summary of results for post-HIPed samples of alumina TM-DAR*

| Samples | HIP | | | HIPed density | s HIPed density | AGS | s AGS | PS density | s PS density |
|---|---|---|---|---|---|---|---|---|---|
| | Temp [°C] | Pressure [MPa] | Time [h] | [% t.d.] | - | [nm] | - | [% t.d.] | - |
| TM-DAR PS | 1360 | 0.1 | 0.02 | - | - | 498 | 23 | 96.2 | 0.3 |
| TM-DAR 1 | 1200 | 200 | 0.5 | 99.6 | 0.2 | 476 | 23 | 96.0 | 0.2 |
| TM-DAR 2 | 1200 | 50 | 1 | 99.6 | 0.1 | 576 | 36 | 96.5 | 0.3 |
| TM-DAR 3 | | | 4 | 99.5 | 0.2 | 750 | 50 | 96.6 | 0.6 |
| TM-DAR 4 | | 200 | 1 | 99.7 | 0.1 | 535 | 55 | 96.1 | 0.2 |
| TM-DAR 5 | | | 3 | 99.5 | 0.1 | 585 | 47 | 96.7 | 0.2 |
| TM-DAR 6 | | | 4 | 99.8 | 0.1 | 571 | 53 | 96.2 | 0.1 |
| TM-DAR 7 | | | 6 | 99.5 | 0.1 | 591 | 45 | 96.6 | 0.1 |
| TM-DAR 8 | | | 9 | 99.6 | 0.1 | 696 | 62 | 96.4 | 0.2 |
| TM-DAR 9 | 1250 | 50 | 1 | 99.5 | 0.2 | 630 | 27 | 95.6 | 0.1 |
| TM-DAR 10 | | | 4 | 99.8 | 0.1 | 800 | 86 | 96.2 | 0.2 |
| TM-DAR 11 | | 200 | 1 | 99.9 | 0.2 | 657 | 62 | 96.5 | 0.2 |
| TM-DAR 12 | | | 4 | 99.9 | 0.1 | 700 | 72 | 96.6 | 0.5 |
| TM-DAR 13 | 1300 | 50 | 1 | 99.9 | 0.2 | 1150 | 114 | 96.1 | 0.2 |
| TM-DAR 14 | | | 4 | 99.8 | 0.2 | 1498 | 222 | 96.1 | 0.1 |
| TM-DAR 15 | | 200 | 1 | 99.8 | 0.1 | 1135 | 95 | 96.7 | 0.2 |
| TM-DAR 16 | | | 4 | 99.8 | 0.2 | 1587 | 279 | 96.1 | 0.1 |
| TM-DAR 17 | 1400 | 200 | 4 | 99.9 | 0.1 | 6870 | 1334 | 95.8 | 0.1 |

HIPed density, s HIPed density → average density and its std. dev. after HIPing calculated from 3 measurements
PS density, s PS density → average density and its std. dev. after pre-sintering calculated from 3 measurements
AGS, s AGS → average grain size and its std. dev. of HIPed samples (except PS sample) calculated from 30 measurements

As it can be seen in Figure 32, the average grain size is strongly connected with the post-HIPing temperature. The grain sizes are separated into 3 regions according to post-HIPing temperatures. Grain sizes of post-HIPing temperatures 1200 °C and 1250 °C are close together (and close to pre-sintering grain size). The grain sizes of post-HIPing temperature of 1300 °C are higher and visibly separated. The third grain size region of post-HIPing temperature 1400 °C (not presented in Figure 32, due to extremely large grains, see Table 8) represents visible argument, that post-HIPing has none stopping power for grain growth at temperatures above the pre-sintering one (in this case 1360 °C).

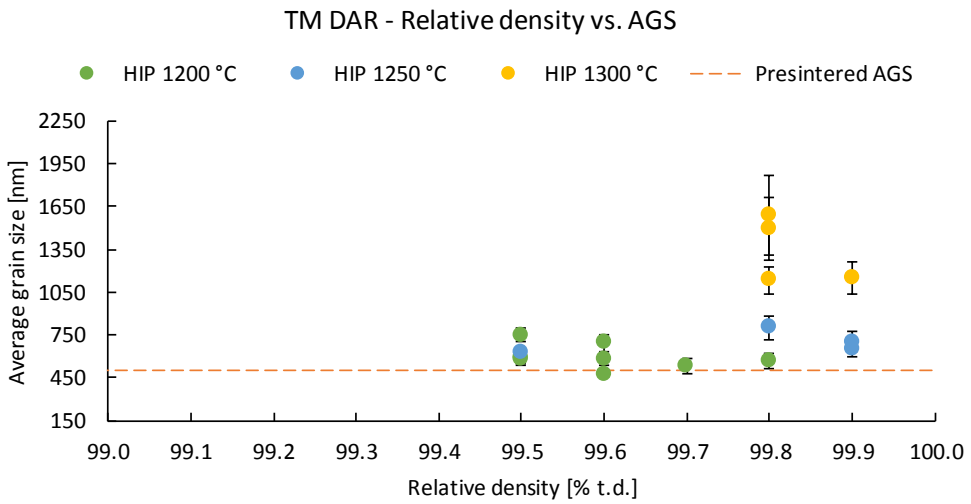


*Figure 32: Summarized plot (average grain size vs. relative density) of post-HIPing experiments for alumina TM-DAR*

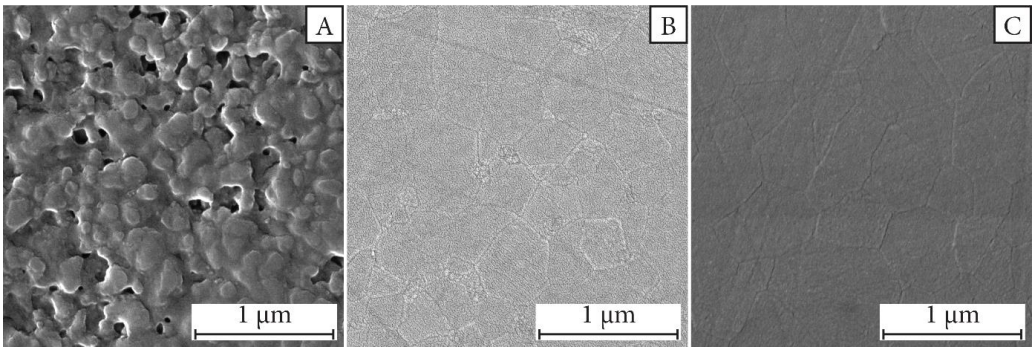


*Figure 33: Representative microstructure of TM-DAR powder type in various states of preparation. A – microstructure of green body, B – pre-sintered microstructure, C – post-HIPed microstructure (1200 °C/ 200 MPa/ 1 h).*

### 8.3.2. Post-HIPed Zirconia TZ3Y

The data obtained after the analysis of post-HIPed zirconia TZ3Y specimens are summarized in Table 9 and important selected data are presented in Figure 34. Samples were densified to the range of 98.4 – 100.0 % t.d. According to grain size and density characteristics, the best post-HIPing regime is 1200 °C/200 MPa/3 hours providing the sample with density 99.8 % t.d. and grain size 203 nm. Representative microstructures of green body, pre-sintered sample and post-HIPed sample are presented in Figure 35.

*Table 9: Detailed summary of results for post-HIPed samples of zirconia TZ3Y*

| Samples | HIP | | | HIPed density | s HIPed density | AGS | s AGS | PS density | s PS density |
|---|---|---|---|---|---|---|---|---|---|
| | Temp [°C] | Pressure [MPa] | Time [h] | [% t.d.] | - | [nm] | - | [% t.d.] | - |
| TZ3Y PS | 1345 | 0.1 | 0.02 | - | - | 204 | 9 | 92.3 | 0.2 |
| TZ3Y 1 | 1200 | 200 | 0.5 | 98.4 | 0.2 | 198 | 16 | 92.2 | 0.2 |
| TZ3Y 2 | 1200 | 50 | 1 | 98.5 | 0.2 | 178 | 12 | 92.6 | 0.2 |
| TZ3Y 3 | | | 4 | 99.1 | 0.1 | 197 | 12 | 92.2 | 0.3 |
| TZ3Y 4 | | 200 | 1 | 99.5 | 0.1 | 192 | 5 | 92.2 | 0.1 |
| TZ3Y 5 | | | 3 | 99.8 | 0.1 | 203 | 6 | 92.8 | 0.1 |
| TZ3Y 6 | | | 4 | 99.3 | 0.1 | 190 | 8 | 92.2 | 0.2 |
| TZ3Y 7 | | | 6 | 100.0 | 0.1 | 204 | 14 | 92.8 | 0.2 |
| TZ3Y 8 | | | 9 | 100.0 | 0.1 | 190 | 5 | 92.7 | 0.1 |
| TZ3Y 9 | 1250 | 50 | 1 | 99.0 | 0.1 | 195 | 11 | 92 | 0.3 |
| TZ3Y 10 | | | 4 | 99.9 | 0.1 | 215 | 9 | 92.5 | 0.1 |
| TZ3Y 11 | | 200 | 1 | 99.2 | 0.1 | 209 | 12 | 92.5 | 0.1 |
| TZ3Y 12 | | | 4 | 99.8 | 0.2 | 203 | 3 | 92.1 | 0.3 |
| TZ3Y 13 | 1300 | 50 | 1 | 99.9 | 0.2 | 209 | 14 | 92.6 | 0.2 |
| TZ3Y 14 | | | 4 | 100.0 | 0.1 | 228 | 16 | 92.8 | 0.1 |
| TZ3Y 15 | | 200 | 1 | 100.0 | 0.1 | 209 | 6 | 92.4 | 0.2 |
| TZ3Y 16 | | | 4 | 99.9 | 0.3 | 209 | 8 | 92.6 | 0.3 |
| TZ3Y 17 | 1400 | 200 | 4 | 99.9 | 0.1 | 303 | 9 | 92.3 | 0.1 |

HIPed density, s HIPed density → average density and its std. dev. after HIPing calculated from 3 measurements
PS density, s PS density → average density and its std. dev. after pre-sintering calculated from 3 measurements
AGS, s AGS → average grain size and its std. dev. of HIPed samples (except PS sample) calculated from 30 measurements

As it can be seen in Figure 34, that changing the post-HIPed parameters have only minimal effect on grain size until the temperature is set to 1400 °C (not in Figure 34) when grain growth is observable (see Table 9).

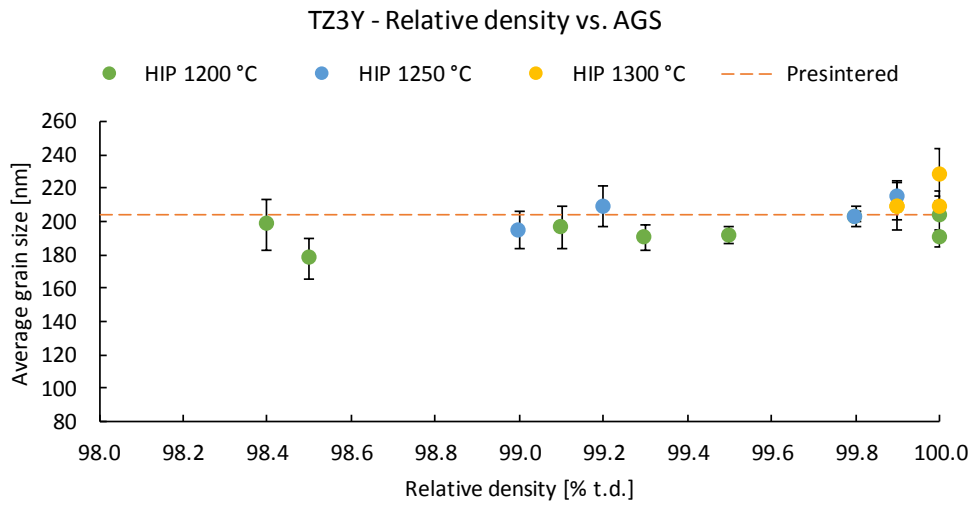


*Figure 34: Summarized plot (average grain size vs. relative density) of HIPing experiments for zirconia TZ3Y*

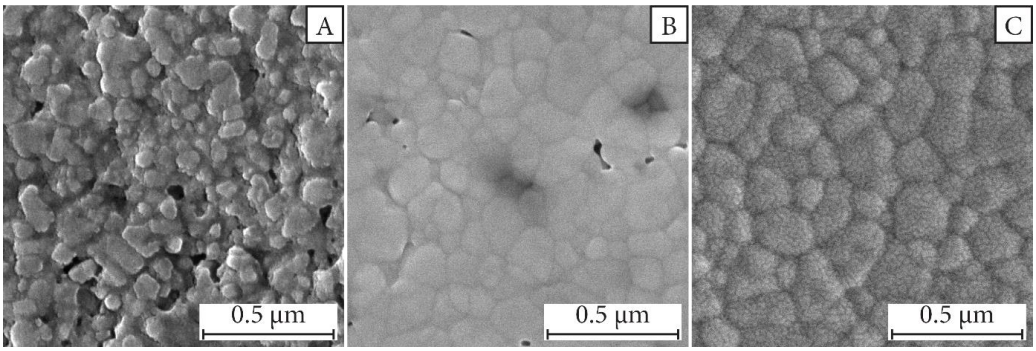


*Figure 35: Representative microstructure of TZ3Y powder type in various states of preparation. A – microstructure of green body, B – pre-sintered microstructure, C – HIPed microstructure (1200 °C/ 200 MPa/ 3 h).*

### 8.3.3. HIPed Zirconia TZ8Y

The data obtained after the analysis of HIPed zirconia TZ8Y specimens are summarized in Table 10 and important selected data are presented in Figure 36. Samples were densified to the range of 97.4 – 100.0 % t.d. According to grain size and density characteristics, the best HIPing regime is 1200 °C/200 MPa/1 h providing the sample with density 99.8 % t.d. and grain size 518 nm. Representative microstructures of green body, pre-sintered sample and post-HIPed sample are shown in Figure 37.

*Table 10: Detailed summary of results for post-HIPed samples of zirconia TZ8Y*

| Samples | HIP | | | HIPed density | s HIPed density | AGS | s AGS | PS density | s PS density |
|---|---|---|---|---|---|---|---|---|---|
| | Temp [°C] | Pressure [MPa] | Time [h] | [% t.d.] | - | [nm] | - | [% t.d.] | - |
| TZ8Y PS | 1380 | 0.1 | 0.02 | - | - | 472 | 33 | 93.5 | 0.4 |
| TZ8Y 1 | 1200 | 50 | 1 | 97.4 | 0.3 | 499 | 27 | 93.3 | 0.2 |
| TZ8Y 2 | | | 4 | 99.6 | 0.1 | 502 | 56 | 92.8 | 0.2 |
| TZ8Y 3 | | 200 | 1 | 99.8 | 0.2 | 518 | 31 | 94.2 | 0.1 |
| TZ8Y 4 | | | 3 | 99.9 | 0.1 | 603 | 27 | 93.6 | 0.2 |
| TZ8Y 5 | | | 4 | 99.9 | 0.1 | 521 | 30 | 93.8 | 0.1 |
| TZ8Y 6 | | | 6 | 99.9 | 0.2 | 599 | 27 | 93.4 | 0.2 |
| TZ8Y 7 | | | 9 | 99.9 | 0.1 | 640 | 25 | 93.5 | 0.1 |
| TZ8Y 8 | 1250 | 50 | 1 | 99.6 | 0.1 | 504 | 41 | 93.8 | 0.1 |
| TZ8Y 9 | | | 4 | 99.9 | 0.1 | 646 | 39 | 92.7 | 0.1 |
| TZ8Y 10 | | 200 | 1 | 99.8 | 0.2 | 558 | 28 | 93.6 | 0.1 |
| TZ8Y 11 | | | 4 | 99.8 | 0.1 | 588 | 22 | 93.9 | 0.1 |
| TZ8Y 12 | 1300 | 50 | 1 | 99.8 | 0.2 | 654 | 59 | 93.7 | 0.2 |
| TZ8Y 13 | | | 4 | 100.0 | 0.1 | 1087 | 47 | 92.7 | 0.1 |
| TZ8Y 14 | | 200 | 1 | 100.0 | 0.1 | 643 | 28 | 93.5 | 0.1 |
| TZ8Y 15 | | | 4 | 99.9 | 0.1 | 902 | 89 | 93.3 | 0.1 |
| TZ8Y 16 | 1400 | 200 | 4 | 100.0 | 0.1 | 3240 | 488 | 92.5 | 0.1 |

HIPed density, s HIPed density → average density and its std. dev. after HIPing calculated from 3 measurements
PS density, s PS density → average density and its std. dev. after pre-sintering calculated from 3 measurements
AGS, s AGS → average grain size and its std. dev. of HIPed samples (except PS sample) calculated from 30 measurements

Again, similarly to TM DAR, it can be seen the influence of excessive HIPing temperature (1400 °C) on extensive grain growth (see Table 10).

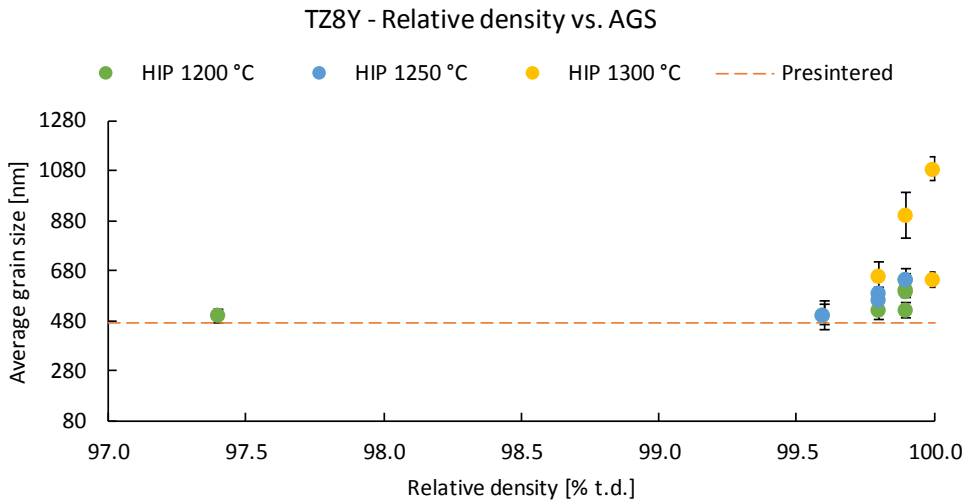


*Figure 36: Summarized plot (average grain size vs. relative density) of post-HIPing experiments for zirconia TZ8Y*

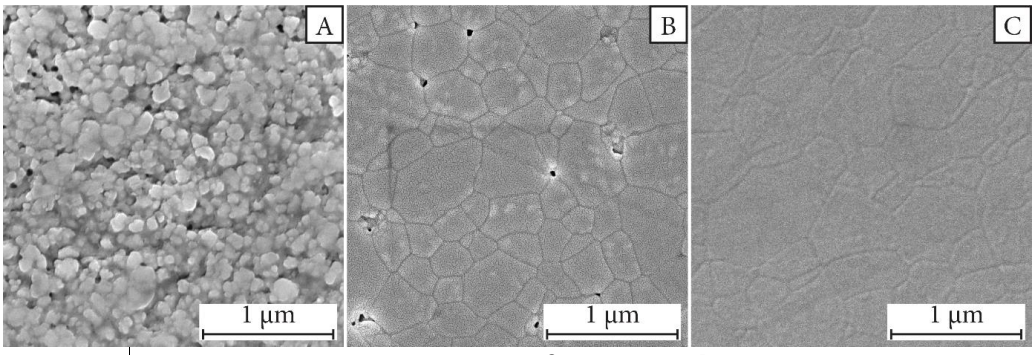


*Figure 37: Representative microstructure of TZ8Y powder type in various states of preparation. A – microstructure of green body, B – pre-sintered microstructure, C – post-HIPed microstructure (1200 °C/ 200 MPa/ 1 h).*

### 8.3.4. Post-HIPed Zirconia TZ8YSB

The data obtained after the analysis of post-HIPed zirconia TZ8YSB specimens are summarized in Table 11 and important selected data are presented in Figure 38. Samples were densified to the range of 93.7 – 99.9 % t.d. According to grain size and density characteristics, the best post-HIPing regime is 1250 °C/200 MPa/4 hours providing the sample with density 99.9 % t.d. and grain size 828 nm. Alternatively, regime 1200°C /200 MPa /9 h provides full density 99.8 % t.d. with 880 nm grain size. Representative microstructures of green body, pre-sintered sample and post-HIPed sample are shown in Figure 39.

*Table 11: Detailed summary of results for post-HIPed samples of zirconia TZ8YSB*

| Samples | HIP | | | HIPed density | s HIPed density | AGS | s AGS | PS density | s PS density |
|---|---|---|---|---|---|---|---|---|---|
| | Temp [°C] | Pressure [MPa] | Time [h] | [% t.d.] | - | [nm] | - | [% t.d.] | - |
| TZ8YSB PS | 1445 | 0.1 | 0.02 | - | - | 757 | 44 | 92.5 | 0.3 |
| TZ8YSB 1 | 1200 | 200 | 0.5 | 95.6 | 0.1 | 725 | 86 | 92.9 | 0.1 |
| TZ8YSB 2 | 1200 | 50 | 1 | 93.7 | 0.2 | 752 | 42 | 93.0 | 0.1 |
| TZ8YSB 3 | | | 4 | 96.3 | 0.1 | 700 | 64 | 91.9 | 0.2 |
| TZ8YSB 4 | | 200 | 1 | 97.1 | 0.3 | 747 | 64 | 93.0 | 0.1 |
| TZ8YSB 5 | | | 3 | 98.7 | 0.1 | 757 | 48 | 92.4 | 0.2 |
| TZ8YSB 6 | | | 4 | 99.5 | 0.1 | 725 | 36 | 92.4 | 0.2 |
| TZ8YSB 7 | | | 6 | 99.6 | 0.1 | 821 | 55 | 92.7 | 0.1 |
| TZ8YSB 8 | | | 9 | 99.8 | 0.1 | 880 | 45 | 92.5 | 0.2 |
| TZ8YSB 9 | 1250 | 50 | 1 | 96.4 | 0.1 | 792 | 47 | 92.8 | 0.1 |
| TZ8YSB 10 | | | 4 | 98.9 | 0.2 | 855 | 22 | 92.2 | 0.3 |
| TZ8YSB 11 | | 200 | 1 | 99.5 | 0.1 | 771 | 19 | 92.6 | 0.1 |
| TZ8YSB 12 | | | 4 | 99.9 | 0.1 | 828 | 30 | 92.8 | 0.1 |
| TZ8YSB 13 | 1300 | 50 | 1 | 98.4 | 0.3 | 842 | 56 | 92.3 | 0.2 |
| TZ8YSB 14 | | | 4 | 99.5 | 0.2 | 1246 | 94 | 92.2 | 0.1 |
| TZ8YSB 15 | | 200 | 1 | 99.8 | 0.2 | 913 | 16 | 92.5 | 0.2 |
| TZ8YSB 16 | | | 4 | 99.9 | 0.1 | 1190 | 33 | 93.0 | 0.1 |
| TZ8YSB 17 | 1400 | 200 | 4 | 99.9 | 0.2 | 4145 | 343 | 92.3 | 0.1 |

HIPed density, s HIPed density → average density and its std. dev. after HIPing calculated from 3 measurements
PS density, s PS density → average density and its std. dev. after pre-sintering calculated from 3 measurements
AGS, s AGS → average grain size and its std. dev. of HIPed samples (except PS sample) calculated from 30 measurements

Unlike the previous powders, where the results of HIPing provides only near full density region (TM DAR and TZ8Y), the post-HIPing results of TZ8YSB present almost whole density range from pre-sintering density (92.5 % t.d.) to full density.

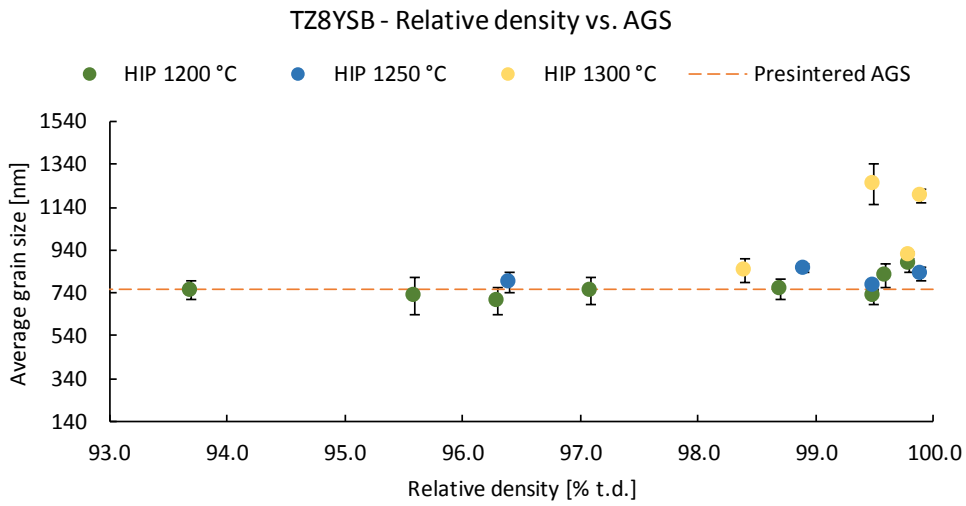


*Figure 38: Summarized plot (average grain size vs. relative density) of post-HIPing experiments for zirconia TZ8YSB*

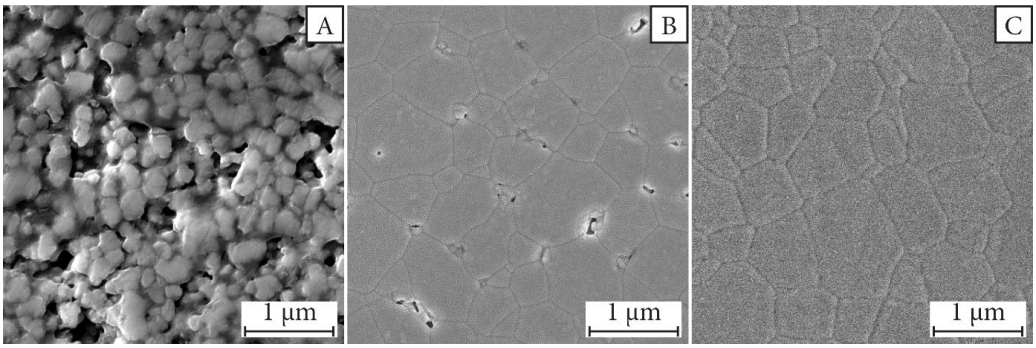


*Figure 39: Representative microstructure of TZ8YSB powder type in various states of preparation. A – microstructure of green body, B – pre-sintered microstructure, C – post-HIPed microstructure (1200 °C/ 200 MPa/ 9 h).*

# 9. Microstructure Development During Post-HIPing - Discussion

The discussion chapter is divided into several subchapters focused on specific steps of the research. The first subchapter is focused on the green body forming and repeatability of the forming process is discussed. Secondly the accuracy of the preparation of pre-sintered samples is discussed. Thirdly the analysis of post-HIPing process and influence of dwell time, pressure and temperature on the grain size and density is presented.

## 9.1. Green Body Preparation

Using the premium powders from renowned producers, provides relatively high powder quality without special powder synthesis optimization. Although there are more sophisticated ways how to shape the powder to the green body, like gel casting or slip casting, the combination of uniaxial and cold isostatic pressing was chosen as a technique of choice.

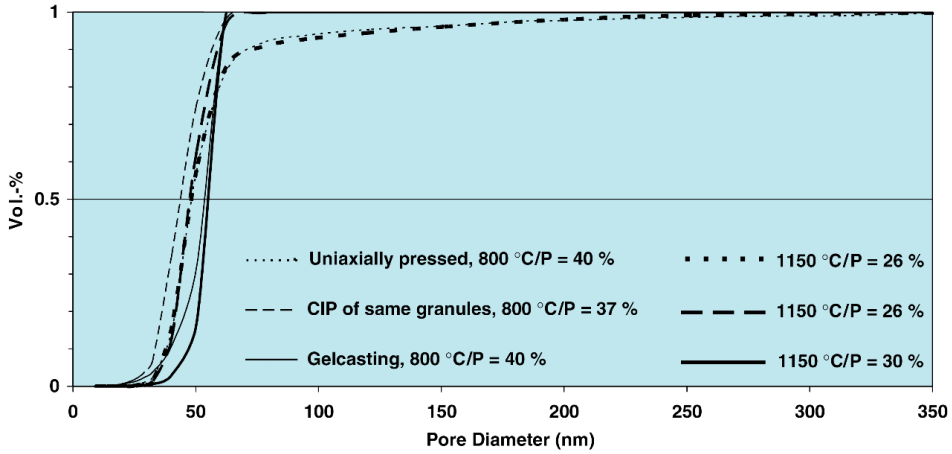


*Figure 40: Difference in the pore distribution among the samples prepared with different consolidation techniques* [96]. *Uniaxially pressed specimen has a visible tail of large pores, which will require higher sintering temperature/time. CIPing (as used in this thesis) removed the majority of the tail of pores and it is comparable to gel casting method.*

This combination provides sufficient quality of green bodies (Figure 40) [96] for subsequent experiments while also provides reproducibility of samples for all of the powders within the batches and also between persons (operators) making the green bodies (Figure 41). Such reproducibility is enormously important in sample-heavy research, such as this one, where several batches by several people (me and bachelor/master student under my supervision [88, 97]) were made during the time of the research.

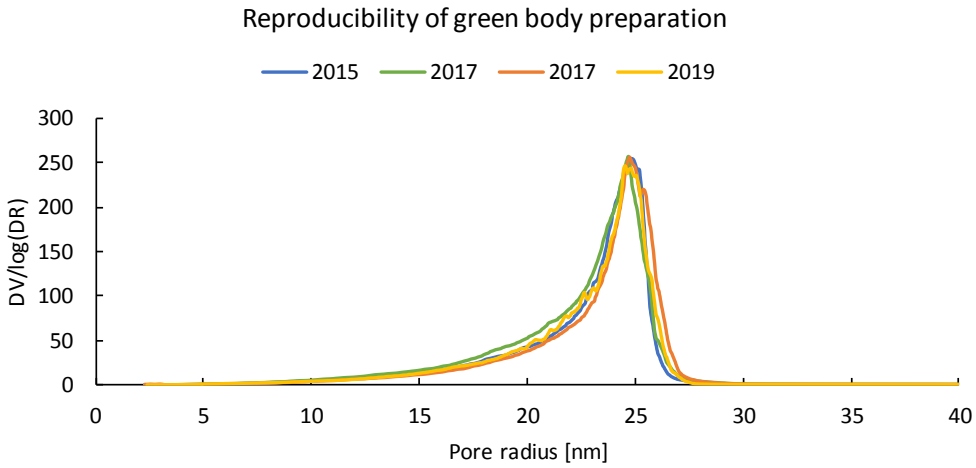


*Figure 41: Porosimetry measurements of the TZ3Y green bodies through the time of the experiment. It is clearly visible, that the green bodies have very similar quality despite the year of consolidation.*

## 9.2. Repeatability of Pre-sintering Process

As is displayed in Figure 31 and Table 7, the preparation of large batch of pre-sintered bodies with same quality (in the terms of grain size at critical density) was more than successful and they are sufficient baseline for the HIPing experiments. Figure 42 shows comparison between already published data [8] for critical densities of studied materials and critical density of the samples prepared for post-HIPing experiments, which exhibits sufficient agreement.

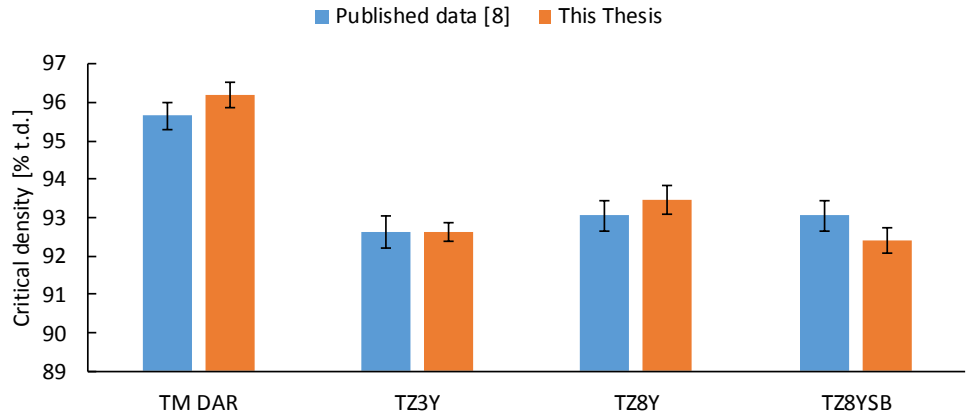


*Figure 42: Comparison of critical density reached in published data [8] and in this thesis.*

## 9.3. Errors of Density and Grain Size Measurements

In order to properly analyse and evaluate the ceramics' microstructure, the limitations of the used experimental methods have to be discussed. The density measurements according to standard [90] "EN 623-2 Advanced technical ceramics – Monolithic ceramics – General and textural properties – Part 2: Determination of density and porosity" are determined by precision of the measuring device (laboratory scales equipped with density kit), the sample's mass and shape. According to mentioned standard the relative accuracy (error) of the Archimedes method is 0.3 %. Which in practice means, that every measured density bares 0.3 % error and therefore every sample which reaches 99.7 % will be qualified as fully dense for the purpose of this thesis.

Also for grain size analysis performed according to [62] "ISO 13383-1:2012. Fine ceramics (advanced ceramics, advanced technical ceramics) - Microstructural characterization - Part 1: Determination of grain size and size distribution" there are limitations which have to be mentioned. The intersection method according to selected standard should provide average grain size present in the whole sample. However, such assumptions are relatively generous, considering the size of surface area being analysed. As an example, the sample in the shape of cylinder with 13 mm diameter (used for the etching experiments) has the surface area of 132.7 $mm^2$. Depending on the average grain size of the sample, the view field required for the proper analysis will have 11.9 $\mu m^2$ (in the case of TZ3Y) up to 1874.9 $\mu m^2$ (in the case of the TZ8YSB with the largest grains). Therefore, the analysed area for TZ3Y is 0.000045 % and for TZ8YSB it is 0.007 % of the whole sample surface. Even though the analysed SEM images were taken as representatives for given microstructure, it has to be taken into account, that slight abnormalities (or variance) in the results of the analysis can appear.

## 9.4. Influence of HIPing Variables on the Microstructure

Planned post-HIPing experiments at mentioned conditions should provide a reasonable dense net of results to cover the density and grain size evolution during various post-HIPing cycles. The majority of HIPing temperatures were chosen to be lower than the pre-sintering temperature in order to monitor the evolution of density and grain size from pre-sintered sample to fully dense sample.

The densification process was quite rapid for TM DAR, TZ3Y and TZ8Y reaching full densities at 1200 °C. On the other hand, densification of TZ8YSB was relatively moderate, with full density at 1250 °C. Such behaviour was expected due to different pore size distribution (Figure 29), which is projected into different pre-sintering temperatures between TM DAR, TZ3Y and TZ8Y (1360, 1345, 1380 °C) versus TZ8YSB (1445 °C).

### 9.4.1. Influence of the Time on the Microstructure

In order to analyse the influence of the dwell time during HIPing, 0.5, 1, 3, 4, 6, 9 hour cycles at constant temperature and pressure (1200 °C and 200 MPa) were performed. It can be seen, that the increase of the post-HIPing dwell time has significant beneficial impact on the densification for every powder grade (Table 8 - Table 11).

For description of the isothermal grain growth behaviour, the parabolic Equation (8) can be used. In the isothermal sintering conditions $k_G$ is constant (not function of time) and the $n$ (grain growth exponent) has to be found experimentally from the data by linear fit the $G^n$ vs time plot. The grain growth exponent according to [81] is 1 for abnormal grain growth, 2 for normal grain growth in pure single phase system, 3 for grain growth in the presence of solutes and 4 for grain growth in presence of pores. Such analysis was performed for every powder type, unfortunately with unsatisfactory results. As can be seen in Table 12 the regression factors (which represent how viable is the fit) are almost identical for every $n$ within the powder types (even when the fits are not precise, the regression factors $R^2$ is lower than 0.9). This could mean that the grain growth is not yet fully activated at 1200 °C and therefore it cannot be analysed by Equation (8).

*Table 12: Regression factors of the linear fit for various growth exponents for analysed powder types.*

| | $G^1\ [nm^1]$ | $G^2\ [nm^2]$ | $G^3\ [nm^3]$ | $G^4\ [nm^4]$ |
|---|---|---|---|---|
| $R^2$ for TM-DAR | 0.8846 | 0.8896 | 0.8854 | 0.8738 |
| $R^2$ for TZ3Y | 0.0242 | 0.0223 | 0.0206 | 0.0189 |

| | | | | |
|---|---|---|---|---|
| $R^2$ for TZ8Y | 0.6010 | 0.6145 | 0.6279 | 0.6411 |
| $R^2$ for TZ8YSB | 0.8118 | 0.8168 | 0.8206 | 0.8233 |

$G^n$ → experimental grain size to power of grain growth exponent n, where n is 1-4

$R^2$ → regression parameter of the fit

Figure 43 shows linear fit for $n = 2$ as an illustration of plausible fit for measured data of TM-DAR experiencing the parabolic behaviour. On the other hand, Figure 44 presents the fit for $n = 2$ for TZ3Y where the grain growth is not activated experiencing the scattered values unable to be fitted correctly. From the obtained results it is evident, that the dwell time in post-HIPing process has parabolic effect on the grain growth when it is activated – for TM-DAR, TZ8Y and TZ8YSB. On the other hand, what is visible on the behaviour of TZ3Y, there are conditions during post-HIPing where the grain growth is not yet activated, while density is close to theoretical. Such information is essential and important information in the optimization process during post-HIPing.

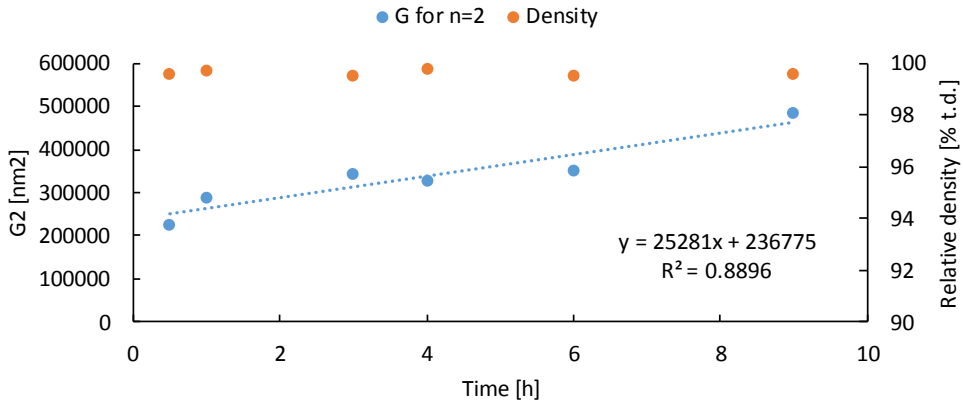


*Figure 43: Plausible fit for $n = 2$ for grain growth development in TM-DAR during isothermal post-HIPing.*

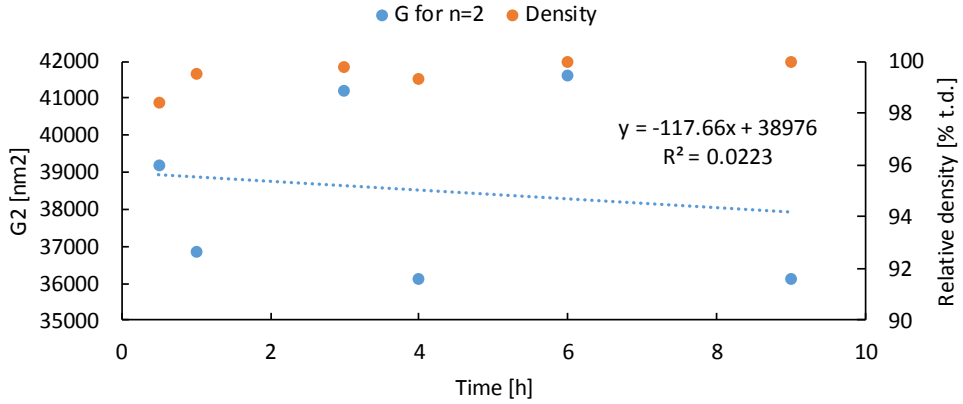


*Figure 44: Invalid fit for $n = 2$ for grain growth development in TZ3Y during isothermal post-HIPing because the grain growth has not been activated yet.*

### 9.4.2. Influence of the Temperature on the Microstructure

Similarly as the influence of the dwell time, the influence of the post-HIPing temperature on grain growth can be evaluated by combining grain growth Equations (8) and (9) into:

$$\ln(G^n - G_0^n) = lnk_0 t + \frac{-Q_G}{R} \cdot \frac{1}{T}, \tag{15}$$

which enables to prepare the plot of $\ln(G^n - G_0^n)$ versus the $1/T$ providing opportunity to make linear fit and ability to calculate the activation energy for grain growth $Q_G$. From the post-HIPing experiment there are 4 sets of grain size data (50 MPa/ 1 h, 50 MPa/ 4 h, 200 MPa/ 1 h, 200 MPa/ 4 h) for 3 different temperatures (1200, 1250, 1300 °C) and one additional temperature 1400 °C for 200 MPa/ 4 h regime.

For the TM-DAR powder type the data for linear fit are shown in Table 13 and the fit for $n = 2$ is presented in Figure 45.

*Table 13: Activation energies and regression factors of linear fit for various n for TM-DAR*

| | 50 MPa/ 1 h | 50 MPa/ 4 h | 200 MPa/ 1 h | 200 MPa/ 4 h | Avg | stdev |
|---|---|---|---|---|---|---|
| $Q_G\ for\ n = 1\ [kJ/mol]$ | 385 | 257 | 501 | 443 | 397 | 104 |
| $Q_G\ for\ n = 2\ [kJ/mol]$ | 467 | 348 | 590 | 649 | 513 | 134 |
| $Q_G\ for\ n = 3\ [kJ/mol]$ | 559 | 451 | 688 | 879 | 644 | 184 |
| $Q_G\ for\ n = 4\ [kJ/mol]$ | 660 | 564 | 794 | 1122 | 785 | 244 |
| $R^2 for\ n = 1$ | 0.9042 | 0.8312 | 0.9988 | 0.9848 | 0.9297 | 0.0778 |
| $R^2 for\ n = 2$ | 0.8905 | 0.8225 | 0.9940 | 0.9819 | 0.9222 | 0.0810 |
| $R^2 for\ n = 3$ | 0.8790 | 0.8164 | 0.9873 | 0.9746 | 0.9143 | 0.0812 |
| $R^2 for\ n = 4$ | 0.8696 | 0.8123 | 0.9798 | 0.9687 | 0.9076 | 0.0806 |

$Q_G \rightarrow$ activation energy for grain growth
$R^2 \rightarrow$ regression parameter of the fit
$Avg \rightarrow$ is average value for $Q_G$ or for $R^2$ respectively, with corresponding standard deviation from 4 items

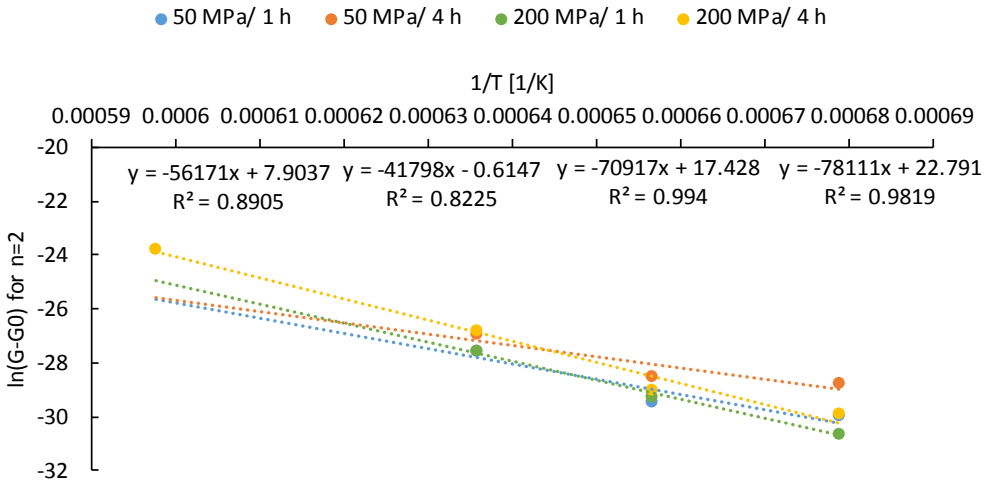


*Figure 45: Linear regression of the grain size for n=2 versus 1/T for TM-DAR.*

Unfortunately, the regression coefficients for all $n$ are almost identical, therefore it is difficult to determine the correct mechanism for grain growth. However, it can be safely stated, that the influence of post-HIPing temperature on grain growth is exponential, due to reasonable fit for all combinations. However, based on the microstructural observation, the proper $n$ could be estimated as 2 or 3 because there is no observed abnormal grain growth (so $n = 1$ is not

expected) and the density of observed samples is above 99.5 % t.d., therefore the $n = 4$ (grain growth in the presence of pores) is also not plausible. The calculated activation energy for grain growth is 513 ± 134 kJ/mol and 644 ± 184 kJ/mol for $n = 2$ and $n = 3$, respectively. In comparison with another authors [98–103] for $n = 2$ activation energies for 50 MPa reache similar values as in this work, however activation energies for 200 MPa exhibit higher values (Figure 46). It seems that the higher post-HIPing pressure retards grain growth, which was rejected in [32]. More probable is, that the grain growth model for pressureless sintering is not applicable for the pressure-assisted sintering at low temperatures, when the grain growth is not yet activated therefore the grain size does not change with temperature (in the range of 1200-1300 °C) as rapidly as expected.

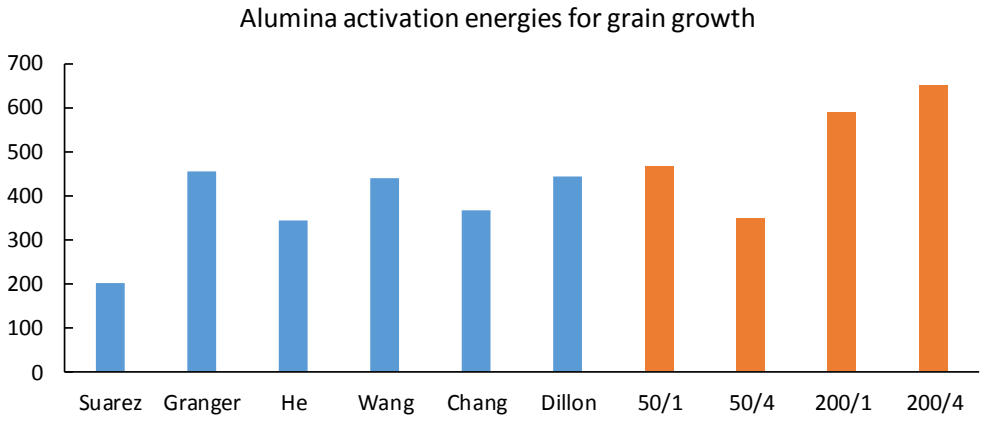


*Figure 46: Comparison of the activation energies of grain growth for alumina ceramics from the literature (blue) and for various post-HIPing cycles of this thesis (orange) in the format pressure/time.*

The similar trend in the fitting is visible for TZ8Y and for TZ8YSB powder types – regression coefficients are very close together and it is difficult to select the proper $n$. However, the visible difference is that the activation energies are divided by the dwell time. Activation energies for 1 and for 4h regimes are significantly different, which is quite expected because of the minimal difference between grain sizes, the model is suggesting higher activation energies for 4h regimes. This is another evidence, that the model is not precise for pressure-assisted sintering at low temperatures where the grain growth is not (fully) activated. For the TZ8Y powder type, the data for linear fit are shown in Table 14 and the fit for $n = 2$ is presented in Figure 47. For the TZ8YSB powder type, the data for linear fit are shown in Table 15 and the fit for $n = 2$ is presented in Figure 48.

Comparing the activation energies for grain growth for cubic zirconia in this thesis with the literature [78, 104–107] provides reasonable agreement for the 1-hour regimes for both TZ8Y and TZ8YSB as is presented in Figure 49. However, 4-hour regimes could only be compared with one source [105].

*Table 14: Activation energies and regression factors of linear fit for various n for TZ8Y*

| | 50 MPa/ 1 h | 50 MPa/ 4 h | 200 MPa/ 1 h | 200 MPa/ 4 h | Avg | stdev |
|---|---|---|---|---|---|---|
| $Q_G\ for\ n = 1\ [kJ/mol]$ | 364 | 583 | 253 | 422 | 405 | 138 |
| $Q_G\ for\ n = 2\ [kJ/mol]$ | 392 | 673 | 276 | 561 | 476 | 176 |
| $Q_G\ for\ n = 3\ [kJ/mol]$ | 422 | 773 | 300 | 719 | 553 | 229 |
| $Q_G\ for\ n = 4\ [kJ/mol]$ | 454 | 881 | 325 | 887 | 637 | 290 |
| $R^2 for\ n = 1$ | 0.8013 | 0.9943 | 0.9979 | 0.9951 | 0.9471 | 0.0972 |
| $R^2 for\ n = 2$ | 0.7984 | 0.9991 | 0.9964 | 0.9873 | 0.9453 | 0.0981 |

| | | | | | | |
|---|---|---|---|---|---|---|
| $R^2 for\ n = 3$ | 0.7956 | 0.9999 | 0.9947 | 0.9750 | 0.9413 | 0.0977 |
| $R^2 for\ n = 4$ | 0.7930 | 0.9982 | 0.9929 | 0.9638 | 0.9370 | 0.0971 |

$Q_G \rightarrow$ activation energy for grain growth

$R^2 \rightarrow$ regression parameter of the fit

$Avg \rightarrow$ is an average value for $Q_G$ or for $R^2$ respectively, with corresponding standard deviation from 4 items

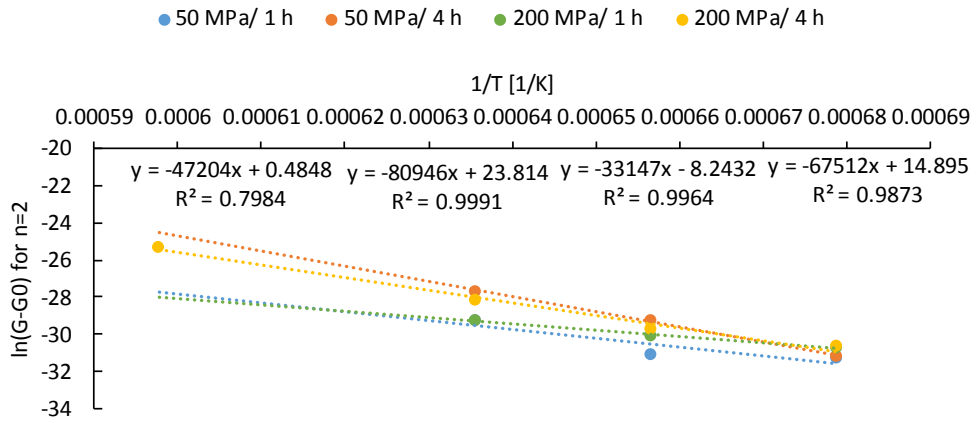


*Figure 47: Linear regression of the grain size for n=2 versus 1/T for TZ8Y*

*Table 15: Activation energies and regression factors of linear fit for various n for TZ8YSB*

| | 50 MPa/ 1 h | 50 MPa/ 4 h | 200 MPa/ 1 h | 200 MPa/ 4 h | Avg | stdev |
|---|---|---|---|---|---|---|
| $Q_G\ for\ n = 1\ [kJ/mol]$ | 181 | 875 | 272 | 481 | 452 | 309 |
| $Q_G\ for\ n = 2\ [kJ/mol]$ | 192 | 939 | 293 | 610 | 508 | 338 |
| $Q_G\ for\ n = 3\ [kJ/mol]$ | 204 | 1007 | 315 | 756 | 570 | 376 |
| $Q_G\ for\ n = 4\ [kJ/mol]$ | 217 | 1080 | 338 | 912 | 637 | 424 |
| $R^2 for\ n = 1$ | 0.9999 | 0.9444 | 0.9205 | 0.9957 | 0.9651 | 0.0390 |
| $R^2 for\ n = 2$ | 1.0000 | 0.9575 | 0.9158 | 0.9995 | 0.9682 | 0.0402 |
| $R^2 for\ n = 3$ | 1.0000 | 0.9687 | 0.9113 | 0.9924 | 0.9681 | 0.0401 |
| $R^2 for\ n = 4$ | 0.9999 | 0.9780 | 0.9071 | 0.9823 | 0.9668 | 0.0409 |

$Q_G \rightarrow$ activation energy for grain growth

$R^2 \rightarrow$ regression parameter of the fit

$Avg \rightarrow$ is an average value for $Q_G$ or for $R^2$ respectively, with corresponding standard deviation from 4 items

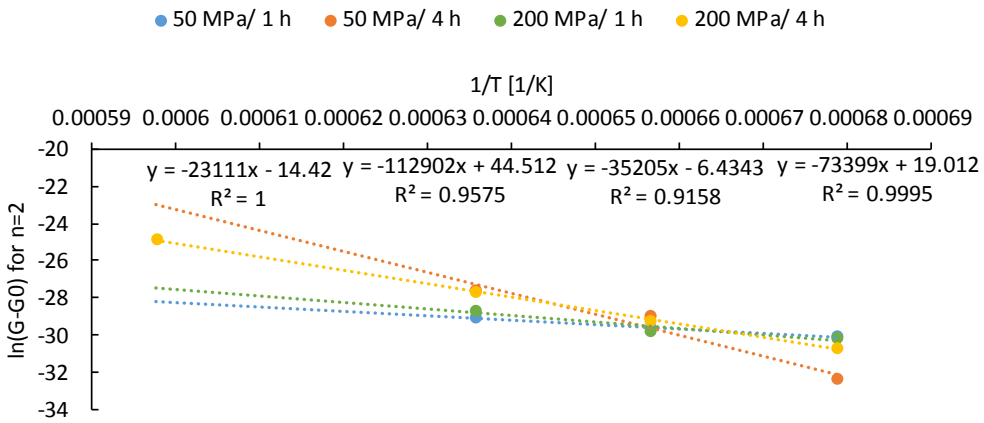


*Figure 48: Linear regression of the grain size for n=2 versus 1/T for TZ8YSB*

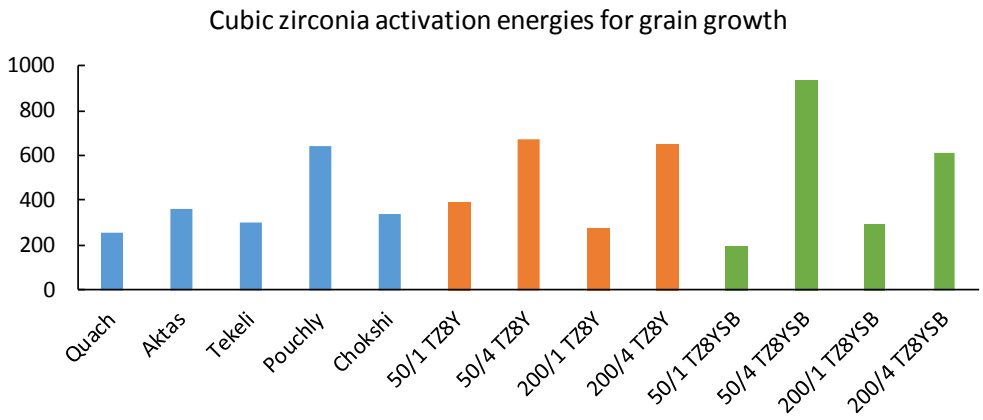


*Figure 49: Comparison of the activation energies of grain growth for cubic zirconia ceramics from the literature (blue) and for various post-HIPing cycles of this thesis for TZ8Y (orange) and TZ8YSB (green) in the format pressure/time.*

Despite the visible inconsistency, it is possible to evaluate the temperature influence on the microstructure during post-HIPing as double-sided. On the one side, the elevated temperature is the another source of energy enabling densification and with applied pressure, the densification effect is evidently more powerful. Unfortunately, the increase in sintering temperature also activated grain boundaries and enhance their mobility (visible in Chapter 8.3 for samples post-HIPed at 1400 °C). Therefore, application the elevated temperature into the sintering process is necessary to activate densification mechanisms, but it has to be done with respect to its negative effects.

### 9.4.3. Influence of the Pressure on the Microstructure

As it was mentioned before in a theoretical review, the pressure has significant densification ability which can be demonstrated in various cases in the literature (see Chapter 2.6) and also in the present research.

When the pre-sintered sample is firstly encountered with the pressure (50 or 200 MPa) even at lowest HIPing temperature (1200 °C), the increase in the density is significant as is documented in Figure 50. It is evident, that the more pressure is applied, the higher densities at the same temperature/time settings are received. Therefore, for the densification, the optimal amount of the applied pressure is the available maximum for the machine.

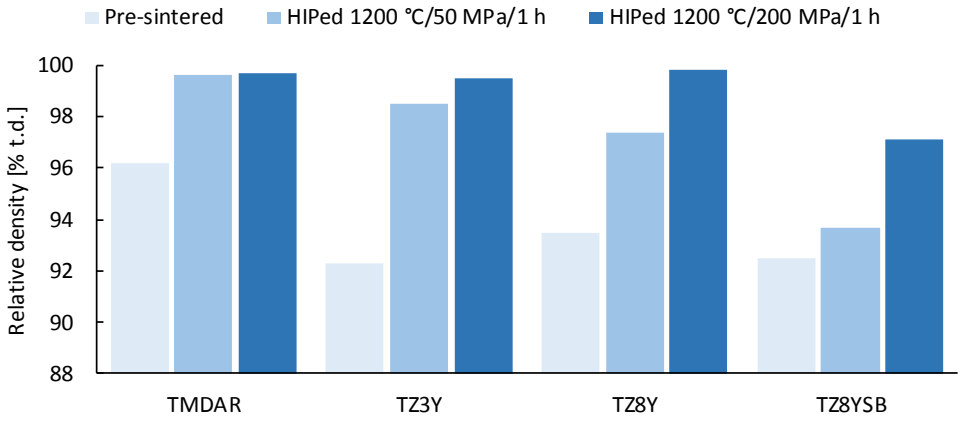


*Figure 50: Influence of pressure on densification during HIPing at constant temperature and time.*

As the influence of the pressure on the densification is quite clear, the influence on the grain growth is rather inconsistent. In the literature, Besson et. al. presented that applied pressure during direct HIPing (with metal/glass container) at constant temperature and time, increases the grain size linearly, which is visible in Figure 11A [30]. However, he also observed, that pressure does not affect grains size of already dense samples with 98 % t.d. and average grain size remained the same after HIPing, which is presented in Table 1 [30]. However, Kishimoto et. al. [35] showed that pressure increases grain size linearly even for the almost dense samples with similar density (Figure 13A). Such contradictory is rather hard to resolve due to the limited amount of legit data in the literature. The presented results of this thesis indicate, that the pressure does not have any influence on the grain growth development during HIPing of pre-sintered samples with 8 to 4 % of remaining pores. Figure 51 - Figure 54 show differences in the average grain size (AGS) between 50 and 200 MPa of HIPing pressure at the same temperature/time settings. In spite of some present irregularities, the trend is sufficiently clear: in the range of the standard error there is none change in the AGS at certain temperature and time (blue bar corresponds to orange bar at given temperature and time combination). Therefore, introducing the pressure during post-HIPing enhance the densification process and additionally do not affect the grain size during sintering.

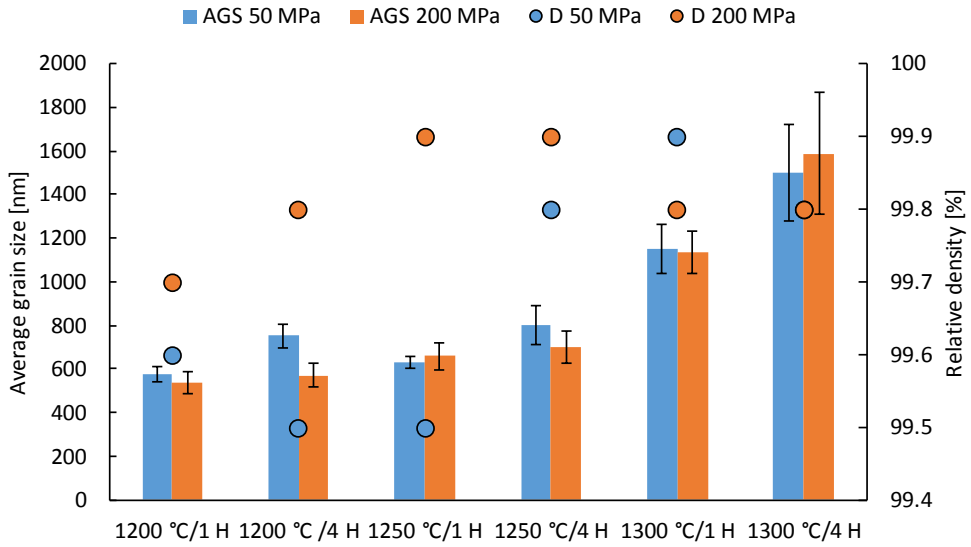


*Figure 51: Influence of applied pressure on average grain size (AGS) and density (D) during post-HIPing of TMDAR*

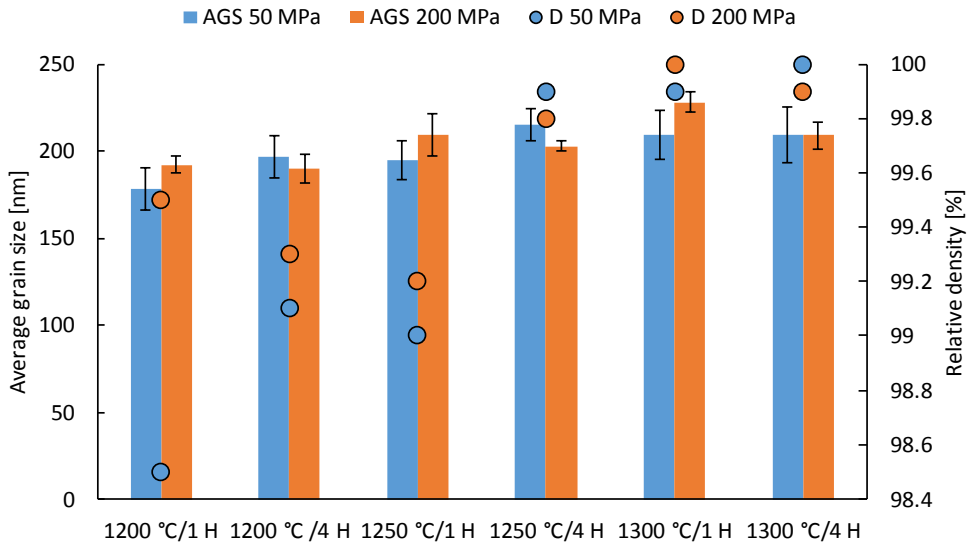


*Figure 52: Influence of applied pressure on average grain size (AGS) and density (D) during post-HIPing of TZ3Y*

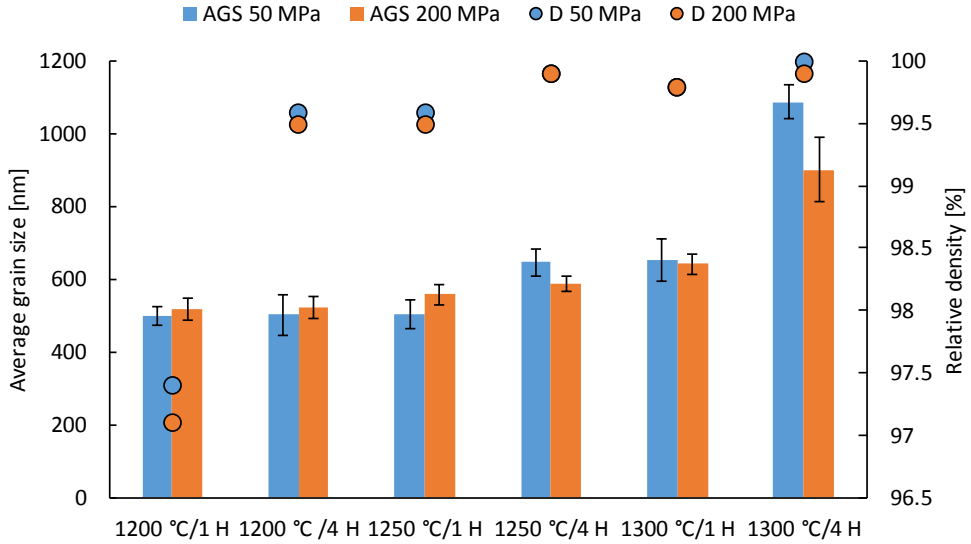


*Figure 53: Influence of applied pressure on average grain size (AGS) and density (D) during post-HIPing of TZ8Y*

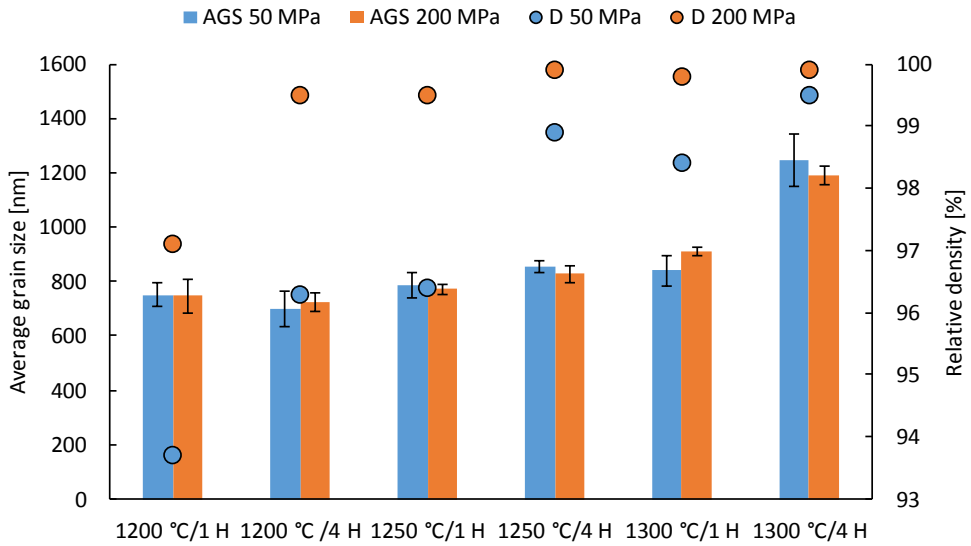


*Figure 54: Influence of applied pressure on average grain size (AGS) and density (D) during post-HIPing of TZ8YSB*

### 9.4.4. Optimization of the HIPing Process

This Chapter is a direct follow up of Chapter 2.8 aiming to confirm the proposed thoughts on the optimization of the post-HIPing process in order to achieve full density and minimum grain growth. The main idea was, that the densification (reaching the full density) is the main process which has to be focused on, however without using the thermal energy as the main densification mechanism, but use the densification influence of the applied pressure instead.

The reason why the temperature utilization in the sintering process has to be limited is visible in Equation (9), where the grain size change is increased exponentially with temperature. Therefore, although the certain temperature is necessary to activate the diffusion processes for densification, the pressure, which does not have any influence on the grain size (visible in Chapter 9.4.2 and from Figure 51 to Figure 54), is the ideal candidate to provide energy for the densification process.

The results of the application of this approach are visible on every powder tested in this work aiming to obtain fully dense specimen with minimal grain growth. In the case of TMDAR, starting from the pre-sintering density of 96.2 % t.d. and grain size 498 nm, the ideal post-HIPing regime is 1200 °C/200 MPa/1 h reaching density 99.7 % t.d. and grain size 535 nm. Considering the errors which are inevitably connected with experimental work and evaluation methods, it can be said, that the density is full and that there is only minimal grain growth. There is a little chance, that lowering the temperature below 1200 °C and significantly increase in the dwell time could bring better results. On the other hand, increasing the temperature above 1200 °C only increase the grain size, without any other benefit.

The post-HIPing results of the TZ3Y are unexpected. While other powder types exhibit grain growth during the post-HIPing process, this powder does not. The TZ3Y starts from the pre-sintering density of 92.3 % t.d. and 204 nm grain size and the ideal cycle is 1200 °C/200 MPa/3 h with 99.8 % t.d. and 203 nm grains. However, increasing the temperature to 1300 °C/200 MPa/4 h do not have effect on the grain size, which remains at 209 nm. Even increasing the temperature to 1400 °C, which is above pre-sintering temperature, increase the grain size only to 303 nm. The hypothetical explanation can be connected to the activation energy of the

grain growth, which can be incredibly high, that grain boundaries are unable to move. However, such behaviour is strange and has to be subjected to more focused research.

The results of post-HIPing the TZ8Y powder show very similar behaviour as TMDAR powder: fast densification from pre-sintering density 93.5 % t.d. and 472 nm grain size to 99.8 % t.d. with grain size 518 nm at 1200 °C/200 MPa/1 h. Increasing in the temperature, again, only increase the grain size of fully dense material.

As it was mentioned earlier, the post-HIPing results of TZ8YSB provide valuable data for the densification procedure during post-HIPing and influence of the combination of the HIPing parameters on microstructure. Because of the coarser starting powder, the pre-sintering temperature is higher and therefore the effect of selected HIPing cycles is moderated, hence the densification is slower and can be observed in detail. The ideal post-HIPing process for the TZ8YSB is 1250 °C/200 MPa/4 h reaching 99.9 % t.d. with 828 nm grains. However, there is a minimal noticeable increase in grain size compared to the pre-sintering sample with 92.2 % t.d. and 757 nm grains. Lowering the dwell time to 1 hour decreases the grain size to 771 nm, but does not provide full density, only 99.5 % t.d.

### 9.4.5. Trading of the HIPing Parameters

Considering, that post-HIPing regime is characterized by 3 main parameters: applied pressure, dwell time and sintering temperature, the idea arises, that there could be various combinations providing similar/same results. Detailed analyse of Table 8 - Table 11 provides evidence of a possibility of time/temperature trade-off – summarized in Table 16.

*Table 16: Evidence of possible temperature/time trade-off for HIPed samples*

| Samples | HIP | | | HIPed density | s HIPed density | AGS | s AGS | PS density | s PS density |
|---|---|---|---|---|---|---|---|---|---|
| | Temp [°C] | Pressure [MPa] | Time [h] | [% t.d.] | - | [nm] | - | [% t.d.] | - |
| TMDAR | 1200 | 200 | 4 | 99.8 | 0.1 | 571 | 53 | 96.2 | 0.1 |
| | 1250 | 200 | 1 | 99.9 | 0.2 | 657 | 62 | 96.5 | 0.2 |
| TZ3Y | 1200 | 50 | 4 | 99.1 | 0.1 | 197 | 12 | 92.2 | 0.3 |
| | 1250 | 50 | 1 | 99.0 | 0.1 | 195 | 11 | 92 | 0.3 |
| | 1200 | 200 | 4 | 99.3 | 0.1 | 190 | 8 | 92.2 | 0.2 |
| | 1250 | 200 | 1 | 99.2 | 0.1 | 209 | 12 | 92.5 | 0.1 |
| | 1250 | 50 | 4 | 99.9 | 0.1 | 215 | 9 | 92.5 | 0.1 |
| | 1300 | 50 | 1 | 99.9 | 0.2 | 209 | 14 | 92.6 | 0.2 |
| | 1250 | 200 | 4 | 99.8 | 0.2 | 203 | 3 | 92.1 | 0.3 |
| | 1300 | 200 | 1 | 100.0 | 0.1 | 209 | 6 | 92.4 | 0.2 |
| TZ8Y | 1200 | 50 | 4 | 99.6 | 0.1 | 502 | 56 | 92.8 | 0.2 |
| | 1250 | 50 | 1 | 99.6 | 0.1 | 504 | 41 | 93.8 | 0.1 |
| | 1200 | 200 | 4 | 99.9 | 0.1 | 521 | 30 | 93.8 | 0.1 |
| | 1250 | 200 | 1 | 99.8 | 0.2 | 558 | 28 | 93.6 | 0.1 |
| | 1250 | 50 | 4 | 99.9 | 0.1 | 646 | 39 | 92.7 | 0.1 |
| | 1300 | 50 | 1 | 99.8 | 0.2 | 654 | 59 | 93.7 | 0.2 |
| | 1250 | 200 | 4 | 99.8 | 0.1 | 588 | 22 | 93.9 | 0.1 |
| | 1300 | 200 | 1 | 100.0 | 0.1 | 643 | 28 | 93.5 | 0.1 |
| TZ8YSB | 1200 | 50 | 4 | 96.3 | 0.1 | 700 | 64 | 91.9 | 0.2 |
| | 1250 | 50 | 1 | 96.4 | 0.1 | 789 | 47 | 92.8 | 0.1 |
| | 1200 | 200 | 4 | 99.5 | 0.1 | 725 | 36 | 92.4 | 0.2 |
| | 1250 | 200 | 1 | 99.5 | 0.1 | 771 | 19 | 92.6 | 0.1 |
| | 1250 | 50 | 4 | 98.9 | 0.2 | 855 | 22 | 92.2 | 0.3 |
| | 1300 | 50 | 1 | 98.4 | 0.3 | 842 | 56 | 92.3 | 0.2 |

HIPed density, s HIPed density → average density and its std. dev. after HIPing calculated from 3 measurements
PS density, s PS density → average density and its std. dev. after pre-sintering calculated from 3 measurements
AGS, s AGS → average grain size and its std. dev. of HIPed samples (except PS sample) calculated from 30 measurements

It seems, that for TZ3Y, TZ8Y and TZ8YSB the time and temperature could be traded in the ration of 50 °C for 3 hours at constant pressure in the upside direction (increasing temperature, decreasing time). Unfortunately, for TMDAR such trading seems to be an unavailable option because there is only one sufficient evidence. On the other hand, for the remaining powders, there are plenty of pairs supporting such an idea (Table 16). As an example for TZ8YSB: 1200 °C/50 MPa/4 h (96.3 % t.d. and 700 nm) is evidently very close (with the respect to experimental errors) to 1250 °C/50 MPa/1 h (96.4 % t.d. and 789 nm). Similarly 1200 °C/200 MPa/4 h (99.5 % t.d. and 725 nm) is close to 1250 °C/200 MPa/1 h (99.5 % t.d. and 771 nm). Unfortunately, there is no evidence that this trade-off can be extended for longer times and higher temperatures (e. g. decrease the temperature by 100 °C and increase the time by 6 hours).

While the trading the temperature for time is very known for the two-step sintering, the trading temperature or time for the pressure is not widely presented in the literature. Unfortunately, data in this work provides only one set of applicable "connected" samples – same density, same grain size, but different pressure/time/temperature to evaluate the parameters of trading (Table 17).

*Table 17: Set TZ8YSB samples applicable for the trading of post-HIPing parameters*

| Samples | HIP | | | HIPed density | s HIPed density | AGS | s AGS | PS density | s PS density |
|---|---|---|---|---|---|---|---|---|---|
| | Temp [°C] | Pressure [MPa] | Time [h] | [% t.d.] | - | [nm] | - | [% t.d.] | - |
| TZ8YSB | 1200 | 200 | 3 | 98.7 | 0.1 | 757 | 48 | 92.4 | 0.2 |
| | 1250 | 50 | 4 | 98.9 | 0.2 | 855 | 22 | 92.2 | 0.3 |
| | 1300 | 50 | 1 | 98.4 | 0.3 | 842 | 56 | 92.3 | 0.2 |

HIPed density, s HIPed density → average density and its std. dev. after HIPing calculated from 3 measurements
PS density, s PS density → average density and its std. dev. after pre-sintering calculated from 3 measurements
AGS, s AGS → average grain size and its std. dev. of HIPed samples (except PS sample) calculated from 30 measurements

It can be seen, that the samples are more or less similar in the density and the grain size. The evaluation of the possibility of the trading parameters is as follows:

- From green (1200/200/3) to blue (1250/50/4) it is necessary to increase the temperature by 50 °C, decrease pressure by 150 MPa and increase the time by 1 hour.
- From green to yellow (1300/50/1) it is necessary to increase the temperature by 100 °C, decrease pressure by 150 MPa and decrease the time by 2 hours.
- From blue to yellow it is necessary to decrease the time by 3 hours and increase the temperature by 50 °C.

If the time and temperature have a trading rate 50 °C for 3 hours, then 150 MPa can be traded for 4 hours which gives 50 °C for 112.5 MPa. Such relations could be expressed as follows:

$$\begin{aligned} \mathbf{50}\ ^{\circ}\boldsymbol{C} &\leftrightarrow 112.5\ MPa \leftrightarrow 3\ h, \\ 66.7\ ^{\circ}C &\leftrightarrow \mathbf{150}\ \boldsymbol{MPa} \leftrightarrow 4\ h, \\ 16.7\ ^{\circ}C &\leftrightarrow 37.5\ MPa \leftrightarrow \mathbf{1}\ \boldsymbol{h}. \end{aligned} \tag{16}$$

Unfortunately, when such trading calculations were performed on other samples and powders, the results were highly inconsistent. There was no acceptable result for TMDAR powder, and due to minimal grain growth it is also unusable for TZ3Y. There were 50 % successful application for TZ8Y and for TZ8YSB with any logical pattern when it is available and when it is not. Therefore, such simplistic relation among the three HIPing variables is generally inapplicable and has to be studied deeper, with larger data set – temperatures below 1200 °C, pressures at 10 MPa, 100 MPa and 150 MPa and broader dwell time options for more temperature/pressure combinations.

# 10. Conclusions

The main goal of this thesis was to discover tailoring potential of post-HIPing procedure on the microstructure of selected advanced ceramic materials in order to produce samples with theoretical density and minimal grain size. The initial step was to analyse the preparation of pre-sintering samples (92 - 96 % t.d.); observations from this research could be summarized as:

- Pore closure is a material characteristic governed by interfacial energies.
- Pore closure is independent on initial microstructure.
- Pore closure is independent on the sintering history.

For the analysis of pre-sintered samples which contains a considerable amount of porosity, the novel approach for thermal etching was developed. It was found out that microstructure of studied ceramic materials (alumina and zirconia) can be revealed independently on sintering temperature by low temperature etching (900 °C for 1 hour). Post-HIPed samples (almost dense ceramic material) can also be etched by such technique.

Conclusions of extensive experimental study of post-HIPed procedure can be summarized as:

- Post-HIPing has enormous potential in the densification process of ceramic materials synchronizing the temperature and applied pressure as densification forces.
- Standard kinetic equation for grain growth used for pressureless sintering is not sufficiently applicable for pressure-assisted sintering due to the synergic combination of processing parameters (temperature, dwell time and pressure), which are sufficient for densification of the specimen without activation of the grain growth.
- When grain growth is activated (at higher post-HIPing temperatures), the grain growth exhibits parabolic dependence on dwell time during the post-HIPing process.
- Post-HIPing temperature exhibits exponential influence on grain growth and therefore it has to be kept on a minimal necessary level to avoid excessive grain growth.
- Applied pressure during post-HIPing process exhibits minimal influence on grain growth and therefore the pressure should be main densification force during post-HIPing process.

Optimized HIPing cycles for studied powder types for full density and minimal grain growth can be summarized as:

- Pre-sintered (density, AGS) → HIPing regime → post-HIPed (density, AGS)
- TM-DAR: 96.2 % t.d., 498 nm → 1200 °C/ 200 MPa/ 1 h → 99.7 % t.d., 535 nm
- TZ3Y: 92.3 % t.d., 204 nm → 1200 °C/ 200 MPa/ 3 h → 99.8 % t.d., 203 nm
- TZ8Y: 93.5 % t.d., 472 nm → 1200 °C/ 200 MPa/ 1 h → 99.8 % t.d., 518 nm
- TZ8YSB: 92.2 % t.d., 757 nm → 1250 °C/ 200 MPa/ 4 h → 99.9 % t.d., 828 nm

Results of the pore closure phenomena and optimization of the post-HIPing process were successfully applied in a preparation of transparent alumina ceramics doped by rare earth elements with photo-luminescent properties.

# 11. Bibliography


[1] KRELL, Andreas, Jens KLIMKE and Thomas HUTZLER. Advanced spinel and sub-um Al2O3 for transparent armour applications. *Journal of the European Ceramic Society*. 2009, **29**(2), 275–281. ISSN 09552219. Doi: 10.1016/j.jeurceramsoc.2008.03.024

[2] WANG, S.F., J. ZHANG, D.W. LUO, F. GU, D.Y. TANG, Z.L. DONG, G.E.B. TAN, W.X. QUE, T.S. ZHANG, S. LI and L.B. KONG. Transparent ceramics: Processing, materials and applications. *Progress in Solid State Chemistry*. 2013, **41**(1–2), 20–54. ISSN 00796786. Doi: 10.1016/j.progsolidstchem.2012.12.002

[3] TRUNEC, Martin, Karel MACA and Radim CHMELIK. Polycrystalline alumina ceramics doped with nanoparticles for increased transparency. *Journal of the European Ceramic Society*. 2015, **35**(3), 1001–1009. ISSN 09552219. Doi: 10.1016/j.jeurceramsoc.2014.09.041

[4] WOLLMERSHAUSER, James A., Boris N. FEIGELSON, Edward P. GORZKOWSKI, Chase T. ELLIS, Ramasis GOSWAMI, Syed B. QADRI, Joseph G. TISCHLER, Fritz J. KUB and Richard K. EVERETT. An extended hardness limit in bulk nanoceramics. *Acta Materialia*. 2014, **69**, 9–16. ISSN 13596454. Doi: 10.1016/j.actamat.2014.01.030

[5] COBLE, R. L. Sintering Crystalline Solids. I. Intermediate and Final State Diffusion Models. *Journal of Applied Physics*. 1961, **32**(5), 787–792. ISSN 0021-8979. Doi: 10.1063/1.1736107

[6] MAYO, M. J. Processing of nanocrystalline ceramics from ultrafine particles. *International Materials Reviews*. 1996, **41**(3), 85–115. ISSN 0950-6608. Doi: 10.1179/imr.1996.41.3.85

[7] LARKER, Hans T. and Richard LARKER. Hot Isostatic Pressing. In: *Materials Science and Technology*. B.m.: Wiley-VCH Verlag GmbH & Co. KGaA, 2006. ISBN 978-3-527-60397-8.

[8] SPUSTA, Tomas, Jiri SVOBODA and Karel MACA. Study of pore closure during pressure-less sintering of advanced oxide ceramics. *Acta Materialia*. 2016, **115**, 347–353. ISSN 13596454. Doi: 10.1016/j.actamat.2016.05.049

[9] SELIVERSTOV, D., V. SAMAROV, V. GOLOVESHKIN, S. ALEXANDROV and Peter EKSTROM. CAPSULE DESIGN FOR HIP OF COMPLEX SHAPE PARTS. In: *Hot Isostatic Pressing '93*. 1994, p. 555–560. ISBN 9780444899590. Doi: 10.1016/B978-0-444-89959-0.50066-9

[10] ATKINSON, Hv and S DAVIES. Fundamental aspects of hot isostatic pressing: an overview. *Metallurgical and Materials Transactions A*. 2000, **31A**(December), 2981–3000. ISSN 1073-5623. Doi: 10.1007/s11661-000-0078-2

[11] GUPTA, T. K. Instability of Cylindrical Voids in Alumina. *Journal of the American Ceramic Society*. 1978, **61**(5–6), 191–195. ISSN 0002-7820. Doi: 10.1111/j.1151-2916.1978.tb09276.x

[12] CARTER, W. Craig, Andreas M. GLAESER and W.D. KINGERY. Dihedral Angle Effects on the Stability of Pore Channels. *Journal of the American Ceramic Society*. 1984, **67**(6), C-124-C–127. ISSN 00027820. Doi: 10.1111/j.1151-2916.1984.tb19717.x

[13] WANG, Xiao Hui, Pei Lin CHEN and I. Wei CHEN. Two-step sintering of ceramics with constant grain-size, I. Y 2O 3. *Journal of the American Ceramic Society*. 2006, **89**(2), 431–437. ISSN 00027820. Doi: 10.1111/j.1551-2916.2005.00763.x

[14] MACA, Karel, Vaclav POUCHLY and Pavel ZALUD. Two-Step Sintering of oxide ceramics with various crystal structures. *Journal of the European Ceramic Society*. 2010, **30**(2), 583–589. ISSN 0955-2219. Doi: 10.1016/J.JEURCERAMSOC.2009.06.008

[15] FANG, Zhigang Zak. *Sintering of advanced materials : fundamentals and processes*. B.m.:

Woodhead Pub, 2010. ISBN 9781845699949.

[16] KANG, S.-J. L. (Suk-Joong L.). *Sintering : densification, grain growth, and microstructure*. B.m.: Elsevier Butterworth-Heinemann, 2005. ISBN 9780750663854.

[17] KANG, Suk Joong L. and Kyung J. YOON. Densification of ceramics containing entrapped gases. *Journal of the European Ceramic Society*. 1989, **5**(2), 135–139. ISSN 09552219. Doi: 10.1016/0955-2219(89)90020-4

[18] YOON, Kyung J. and Suk Joong L. KANG. Densification of ceramics containing entrapped gases during pressure sintering. *Journal of the European Ceramic Society*. 1990, **6**(3), 201–202. ISSN 09552219. Doi: 10.1016/0955-2219(90)90018-B

[19] HÄRDTL, K. H. A simplified method for the isostatic hot pressing of ceramics. *Phillips Tech Rev*. 1975, **35**(2–3), 65–72.

[20] MACA, Karel, Martin TRUNEC and Radim CHMELIK. Processing and properties of fine-grained transparent MgAl2O4 ceramics. *Ceramics − Silikáty*. 2007, **51**(2), 94–97.

[21] SWINKELS, F.B. and M.F. ASHBY. A second report on sintering diagrams. *Acta Metallurgica*. 1981, **29**(2), 259–281. ISSN 00016160. Doi: 10.1016/0001-6160(81)90154-1

[22] ARZT, E., M. F. ASHBY and K. E. EASTERLING. Practical applications of hotisostatic Pressing diagrams: Four case studies. *Metallurgical Transactions A*. 1983, **14**(1), 211–221. ISSN 03602133. Doi: 10.1007/BF02651618

[23] ARZT, E. Optimization of HIP Parameters by Considering the Densification Mechanism. *Keramische Zeitschrift*. 1985, **37**(7), 350–353. ISSN 0048-5012. Available at: http://www.scopus.com/scopus/inward/record.url?eid=2-s2.0-0022089667&partnerID=40&rel=R5.6.0

[24] WEB OF SCIENCE. *Web of Science*. 2019. Available at: https://www.webofknowledge.com/

[25] KWON, Sung-Tae, Doh-Yeon KIM, Thae-Khapp KANG and Duk N. YOON. Effect of Sintering Temperature on the Densification of Al2O3. *Journal of the American Ceramic Society*. 1987, **70**(4), C-69-C–70. ISSN 0002-7820. Doi: 10.1111/j.1151-2916.1987.tb04987.x

[26] KIM, Jin-Young, Nozomu UCHIDA, Katsuichi SAITO and Keizo UEMATSU. Analysis of Hot Isotatic Pressing of Presintered Zirconia. *Journal of the American Ceramic Society*. 1990, **73**(4), 1069–1073. ISSN 0002-7820. Doi: 10.1111/j.1151-2916.1990.tb05158.x

[27] KIM, J. -Y., S. OKAMOTO, N. UCHIDA and K. UEMATSU. Hot isostatic pressing of Y-TZP powder compacts. *Journal of Materials Science*. 1990, **25**(11), 4634–4638. ISSN 0022-2461. Doi: 10.1007/BF01129918

[28] UEMATSU, Keizo, Kazuhisa ITAKURA, Nozomu UCHIDA, Katsuichi SAITO, Akira MIYAMOTO and Tsuneo MIYASHITA. Hot Isostatic Pressing of Alumina and Examination of the Hot Isostatic Pressing Map. *Journal of the American Ceramic Society*. 1990, **73**(1), 74–78. ISSN 0002-7820. Doi: 10.1111/j.1151-2916.1990.tb05093.x

[29] UEMATSU, Keizo, Kazuhisa ITAKURA, Masahiko SEKIGUCHI and Nozomu UCHIDA. Grain Growth During Hot Isostatic Pressing of Presintered Alumina. 1989, **40**, 1239–1240.

[30] BESSON, J. and M. ABOUAF. Microstructural changes in alumina during hot isostatic pressing. *Materials Science and Engineering: A*. 1989, **109**, 37–43. ISSN 09215093. Doi: 10.1016/0921-5093(89)90562-5

[31] BESSON, J. and M. ABOUAF. Grain growth enhancement in alumina during hot isostatic

pressing. *Acta Metallurgica Et Materialia*. 1991, **39**(10), 2225–2234. ISSN 09567151. Doi: 10.1016/0956-7151(91)90004-K

[32] HAHN, H and H GLEITER. The effect of pressure on grain growth and boundary mobility. *Scripta Metallurgica*. 1979, **13**(1), 3–6. ISSN 00369748. Doi: 10.1016/0036-9748(79)90378-8

[33] UEMATSU, K., M. SEKIGUCHI, J. Y. KIM, K. SAITO, Y. MUTOH, M. INOUE, Y. FUJINO and A. MIYAMOTO. Effect of processing conditions on the characteristics of pores in hot isostatically pressed alumina. *Journal of Materials Science*. 1993, **28**(7), 1788–1792. ISSN 00222461. Doi: 10.1007/BF00595746

[34] PARK, H. and S. Y. PARK. Grain growth behavior of alumina during sinter-HIP process. *Journal of Materials Science Letters*. 2001, **20**(7), 601–603. ISSN 02618028. Doi: 10.1023/A:1010957014567

[35] KISHIMOTO, Akira, Masaaki HANAO and Hidetaka HAYASHI. Anomalous grain growth during hot isostatic pressing of magnesia ceramics made from starting powders with different coarse/fine mixing ratios. *Scripta Materialia*. 2007, **57**(4), 321–324. Available at: https://www.sciencedirect.com/science/article/pii/S135964620700317X

[36] LOH, N.L. and K.Y. SIA. An overview of hot isostatic pressing. *Journal of Materials Processing Technology*. 1992, **30**(1), 45–65. ISSN 0924-0136. Doi: 10.1016/0924-0136(92)90038-T

[37] BOCANEGRA-BERNAL, M. H. Hot Isostatic Pressing (HIP) technology and its applications to metals and ceramics. *Journal of Materials Science*. 2004, **39**(21), 6399–6420. ISSN 0022-2461. Doi: 10.1023/B:JMSC.0000044878.11441.90

[38] HOFFMANN, Michael J., Stefan FÜNFSCHILLING and Deniz KAHRAMAN. Hot Isostatic Pressing and Gas-Pressure Sintering. In: *Ceramics Science and Technology*. Weinheim, Germany: Wiley-VCH Verlag GmbH & Co. KGaA, 2014 [accessed. 2017-03-05], p. 171–187. ISBN 9783527631940. Doi: 10.1002/9783527631940.ch38

[39] NAIR, Sv V and Jk K TIEN. Densification mechanism maps for hot isostatic pressing (HIP) of unequal sized particles. *Metallurgical Transactions A*. 1987, **18**(1), 97–107. ISSN 1543-1940. Doi: 10.1007/BF02646226

[40] BESSON, J. and M. ABOUAF. Behaviour of cylindrical hip containers. *International Journal of Solids and Structures*. 1991, **28**(6), 691–702. ISSN 00207683. Doi: 10.1016/0020-7683(91)90150-E

[41] LI, W. B. and H.-Å HÄGGBLAD. Constitutive Laws for Hot Isostatic Pressing of Powder Compact. *Powder Metallurgy*. 1997, **40**(4), 279–281. ISSN 0032-5899. Doi: 10.1179/pom.1997.40.4.279

[42] REARDON, Brian J. Optimizing the hot isostatic pressing process. *Materials and Manufacturing Processes*. 2003, **18**(3), 493–508. ISSN 10426914. Doi: 10.1081/AMP-120022024

[43] KIM, B. N., K. HIRAGA, K. MORITA, H. YOSHIDA and H. ZHANG. Diffusive model of pore shrinkage in final-stage sintering under hydrostatic pressure. *Acta Materialia*. 2011, **59**(10), 4079–4087. ISSN 13596454. Doi: 10.1016/j.actamat.2011.03.032

[44] KIM, Byung Nam, Keijiro HIRAGA, Koji MORITA, Hidehiro YOSHIDA, Yoshio SAKKA and Young Jo PARK. Grain-boundary sliding model of pore shrinkage in late intermediate sintering stage under hydrostatic pressure. *Acta Materialia*. 2013, **61**(18), 6661–6669. ISSN 13596454. Doi: 10.1016/j.actamat.2013.07.014

[45] KIM, Byung Nam, Tohru S. SUZUKI, Koji MORITA, Hidehiro YOSHIDA, Yoshio SAKKA and Hideaki MATSUBARA. Densification kinetics during isothermal sintering of 8YSZ. *Journal of the European*

*Ceramic Society*. 2016, **36**(5), 1269–1275. ISSN 1873619X. Doi: 10.1016/j.jeurceramsoc.2015.11.041

[46] KIM, Byung-Nam, Tohru S. SUZUKI, Koji MORITA, Hidehiro YOSHIDA, Ji-Guang LI and Hideaki MATSUBARA. Evaluation of densification and grain-growth behavior during isothermal sintering of zirconia. *Journal of the Ceramic Society of Japan*. 2017, **125**(4), 357–363. ISSN 1882-0743. Doi: 10.2109/jcersj2.16306

[47] UEMATSU, Keizo, Masaki TAKAGI, Tsunehiro HONDA, Nozomu UCHIDA and Katsuichi SAITO. Transparent Hydroxyapatite Prepared by Hot Isostatic Pressing of Filter Cake. *Journal of the American Ceramic Society*. 1989, **72**(8), 1476–1478. ISSN 15512916. Doi: 10.1111/j.1151-2916.1989.tb07680.x

[48] IKESUE, Akio and Kiichiro KAMATA. *Microstructure and optical properties of hot isostatically pressed Nd:YaG ceramics*. 1996. ISSN 00027820. Doi: 10.1111/j.1151-2916.1996.tb08015.x

[49] TSUKUMA, Koji. Transparent MgAl2O4 Spinel Ceramics Produced by HIP Post-Sintering. *Journal of the Ceramic Society of Japan*. 2006, **114**(1334), 802–806. ISSN 0914-5400. Doi: 10.2109/jcersj.114.802

[50] PROMDEJ, Chutinan, Varong PAVARAJARN, Shigetaka WADA, Thanakorn WASANAPIARNPONG and Tawatchai CHARINPANITKUL. Effect of hot isostatically pressed sintering on microstructure of translucent alumina compact. *Current Applied Physics*. 2009, **9**(5), 960–966. ISSN 15671739. Doi: 10.1016/j.cap.2008.09.011

[51] CHRÉTIEN, Lucie, Loïck BONNET, Rémy BOULESTEIX, Alexandre MAÎTRE, Christian SALLÉ and Alain BRENIER. Influence of hot isostatic pressing on sintering trajectory and optical properties of transparent Nd:YAG ceramics. *Journal of the European Ceramic Society*. 2016, **36**(8), 2035–2042. ISSN 0955-2219. Doi: 10.1016/J.JEURCERAMSOC.2016.02.021

[52] TRUNEC, Martin, Jens KLIMKE and Zhijian James SHEN. Transparent alumina ceramics densified by a combinational approach of spark plasma sintering and hot isostatic pressing. *Journal of the European Ceramic Society*. 2016, **36**(16), 4333–4337. ISSN 0955-2219. Doi: 10.1016/J.JEURCERAMSOC.2016.06.004

[53] GAJDOWSKI, Caroline, Judith BÖHMLER, Yannick LORGOUILLOUX, Sébastien LEMONNIER, Sophie D'ASTORG, Elodie BARRAUD and Anne LERICHE. Influence of post-HIP temperature on microstructural and optical properties of pure MgAl2O4 spinel: From opaque to transparent ceramics. *Journal of the European Ceramic Society*. 2017, **37**(16), 5347–5351. ISSN 0955-2219. Doi: 10.1016/J.JEURCERAMSOC.2017.07.031

[54] MUÑOZ-SALDAÑA, J., H. BALMORI-RAMÍREZ, D. JARAMILLO-VIGUERAS, T. IGA and G. A. SCHNEIDER. Mechanical properties and low-temperature aging of tetragonal zirconia polycrystals processed by hot isostatic pressing. *Journal of Materials Research*. 2003, **18**(10), 2415–2426. ISSN 0884-2914. Doi: 10.1557/JMR.2003.0337

[55] YAMASHITA, Isao, Hitoshi NAGAYAMA, Naoki SHINOZAKI and Koji TSUKUMA. Toughening and strengthening of translucent alumina. *Journal of the Ceramic Society of Japan*. 2009, **117**(1369), 1052–1054. ISSN 1882-0743. Doi: 10.2109/jcersj2.117.1052

[56] MALLIK, A. K., S. GANGADHARAN, S. DUTTA and D. BASU. Micrometer size grains of hot isostatically pressed alumina and its characterization. *Bulletin of Materials Science*. 2010, **33**(4), 445–449. ISSN 0250-4707. Doi: 10.1007/s12034-010-0068-y

[57] SEELEY, Z.M., J.D. KUNTZ, N.J. CHEREPY and S.A. PAYNE. Transparent Lu2O3:Eu ceramics by sinter and HIP optimization. *Optical Materials*. 2011, **33**(11), 1721–1726. ISSN 09253467. Doi:

10.1016/j.optmat.2011.05.031

[58] SCHERRER, S. S., M. CATTANI-LORENTE, S. YOON, L. KARVONEN, S. POKRANT, F. ROTHBRUST and J. KUEBLER. Post-hot isostatic pressing: A healing treatment for process related defects and laboratory grinding damage of dental zirconia? *Dental Materials*. 2013, **29**(9), e180–e190. ISSN 01095641. Doi: 10.1016/j.dental.2013.04.014

[59] GIONEA, Alin, Ecaterina ANDRONESCU, Georgeta VOICU, Coralia BLEOTU and Vasile-Adrian SURDU. Influence of hot isostatic pressing on ZrO2–CaO dental ceramics properties. *International Journal of Pharmaceutics*. 2016, **510**(2), 439–448. ISSN 0378-5173. Doi: 10.1016/J.IJPHARM.2015.10.044

[60] CHINN, Richard E. *Ceramography: preparation and analysis of ceramic microstructures*. B.m.: Materials Park, OH: ASM International, 2002. ISBN 0871707705.

[61] TAFFNER, Ulrike, Veronika CARLE and Ute SCHAFER. Preparation and microstructural analysis of high-performance ceramics. *ASM Handbook: Metallography and Microstructures*. 2004, **9**, 1057–1066. ISSN 0028-3878 (Print). Doi: 10.1361/asmhba0003795

[62] CEN. ISO 13383-1:2012. Fine ceramics (advanced ceramics, advanced technical ceramics) - Microstructural characterization - Part 1: Determination of grain size and size distribution. *EN ISO 13383-1*. 2012.

[63] COOK, Simon G., John A. LITTLE and Julia E. KING. Etching and microstructure of engineering ceramics. *Materials Characterization*. 1995, **34**(1), 1–8. ISSN 10445803. Doi: 10.1016/1044-5803(94)00044-L

[64] CHOKSHI, A. H., A. ROSEN, J. KARCH and H. GLEITER. On the validity of the hall-petch relationship in nanocrystalline materials. *Scripta Metallurgica*. 1989, **23**(10), 1679–1683. ISSN 00369748. Doi: 10.1016/0036-9748(89)90342-6

[65] HALL, E. O. The deformation and ageing of mild steel: III Discussion of results. *Proceedings of the Physical Society. Section B*. 1951, **64**(9), 747–753. ISSN 03701301. Doi: 10.1088/0370-1301/64/9/303

[66] RICE, Roy. *Mechanical Properties of Ceramics and Composites*. B.m.: CRC Press, 2000 [accessed. 2019-10-21]. ISBN 978-0-8247-8874-2. Doi: 10.1201/9780203908471

[67] EHRE, David and Rachman CHAIM. Abnormal Hall–Petch behavior in nanocrystalline MgO ceramic. *Journal of Materials Science*. 2008, **43**(18), 6139–6143. ISSN 0022-2461. Doi: 10.1007/s10853-008-2936-z

[68] KITAMURA, Akira, Shoji KUBODERA, Hideharu YAMAMOTO, Akira MIYAMOTO and Takashi TSUKUI. Prevention of the Color Change in Hip'ing of Zirconia Ceramics. In: *Hot Isostatic Pressing— Theory and Applications*. Dordrecht: Springer Netherlands, 1992 [accessed. 2017-06-25], p. 171–174. Doi: 10.1007/978-94-011-2900-8_27

[69] IKESUE, Akio and Yan Lin AUNG. Ceramic laser materials. *Nature Photonics*. 2008, **2**(12), 721–727. ISSN 1749-4885. Doi: 10.1038/nphoton.2008.243

[70] KRELL, Andreas, Elmar STRASSBURGER, Thomas HUTZLER and Jens KLIMKE. Single and Polycrystalline Transparent Ceramic Armor with Different Crystal Structure. *Journal of the American Ceramic Society*. 2013, **96**(9), 2718–2721. ISSN 00027820. Doi: 10.1111/jace.12530

[71] KRELL, Andreas, Thomas HUTZLER and Jens KLIMKE. Transmission physics and consequences for materials selection, manufacturing, and applications. *Journal of the European Ceramic Society*. 2009, **29**(2), 207–221. ISSN 09552219. Doi: 10.1016/j.jeurceramsoc.2008.03.025

[72] APETZ, Rolf and Michel P. B. BRUGGEN. Transparent Alumina: A Light-Scattering Model. *Journal of the American Ceramic Society*. 2003, **86**(3), 480–486. ISSN 00027820. Doi: 10.1111/j.1151-2916.2003.tb03325.x

[73] BAI, Yang, Ales MATOUSEK, Pavel TOFEL, Vijay BIJALWAN, Bo NAN, Hana HUGHES and Tim W. BUTTON. (Ba,Ca)(Zr,Ti)O3 lead-free piezoelectric ceramics—The critical role of processing on properties. *Journal of the European Ceramic Society*. 2015, **35**(13), 3445–3456. ISSN 0955-2219. Doi: 10.1016/J.JEURCERAMSOC.2015.05.010

[74] MALIC, Barbara, Janez BERNARD, Andreja BENCAN and Marija KOSEC. Influence of zirconia addition on the microstructure of K0.5Na0.5NbO3ceramics. *Journal of the European Ceramic Society*. 2008, **28**(6), 1191–1196. ISSN 09552219. Doi: 10.1016/j.jeurceramsoc.2007.11.004

[75] RATZKER, Barak, Avital WAGNER, Maxim SOKOL, Sergey KALABUKHOV and Nachum FRAGE. Stress-enhanced dynamic grain growth during high-pressure spark plasma sintering of alumina. *Acta Materialia*. 2019, **164**, 390–399. ISSN 13596454. Doi: 10.1016/j.actamat.2018.11.001

[76] ANSELMI-TAMBURINI, U., J.E. GARAY, Z.A. MUNIR, A. TACCA, F. MAGLIA and G. SPINOLO. Spark plasma sintering and characterization of bulk nanostructured fully stabilized zirconia: Part I. Densification studies. *Journal of Materials Research*. 2004, **19**(11), 3255–3262. ISSN 0884-2914. Doi: 10.1557/JMR.2004.0423

[77] KIM, Byung-Nam, Keijiro HIRAGA, Salvatore GRASSO, Koji MORITA, Hidehiro YOSHIDA, Haibin ZHANG and Yoshio SAKKA. High-pressure spark plasma sintering of MgO-doped transparent alumina. *Journal of the Ceramic Society of Japan*. 2012, **120**(1399), 116–118. ISSN 1882-0743. Doi: 10.2109/jcersj2.120.116

[78] QUACH, Dat V., Hugo AVILA-PAREDES, Sangtae KIM, Manfred MARTIN and Zuhair A. MUNIR. Pressure effects and grain growth kinetics in the consolidation of nanostructured fully stabilized zirconia by pulsed electric current sintering. *Acta Materialia*. 2010, **58**(15), 5022–5030. ISSN 13596454. Doi: 10.1016/j.actamat.2010.05.038

[79] BURKE, J.E. and D. TURNBULL. Recrystallization and grain growth. *Progress in Metal Physics*. 1952, **3**, 220–292. ISSN 0502-8205. Doi: 10.1016/0502-8205(52)90009-9

[80] ATKINSON, H. V. Theories of normal grain growth in pure single phase systems. *Acta Metallurgica*. 1988, **36**(3), 469–491. ISSN 00016160. Doi: 10.1016/0001-6160(88)90079-X

[81] BROOK, R.J. Controlled Grain Growth. In: . 1976 [accessed. 2019-11-02], p. 331–364. Doi: 10.1016/B978-0-12-341809-8.50024-3

[82] SPUSTA, Tomas, Marek JEMELKA and Karel MACA. The comprehensive study of the thermal etching conditions for partially and fully dense ceramic samples. *Science of Sintering*. 2019, **51**(3), 257–264. ISSN 0350-820X. Doi: 10.2298/SOS1903257S

[83] DRDLÍKOVÁ, Katarína, Róbert KLEMENT, Daniel DRDLÍK, Tomáš SPUSTA, Dušan GALUSEK and Karel MACA. Luminescent Er 3+ doped transparent alumina ceramics. *Journal of the European Ceramic Society*. 2017, **37**(7), 2695–2703. ISSN 09552219. Doi: 10.1016/j.jeurceramsoc.2017.02.017

[84] BUDWORTH, W.D. Theory of Pore Closure during Sintering. *Transactions of the British Ceramic Society*. 1970, **69**, 29–31.

[85] BEERE, W. A unifying theory of the stability of penetrating liquid phases and sintering pores. *Acta Metallurgica*. 1975, **23**(1), 131–138. ISSN 00016160. Doi: 10.1016/0001-6160(75)90078-4

[86] CARTER, W. Craig and Andreas M. GLAESER. The Morphological Stability of Continuous

Intergranular Phases. In: *Tailoring Multiphase and Composite Ceramics*. Boston, MA: Springer US, 1986 [accessed. 2017-04-25], p. 15–26. Doi: 10.1007/978-1-4613-2233-7_2

[87] SVOBODA, J., H. RIEDEL and H. ZIPSE. Equilibrium pore surfaces, sintering stresses and constitutive equations for the intermediate and late stages of sintering—I. computation of equilibrium surfaces. *Acta Metallurgica et Materialia*. 1994, **42**(2), 435–443. ISSN 09567151. Doi: 10.1016/0956-7151(94)90498-7

[88] JEMELKA, Marek. *Studium vývoje mikrostruktury pokročilých keramických materiálů ve druhé fázi slinování*. Brno: Brno University of Thechnology. 2019

[89] DRDLIK, Daniel, Katarina DRDLIKOVA, Hynek HADRABA and Karel MACA. Optical, mechanical and fractographic response of transparent alumina ceramics on erbium doping. *Journal of the European Ceramic Society*. 2017, **37**(14), 4265–4270. ISSN 1873619X. Doi: 10.1016/j.jeurceramsoc.2017.02.043

[90] *ČSN EN 623-2 (727512) Speciální technická keramika monolitická keramika. Všeobecné a strukturální vlastnosti. Část 2: Stanovení hustoty a pórovitosti*. 1995

[91] MUNRO, Munro. Evaluated Material Properties for a Sintered alpha-Alumina. *Journal of the American Ceramic Society*. 2005, **80**(8), 1919–1928. ISSN 1551-2916. Doi: 10.1111/j.1151-2916.1997.tb03074.x

[92] MATSUMOTO, Roger L. K. and B. J. MCENTIRE. Properties of Yttria Stabilized Tetragonal Zirconia Polycrystals. *MRS Proceedings*. 1985, **60**. ISSN 0272-9172. Doi: 10.1557/proc-60-483

[93] TRUNEC, Martin, Klara CASTKOVA and Pavla ROUPCOVA. Effect of phase structure on sintering behavior of zirconia nanopowders. *Journal of the American Ceramic Society*. 2013, **96**(12), 3720–3727. ISSN 00027820. Doi: 10.1111/jace.12624

[94] MENDELSON, MEL I. Average Grain Size in Polycrystalline Ceramics. *Journal of the American Ceramic Society*. 1969, **52**(8), 443–446. ISSN 0002-7820. Doi: 10.1111/j.1151-2916.1969.tb11975.x

[95] INKSCAPE. *Inkscape*. B.m.: Inkscape. 2019. Available at: https://inkscape.org

[96] KRELL, Andreas and Jens KLIMKE. Effects of the Homogeneity of Particle Coordination on Solid-State Sintering of Transparent Alumina. *Journal of the American Ceramic Society*. 2006, **89**(6), 1985–1992. ISSN 0002-7820. Doi: 10.1111/j.1551-2916.2006.00985.x

[97] JEMELKA, Marek. *Zviditelnění a analýza mikrostruktury částečně slinutých oxidových keramických materiálů*. B.m., 2016. b.n.

[98] SUÁREZ, M., A. FERNÁNDEZ, J. L. MENÉNDEZ and R. TORRECILLAS. Grain growth control and transparency in spark plasma sintered self-doped alumina materials. *Scripta Materialia*. 2009, **61**(10), 931–934. ISSN 13596462. Doi: 10.1016/j.scriptamat.2009.07.026

[99] HE, Zeming and J. MA. Constitutive modeling of alumina sintering: Grain-size effect on dominant densification mechanism. *Computational Materials Science*. 2005, **32**(2), 196–202. ISSN 09270256. Doi: 10.1016/j.commatsci.2004.08.006

[100] BERNARD-GRANGER, Guillaume, Christian GUIZARD and Ahmed ADDAD. Sintering of an ultra pure α-alumina powder: I. Densification, grain growth and sintering path. *Journal of Materials Science*. 2007, **42**(15), 6316–6324. ISSN 15734803. Doi: 10.1007/s10853-006-1206-1

[101] WANG, Jun, Kaijie NING, Jian ZHANG, Dewei LUO, Jie MA, Danlei YIN, Dingyuan TANG and Ling Bing KONG. Rapid Rate Sintering of Yttria Transparent Ceramics. *Journal of the American Ceramic Society*. 2016, **99**(6), 1935–1942. ISSN 00027820. Doi: 10.1111/jace.14209

[102] CHANG, Sekyung, Robert H. DOREMUS, Linda S. SCHADLER and Richard W. SIEGEL. Hot-Pressing of Nano-Size Alumina Powder and the Resulting Mechanical Properties. *International Journal of Applied Ceramic Technology*. 2005, **1**(2), 172–179. ISSN 1546542X. Doi: 10.1111/j.1744-7402.2004.tb00167.x

[103] DILLON, Shen J. and Martin P. HARMER. Intrinsic Grain Boundary Mobility in Alumina. *Journal of the American Ceramic Society*. 2006, **89**(12), 3885–3887. ISSN 0002-7820. Doi: 10.1111/j.1551-2916.2006.01331.x

[104] TEKELI, S. and U. DEMIR. Colloidal processing, sintering and static grain growth behaviour of alumina-doped cubic zirconia. *Ceramics International*. 2005, **31**(7), 973–980. ISSN 02728842. Doi: 10.1016/j.ceramint.2004.10.011

[105] POUCHLY, Vaclav and Karel MACA. Sintering kinetic window for yttria-stabilized cubic zirconia. *Journal of the European Ceramic Society*. 2016, **36**(12), 2931–2936. ISSN 1873619X. Doi: 10.1016/j.jeurceramsoc.2015.12.044

[106] CHOKSHI, Atul H. Diffusion, diffusion creep and grain growth characteristics of nanocrystalline and fine-grained monoclinic, tetragonal and cubic zirconia. *Scripta Materialia*. 2003, **48**(6), 791–796. ISSN 13596462. Doi: 10.1016/S1359-6462(02)00519-5

[107] AKTAS, Bulent, Suleyman TEKELI and Serdar SALMAN. Crystallization and grain growth behavior of La2O3-doped yttria-stabilized zirconia. *Advanced Materials Letters*. 2014, **5**(5), 260–264. ISSN 09763961. Doi: 10.5185/amlett.2014.amwc1011

# 12. Appendix

**Appendix 1**: SPUSTA, Tomas, Jiri SVOBODA and Karel MACA. Study of pore closure during pressure-less sintering of advanced oxide ceramics. *Acta Materialia*. 2016, **115**, 347–353. ISSN 13596454. Doi: 10.1016/j.actamat.2016.05.049

**Appendix 2:** SPUSTA, Tomas, Marek JEMELKA and Karel MACA. The comprehensive study of the thermal etching conditions for partially and fully dense ceramic samples. *Science of Sintering*. 2019, **51**(3), 257–264. ISSN 0350-820X. Doi: 10.2298/SOS1903257S

**Appendix 3:** DRDLÍKOVÁ, Katarína, Róbert KLEMENT, Daniel DRDLÍK, Tomáš SPUSTA, Dušan GALUSEK and Karel MACA. Luminescent Er 3+ doped transparent alumina ceramics. *Journal of the European Ceramic Society*. 2017, **37**(7), 2695–2703. ISSN 09552219. Doi: 10.1016/j.jeurceramsoc.2017.02.017

# 13. Author's publications and other outputs

## *Publications*

- SPUSTA, T.; JEMELKA, M.; MACA, K. The Comprehensive Study of the Thermal Etching Conditions for Partially and Fully Dense Ceramic Samples. Science of Sintering, 2019, vol. 51, no. 3, p. 257-264. ISSN: 0350-820X.
- POUCHLÝ, V.; RÁHEĽ, J.; SPUSTA, T.; ILČÍKOVÁ, M.; PAVLIŇÁK, D.; MORÁVEK, T.; MACA, K. Improved microstructure of alumina ceramics prepared from DBD plasma activated powders. JOURNAL OF THE EUROPEAN CERAMIC SOCIETY, 2019, vol. 39, no. 4, p. 1297-1303. ISSN: 1873-619X.
- HOLEŇÁK, R.; SPUSTA, T.; POTOČEK, M.; SALAMON, D.; ŠIKOLA, T.; BÁBOR, P. 3D localization of spinel (MgAl2O4) and sodium contamination in alumina by TOF-SIMS. MATERIALS CHARACTERIZATION, 2019, vol. 148, no. 1, p. 252-258. ISSN: 1044-5803.
- DRDLÍKOVÁ, K.; KLEMENT, R.; DRDLÍK, D.; SPUSTA, T.; GALUSEK, D.; MACA, K. Luminescent Er3+ doped transparent alumina ceramics. Journal of the European Ceramic Society, 2017, vol. 37, no. 7, p. 2695-2703. ISSN: 0955-2219.
- SPUSTA, T.; SVOBODA, J.; MACA, K. Study of pore closure during pressure-less sintering of advanced oxide ceramics. Acta materialia, 2016, vol. 115, no. 1, p. 347-353. ISSN: 1359-6454.

## *Functional samples*

- SALAMON, D.; ROLEČEK, J.; DRDLÍK, D.; KACHLÍK, M.; SPUSTA, T.: HR; Hybridní kompozit keramika-polymer pro balistickou ochranu. Vysoké učení technické v Brně, Středoevropský technologický institut, Purkyňova 123, 612 00, Brno. (Functional sample)

## *Conferences*

- "Anorganické nekovové materiály 2019", Prague, Czech Republic – Oral presentation.
- "Anorganické nekovové materiály 2017", Prague, Czech Republic – Oral presentation.
- ACerS Winter Workshop 2017 at Orlando, Florida, USA – Participation on the workshop, poster presentation.
- "Príprava a vlastnosti progresívnych keramických materiálov" 2015, Košická Belá, Slovakia – Oral presentation.

## *Research internships*

- Norwegian University of Science and Technology, Trondheim, Norway, 2018. 2-month stay at NTNU Trondheim. Main goal was preparation of Potasium sodium niobate (KNN) samples to achieve fine grain and high density specimens.